UNIVERSITÄT ZU LÜBECK

From the Research Center Borstel
Leibniz Lung Center
Priority Research Area Infections
Director: Prof. Dr. Stefan Niemann

Host Determinants in Lung Infections
Dr. Bianca Schneider

The impact of murine cytomegalovirus infection on the outcome of *Mycobacterium tuberculosis* infection in C57BL/6 mice

Dissertation
for Fulfilment of Requirements
for the Doctoral Degree
of the University of Lübeck

from the Department of Natural Sciences

Submitted by
Jaqueline Marschner
from Hamburg

Lübeck 2025

First referee: PD Dr. Norbert Reiling

Second referee: Prof. Dr. Stefan Taube

Date of oral examination: 15.10.2025

Approved for printing. Lübeck:

Table of contents

Abbreviations

µ

µL ..... Microliter

µM ..... Micromolar

2

26-G 26-gauge

A

AIDS ..... Acquired Immunodeficiency Syndrome

AM ..... Alveolar Macrophage

APC ..... Antigen Presenting Cell

B

BCG ..... Bacillus Calmette-Guérin

BEB ..... Back Extraction Buffer

BMDM ..... Bone Marrow Derived Macrophages

C

CFP-10 ..... Culture Filtrate Protein-10 kDa

CFU ..... Colony-Forming Unit

cGAS ..... Cyclic GMP-AMP Synthase

CPE ..... Cytopathic Effects

D

DC ..... Dendritic Cell

dH_2O ..... Distilled Water

dLN ..... Draining Lymph Node

DMEM ..... Dulbecco's Modified Eagle Medium

DMSO ..... Dimethyl sulfoxide

DNA ..... Deoxyribonucleic Acid

dNTP ..... Deoxynucleotide Triphosphate

ds ..... Double-Stranded

E

e.g ..... For example (exmpli gratia)

E ..... Early

EDTA ..... Ethylenediaminetetraacetic Acid

EPTB ..... Extrapulmonary Tuberculosis

ER ..... Endoplasmic Reticulum

ESAT-6 ..... Early Secreted Antigenic Target 6 kDa Protein

EtBr ..... Ethidium Bromide

EtOH ..... Ethanol

F

FACS ..... Fluorescence-Activated Cell Sorting

FCS ..... Fetal Calf Serum

fw ..... Forward

G

g ..... Glycoprotein

H

HCl ..... Hydrochloric Acid

HCMV ..... Human Cytomegalovirus

HEPES ..... 2-[4-(2-hydroxyethyl)piperazin-1-yl]ethanesulfonic Acid

HIV ..... Human Immunodeficiency Virus

HSCT ..... Hematopoietic Stem Cell Transplant

I

i.p. ..... Intraperitoneal

IE ..... Immediate-Early

IFN ..... Interferon

IL ..... Interleukin

IVC ..... Individually Ventilated Cages

K

kb ..... Kilobases

KCl ..... Potassium chloride

$KHCO_3$ ..... Potassium bicarbonate

L

L ..... Late

LTBI ..... Latent Tuberculosis Infection

M

MCMV ..... Murine Cytomegalovirus

MDR ..... Multidrug-Resistant

MEM ..... Minimum Essential Medium

MeOH ..... Methanol

MHC ..... Major Histocompatibility Complex

min ..... Minutes

mLN ..... Mediastinal lymph node

mm ..... Millimeter

MOI ..... Multiplicity of Infection

MQ10 ..... MACSQuant® Analyzer 10 flow cytometer

mRNA ..... Messenger Ribonucleic Acid

Mtb ..... *Mycobacterium tuberculosis*

MTBC ..... *Mycobacterium tuberculosis* Complex

N

Na_2EDTA ..... Ethylenedinitrilotetraacetic Acid Disodium Salt Dihydrate

NaCl ..... Sodium Chloride

$NaHCO_3$ ..... Sodium Hydrogencarbonate

NaN_3 ..... Sodium Azide

NaOH ..... Sodium Hydroxide

NF-κB ..... Nuclear Factor 'Kappa-light-chain-enhancer' of Activated B-Cells

ng ..... Nanogram

nIF ..... Nodular Inflammatory Foci

NK ..... Natural Killer Cell

NKT ..... Natural Killer T Cell

O

OADC ..... Oleic Acid-Derived Component

P

PAMP ..... Pathogen-Associated Molecular Pattern
PBS ..... Phosphate Buffered Saline
PCR ..... Polymerase Chain Reaction
PFA ..... Paraformaldehyde
PFU ..... Plaque Forming Units
PLHIV ..... People Living with HIV
pp ..... Phosphoprotein
PRR ..... Pattern Recognition Receptor

Q

qPCR ..... Quantitative Polymerase Chain Reaction

R

Rab GTPases ..... Ras-related in Brain Guanosintriphosphatases
RhCMV ..... Rhesus Cytomegalovirus
rv ..... Reverse

S

SDS ..... Sodium Dodecyl Sulfate
sec ..... Seconds
SG ..... Salivary Gland
SOT ..... Solid Organ Transplant
STING ..... Stimulator of Interferon Genes

T

TAE ..... Tris-Acetate-EDTA
TB ..... Tuberculosis
TBE ..... Tris-Borate-EDTA
TC ..... Tissue Culture
TE ..... Tris-EDTA
TLR ..... Toll-Like Receptor
™ ..... Trademark
TNF ..... Tumor Necrosis Factor
Treg ..... Regulatory T cell

TRIS ..... Tris(hydroxymethyl)aminomethane

V

VSB ..... Virus Storage Buffer

W

WHO ..... World Health Organization

WT ..... Wild Type

WTA ..... Wilkins-Chalgren Anaerobic

X

XDR ..... Extensively Drug-Resistant

Abstract

Tuberculosis (TB), caused by *Mycobacterium tuberculosis* (*Mtb*), remains a major global health challenge. While HIV (human immunodeficiency virus) coinfection has long been known to influence TB progression, recent observations suggest that human cytomegalovirus (HCMV) might also affect disease outcomes. However, the nature of this interaction has remained largely unclear. In this study, a C57BL/6 mouse model was used to explore how murine CMV (MCMV) coinfection shapes the course of *Mtb* infection, focusing on disease progression, inflammatory responses, lung pathology, and immune cell infiltration.

When MCMV infection preceded an *Mtb* challenge, mice showed improved disease tolerance and reduced mortality, without changes in bacterial load. Coinfected animals exhibited increased levels of selected inflammatory mediators (including IL-1α, IL-1β, TNF, IFN-γ, CXCL9, CXCL10, and CCL2) and a lung immune environment characterized by fewer lymphocytes and a tendency towards increased macrophage presence. No signs of viral reactivation were observed during coinfection. However, when MCMV infection occurred after *Mtb* infection had become established and chronic, disease progression deteriorated, despite stable pathogen loads. This was not accompanied by major changes in cytokine levels but was associated with earlier onset of symptoms.

At the cellular level in vitro analyzes indicated that macrophages coinfected with *Mtb* after MCMV infection were earlier responsive in producing TNF and showed a lower bacterial burden compared to macrophages infected with *Mtb* alone.

The findings suggest that the timing of MCMV infection in a coinfection with *Mtb* plays a critical role and emphasize the importance of considering the phase of viral infection when interpreting immune dynamics. Further research is needed to explore the molecular mechanisms by which different phases of CMV infection influence the progression to active TB disease, with the aim of applying this knowledge to future disease management strategies.

Zusammenfassung

Tuberkulose (TB), verursacht durch *Mycobacterium tuberculosis* (*Mtb*), stellt nach wie vor eine große Herausforderung für das globale Gesundheitssystem dar. Während das Humane Immundefizienz-Virus (HIV) seit langem als bedeutendster Risikofaktor für die Entwicklung einer TB gilt, weisen neuere Studien darauf hin, dass auch das Humane Zytomegalievirus (HCMV) den Krankheitsverlauf beeinflussen könnte. Die genaue Natur dieser Wechselwirkung ist bislang jedoch weitgehend ungeklärt.

In dieser Studie wurde ein C57BL/6-Mausmodell eingesetzt, um zu untersuchen, wie eine Koinfektion mit murinem Zytomegalievirus (MCMV) den Verlauf einer *Mycobacterium tuberculosis* (*Mtb*)-Infektion beeinflusst. Der Fokus lag auf dem allgemeinen Krankheitsverlauf, der Keimlast, der Entzündungsreaktion, der pulmonalen Pathologie sowie der Infiltration von Immunzellen in die Lunge. Bei Mäusen mit einer MCMV-Infektion vor der *Mtb*-Infektion zeigte sich ein insgesamt günstigerer Krankheitsverlauf und eine reduzierte Sterblichkeit – ohne signifikante Veränderungen in der Kontrolle der *Mtb*-Keimlast. Koinfizierte Tiere wiesen erhöhte Spiegel ausgewählter Entzündungsmediatoren auf, darunter IL-1α, IL-1β, TNF, IFN-γ, CXCL9, CXCL10 und CCL2. Zudem kam es zu einer veränderten Immunzellzusammensetzung in der Lunge mit einer Abnahme von Lymphozyten und einer Zunahme von Makrophagen. Hinweise auf eine Reaktivierung des MCMV während der latenten Infektion wurden nicht festgestellt. Im Gegensatz dazu führte eine akute MCMV-Infektion während einer bestehenden *Mtb*-Infektion zu einem verschlechterten Krankheitsverlauf – trotz stabiler Keimlast. Diese Verschlechterung war weniger mit Veränderungen im Zytokinprofil, sondern vielmehr mit einem früheren Auftreten klinischer Symptome assoziiert. In-vitro-Analysen zeigten, dass Makrophagen, die vor der Infektion mit *Mtb* durch MCMV infiziert worden waren, eine frühere TNF-Produktion aufwiesen und eine geringere bakterielle Keimlast zeigten als Makrophagen, die nur mit *Mtb* infiziert waren.

Die Ergebnisse legen nahe, dass der Zeitpunkt der MCMV-Infektion in einer Koinfektion mit *Mtb* eine entscheidende Rolle spielt und bei der Interpretation immunologischer Abläufe unbedingt berücksichtigt werden muss. Zukünftige Studien sind erforderlich, um die molekularen Mechanismen zu verstehen, durch die unterschiedliche Stadien einer CMV-Infektion den Verlauf hin zur aktiven Tuberkulose beeinflussen können – mit dem langfristigen Ziel, darauf basierende Behandlungsstrategien zu entwickeln.

1 Introduction

1.1 Tuberculosis

Tuberculosis (TB) remains one of the most significant infectious diseases globally and is the world's leading cause of death from a single infectious agent. The World Health Organization (WHO) estimated that 10.8 million people developed TB in 2023, resulting in approximately 1.25 million deaths—nearly twice as many as those caused by HIV (human immunodeficiency virus) (1). In 2023, over half of global TB cases were reported from five countries, such as India, where the incidence rate (Figure 1) was 195 per 100,000 inhabitants—in contrast to 4.8 per 100,000 in low-burden countries like Germany (1–3).

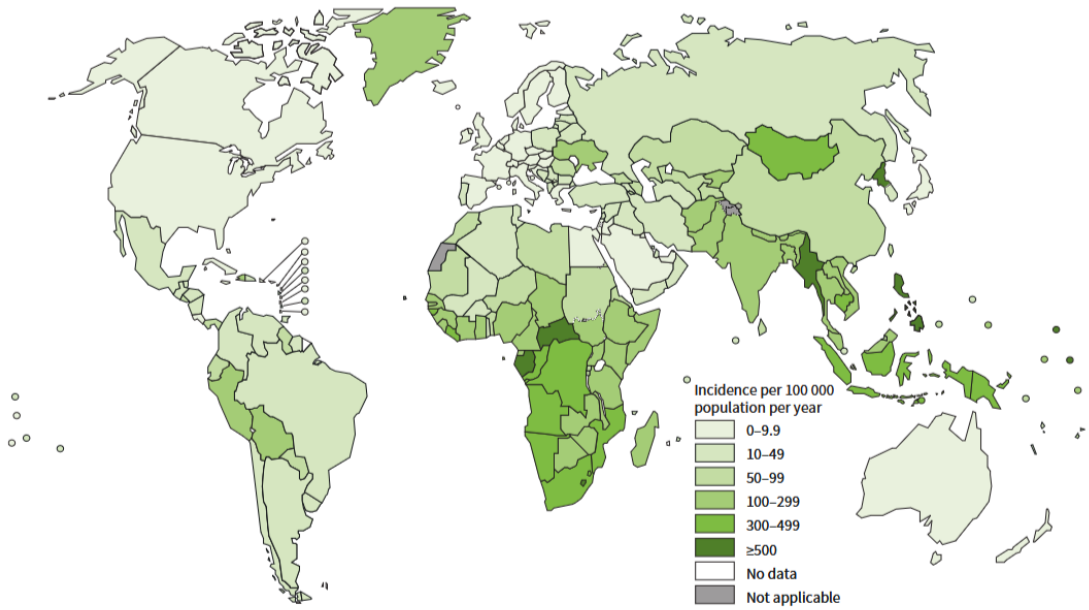

Figure 1: World map showing the estimated TB incidence rates in 2023. (1).

TB is a chronic infectious disease primarily affecting the lungs, although it can disseminate to other organs (4). It manifests in various forms, ranging from latent infection to active disease (5). The most common form is pulmonary TB, which presents with symptoms such as chronic cough and haemoptysis (6). A less common form of TB is extrapulmonary disease, which affects 15–20% of all TB cases (7). Extrapulmonary TB (EPTB) can affect lymph nodes (50%), the pleura (18%), the central nervous system (CNS) (3%), the genitourinary system (13%), bones, and joints (6%) (8,9). The causative agent of TB is *Mycobacterium tuberculosis* (*Mtb*), a slow-growing, aerobic, and non-motile bacillus of the genus *Mycobacterium*, characterized by its unique, lipid-rich cell wall, which contains large amounts of mycolic acids (10,11). This complex cell wall determines the specific properties of *Mtb* such as its long generation time (18-24 hours), its high resistance to desiccation and many

disinfectants, contributing to its virulence and persistence in the environment (12). The organism is also acid-fast, retaining the primary stain when subjected to acid-alcohol decolorization, a property that is used in the Ziehl-Neelsen staining method for diagnostic purposes (13,14). On March 24, 1882, German physician and microbiologist Robert Koch identified *Mycobacterium tuberculosis* as the causative agent of TB—a groundbreaking discovery that revolutionized the field of bacteriology and infectious diseases (15,16). *Mtb* belongs to the *Mycobacterium tuberculosis* complex (MTBC), a group of genetically related mycobacterial species that can cause TB (17). Other notable members of this complex include *Mycobacterium bovis* and *Mycobacterium africanum* (18). These species differ in their host specificity and geographic distribution (19). For instance*, M. bovis* primarily infects cattle but can also cause zoonotic infections in humans, while *M. africanum* is predominantly found in West Africa (20,21).

In the fight against TB, vaccination is arguably the most important tool for prevention and disease management. The Bacillus Calmette-Guérin (BCG) vaccine, developed in the early 20th century, is the only licensed TB vaccine but provides limited protection against pulmonary TB in adults (22–24). This has driven research into novel vaccines, including protein subunit, viral vector-based, and live attenuated vaccines, some of which show promise in clinical trials, each aiming to enhance immune responses and offer broader protection across different age groups (25–28). Developing an effective TB vaccine remains a significant challenge due to the complexity of the pathogen and the need for robust, long-lasting immunity. Despite more than a century of advances—including the discovery of the causative agent, the development of the BCG vaccine, and the introduction of effective antibiotics—TB remains a major public health concern. The WHO has set the ambitious goal of eliminating TB as a public health threat by 2050, but achieving this will require sustained global commitment and new scientific breakthroughs (1). At the same time, the rise of multidrug-resistant (MDR) and extensively drug-resistant (XDR) TB poses an additional global health threat (29). MDR-TB is resistant to the first-line drugs isoniazid and rifampicin, while XDR-TB shows additional resistance to any fluoroquinolone and at least one Group A drug (e.g., bedaquiline or linezolid) (30,31). These resistant strains arise from incomplete treatment, making TB more difficult and expensive to treat (32–34). While drug-resistant TB does not directly impede vaccine development, an effective vaccine could lower TB incidence and help limit the spread of resistant strains. The growing challenge of multidrug resistance underscores the need for better diagnostics, innovative treatments, and robust public health measures (35).

A major challenge in global TB management is the estimated reservoir of approximately 1.7 to 2.3 billion individuals who are likely to be latently infected with tuberculosis (LTBI) (36). According to

the WHO, LTBI is characterized by a persistent immune response that controls *Mtb* infection, without clinical manifestations or dissemination of the bacteria (37). These individuals carry a lifetime risk of reactivation, which occurs in about 5–15% of those with latent TB infection, leading to active TB disease, which is symptomatic and transmissible (38,39). This transition from latent to active TB contributes to the ongoing transmission of the disease and complicates efforts to control and ultimately eliminate TB globally (40). Therefore, in addition to the development of more effective antibiotics, it is essential to identify the risk factors that drive disease progression in order to reduce the global TB burden and to prevent future outbreaks (41). To fully appreciate the challenges in TB control, it is essential to understand the biology of the pathogen and the host immune response.

1.1.1 Tuberculosis pathogenesis

Mtb infection (Figure 2) begins with the inhalation of airborne droplets from individuals with active pulmonary TB (42,43). The lung is both the primary entry site and the main site of disease manifestation (44). Once in the alveoli, *Mtb* bacilli are phagocytosed by alveolar macrophages (AM) (45,46). AMs migrate into the lung interstitium, triggering a proinflammatory response that induces the production of cytokines and chemokines, which recruit mononuclear cells from nearby blood vessels (46–49). Neutrophils and monocytes arrive first, phagocytose bacteria, and amplify the inflammatory response. Dendritic cells (DC), which are superior antigen presenting cells (APCs) transport *Mtb* to lung-draining lymph nodes (dLN), where they present bacterial antigens to lymphocytes, initiating adaptive immunity (50). Activated T and B cells return to the lungs, contributing to bacterial containment (51,52).

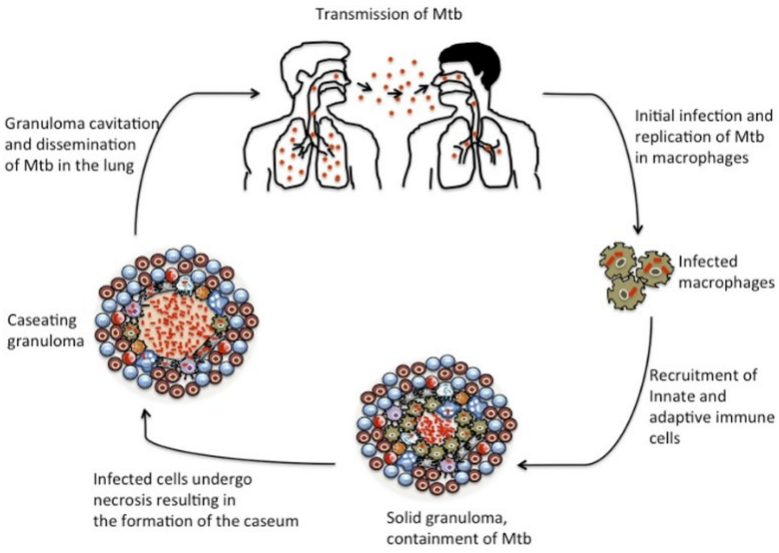

Figure 2: Granuloma Formation and Progression in TB. During early TB infection, inhaled *Mtb* bacilli are phagocytosed by alveolar macrophages, triggering inflammation and recruiting monocytes and macrophages. These differentiate into specialized cells, forming a solid granuloma surrounded by a lymphocytic cuff of B and T cells. While granulomas often contain *Mtb*, disease progression leads to necrosis, caseum accumulation, and cavitation. In advanced stages, granulomas collapse, releasing *Mtb* into the airways and promoting transmission. (Adapted from (53)).

The recruitment of immune cells remodels the site of infection into a cellular mass, called the tubercle or early granuloma (46,54). The granuloma (Figure 3), a hallmark of TB, consists of infected macrophages surrounded by foamy macrophages and lymphocytes, all enclosed by a fibrous cuff (55). As it matures, the granuloma stabilizes, limiting bacterial spread during latent infection (56). In this containment phase, the host does not show overt signs of disease and does not transmit the bacilli to others. Over time, vascularization decreases, and necrosis may develop at the center (57). In progressive cases, caseation occurs, leading to granuloma breakdown and bacterial release into the airways, enabling transmission via coughing or sneezing (58).

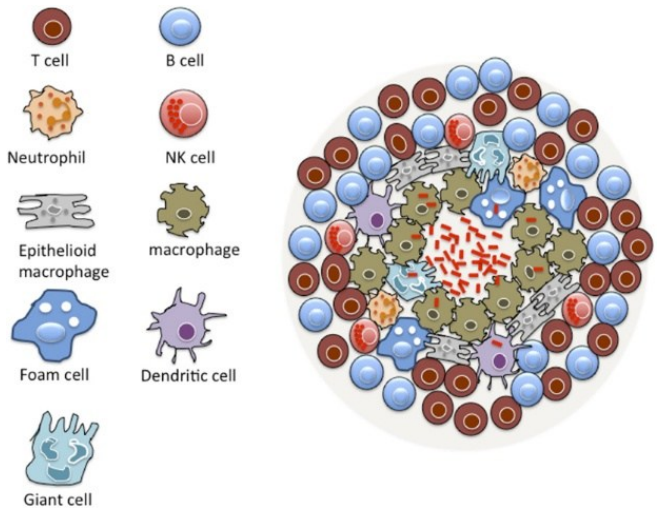

Figure 3: Fundamental structure of a TB granuloma. A granuloma is a compact immunological structure primarily composed of macrophages at its core. These macrophages can undergo specialized differentiation, giving rise to epithelioid cells, multinucleated giant cells, and foamy macrophages, the latter being characterized by their accumulation of lipid droplets. Surrounding the core, a dense lymphocytic cuff, predominantly composed of B and T cells, defines the granuloma's periphery. In addition to these key cell types, neutrophils, dendritic cells, natural killer cells, and fibroblasts contribute to the granuloma's structural and immunological dynamics. (Adapted from (53)).

Granulomas play a dual role in tuberculosis pathogenesis: while they localize infection and limit tissue damage through immune cell containment, they simultaneously shield *Mtb* from host defenses and antibiotics, creating protected niches for bacterial persistence. Within the granuloma, *Mtb* can persist for years in a dormant state, with the potential to reactivate.

1.1.2 Immune response to *Mycobacterium tuberculosis* infection

The immune response to *Mtb* infection is complex and involves both the innate and adaptive immune systems. Most individuals develop an apparently adequate immune response following infection with *Mtb*, but this response is insufficient to completely eliminate the bacteria (59). Instead, a clinically asymptomatic latent infection develops, during which the immune system controls the bacteria in their dormant state. If the host's immune status changes, the bacteria can be reactivated (60,61). After transmission of aerosol droplets containing *Mtb* bacilli from an infected person to a healthy person, AMs are the first cells to come into contact with the bacteria, as they reside in the alveolar space (50). Epithelial cells also interact with *Mtb*, contributing to the initial immune response (62). After binding via toll-like receptors (TLR) and scavenger receptors, AMs phagocytose *Mtb*, serving as a permissive niche for infection establishment (60). *Mtb* resides in a compartment called phagosome, which usually undergoes maturation and fusion with multiple lysosomes, allowing degradation of the pathogen by the lysosomal digestive enzymes (63,64). However, *Mtb* has developed strategies to block phagosome maturation, such as manipulating the

recruitment of Ras-related in brain GTPases (Rab GTPases), which control intracellular trafficking within mammalian cells (65,66). As a result, *Mtb* remains in an early phagosome which does not recruit the vacuolar proton ATPase, responsible for phagosomal acidification (67,68). Moreover, *Mtb* is able to induce phagosomal rupture at later stages of infection, which is facilitated by the type VII secretion system ESX-1. This system includes the proteins early secreted antigenic target 6 kDa protein (ESAT-6) and culture filtrate protein-10 kDa (CFP-10), two immunodominant antigens and major virulence factors of *Mtb* (69–71). Phagosome membrane disruption enables the translocation of *Mtb* into the nutrient-rich cytosol, allowing the bacteria to further replicate and survive within the macrophage (72).

The internalization of the bacilli stimulates AMs to migrate into the lung interstitium. The recognition of pathogen-associated molecular patterns (PAMPs) by TLRs activates the translocation of nuclear factor 'kappa-light-chain-enhancer' of activated B-cells (NF-κB) to the nucleus, resulting in the production of various proinflammatory cytokines such as tumor necrosis factor (TNF), interleukin-1β (IL-1β), and IL-6, which help AMs recruit other cells, such as monocytes, to the site of infection (45,73–77). DCs also play a critical role in *Mtb* infection by activating the adaptive immune system and producing IL-1 and IL-6, further recruiting immune cells to the site of infection (78). DCs phagocytose *Mtb* and migrate to the dLNs, where they process mycobacterial antigens and present them on their surface via the major histocompatibility complex-II (MHC) to naive $CD4^+$ T cells (79). They also upregulate costimulatory molecules (e.g., CD80, CD86) and secrete cytokines such as IL-12, which are crucial for the differentiation of naive T cells into T helper 1 (Th1) cells (80). Activated Th1 cells then produce cytokines like interferon-γ (IFN), IL-2 and TNF, which in turn activate infected macrophages (81). IFN-γ enhances the macrophage's ability to control *Mtb* by overcoming the inhibition of phagosome maturation, increasing phagosome-lysosome fusion, boosting the production of reactive nitrogen intermediates (RNI) and reactive oxygen intermediates (ROI), and stimulating the secretion of IL-6 and TNF (81,82). Further, TNF not only supports the activation of macrophages but also promotes granuloma formation and the recruitment of additional immune cells to the site of infection (83). *Mtb* antigens can also be presented via MHC-I pathways, leading to the activation of cytotoxic $CD8^+$ T cells, which can directly kill infected cells and stimulate the secretion of IFN-γ, thereby contributing to macrophage activation (84,85). Additionally, natural killer (NK) cells and natural killer T (NKT) cells contribute to the immune response by producing IFN-γ and other cytokines (86). Regulatory T cells (Tregs) help modulate this response by preventing excessive inflammation, though they may also facilitate *Mtb* persistence by

dampening the immune response (87). Memory T cells provide a rapid response upon re-exposure to *Mtb*, playing a crucial role in long-term immunity (88,89).

1.1.3 Risk factors

Identifying and understanding the risk factors that promote progression from latent to active TB is essential for elucidating the mechanisms underlying TB pathogenesis (90). Environmental and socioeconomic factors that impair immune function are key risk factors for LTBI reactivation. Recent studies have shown that substance abuse—such as alcohol consumption and smoking—can increase the risk of developing active TB by two- to threefold (90). Additionally, poor living conditions, overcrowding, and limited healthcare access further exacerbate susceptibility. Notably, air pollution, rapid urbanization, and malnutrition—especially severe undernutrition—can increase the risk by up to fourfold (90–92). Beyond environmental and socioeconomic influences, underlying chronic diseases such as type 2 diabetes and immunosuppression play a pivotal role in the progression from LTBI to active TB (1,93). Accordingly, anti-TNF therapy has highlighted the crucial role of TNF in immune defense against *Mtb*, as it increases the risk of developing active TB and necessitates testing for latent TB infection before treatment initiation (94–97). The most significant risk factor for TB is HIV coinfection, which severely compromises the immune system. People living with HIV (PLHIV) are 18 times more likely to develop active TB compared to HIV-negative individuals (98). HIV infection progressively depletes $CD4^+$ lymphocytes, weakening the immune system and increasing susceptibility to opportunistic infections. If left untreated, this immune deterioration can lead to acquired immunodeficiency syndrome (AIDS). As a result, HIV infection impairs the host's ability to control *Mtb*, significantly increasing the risk of LTBI progression to active TB (99). While additional, yet unidentified, risk factors may exist, viral coinfections beyond HIV —such as human cytomegalovirus (HCMV)—have been implicated in TB pathogenesis, with epidemiological evidence supporting an association between HCMV and TB disease progression (100–102).

1.2 Human Cytomegalovirus

HCMV is a ubiquitous herpesvirus with seroprevalence rates approaching 100% in Africa and Asia and around 80% in Europe and North America (103–105). Geographic variations in seroprevalence are largely influenced by socioeconomic factors, as well as age, race, sex, and ethnicity (105,106). In Germany, a low seroprevalence country, between 2009 and 2018, approximately 56.5% of the adults tested HCMV seropositive (107–109). Transmission occurs mainly via mucosal contact, but can also result from blood transfusions or organ transplantation (110). Primary infection involves an acute viremic phase, characterized by active viral replication and shedding in body fluids

(111,112). Following the establishment of a robust immune response, the virus enters a latent phase, during which viral replication is inactive but the risk of lifelong reactivation persists, particularly if the immune system is compromised (113,114). HCMV can be transmitted vertically during pregnancy, either through primary infection or reactivation in the mother, potentially leading to congenital infection in the fetus. Affecting 0.15–2% of all live births, HCMV is the most common cause of congenital infection worldwide (115–119). In utero HCMV infection can have life-long consequences, including birth defects and developmental disabilities (120–122). Most primary HCMV infections are asymptomatic, so individuals are often unaware of their infection. However, in some cases, healthy individuals may experience mild flu-like symptoms, such as fever or swollen glands (123). Individuals at risk of developing clinical manifestations of HCMV include fetuses, neonates, the elderly, and people with weakened immunity, such as those receiving immunosuppressive therapy. In these individuals, primary HCMV infection or reactivation can cause severe disease, with the highest mortality observed in hematopoietic stem cell transplant (HSCT) and solid organ transplant (SOT) recipients (124–126).

HCMV, also known as human herpesvirus 5, belongs to the *Herpesviridae* family (113). Other notable members of this family include Epstein-Barr virus, Kaposi's sarcoma virus and herpes simplex virus types 1 and 2, all of which can infect humans (127,128). Among known herpesviruses, CMV reveals the strictest species specificity with HCMV exclusively infecting humans, rhesus cytomegalovirus (RhCMV) restricted to nonhuman primates and murine cytomegalovirus (MCMV) specific to mice (129). Herpesviruses are enveloped, linear double-stranded DNA viruses, with HCMV having the largest genome (about 236 kb) among them (130,131). The first description of HCMV dates back to 1881, when abnormally large cells with a central nuclear body surrounded by a clear halo were observed (132). Initially misclassified as a protozoan infection, these cells were later identified as a hallmark of HCMV infection. German scientists subsequently detected similar abnormal cells in lesions of herpes-infected patients, leading to the realization that these morphological changes resulted from a viral infection, later confirmed to be HCMV (133,134). A common method for determining whether an individual has been previously infected with CMV is serological testing for CMV-specific antibodies, particularly IgG, in the blood. This serological status, known as seropositivity, indicates a past infection and the development of immunity, providing essential information for assessing the risk of primary infection in seronegative individuals (135). Currently, no approved vaccine exists for HCMV, although several candidates are in clinical development (136). Among them, messenger ribonucleic acid (mRNA) 1674-, a prophylactic vaccine candidate, is currently in Phase 3 clinical evaluation until 2026, targeting women of childbearing

age to prevent primary HCMV infection and reduce the risk of congenital transmission (137). While vaccines remain under investigation, antiviral drugs such as Ganciclovir-which inhibits viral DNA polymerase and replication-are widely used, particularly in organ and stem cell transplant patients (138–140). Valganciclovir, a prodrug of Ganciclovir, is employed for long-term prophylaxis (136,141). Despite available treatments, HCMV remains a significant clinical challenge, especially in immunocompromised individuals. The emergence of multidrug-resistant (MDR) strains, driven by prolonged antiviral use, further complicates treatment, as Ganciclovir-resistant variants harbor mutations in the viral DNA polymerase, reducing drug efficacy (142,143). The development of an effective HCMV vaccine is hindered by the virus's immune evasion mechanisms, its capacity for latent infection, and individual variability in immune responses. Nonetheless, ongoing research continues to explore novel vaccine strategies to address these challenges.

1.2.1 Human Cytomegalovirus pathogenesis

For a long time, it was debated whether HCMV entry primarily occurs via the oral route; however, recent evidence suggests that nasal entry is the more prominent pathway into the host (144). HCMV exhibits a broad tropism, infecting a wide range of cell types, including endothelial cells, epithelial cells, smooth muscle cells, fibroblasts, leukocytes, and DCs (145). This broad tropism facilitates viral transmission and pathogenesis within the human host (146). Following primary infection, HCMV establishes latency in myeloid progenitor cells in the bone marrow, ensuring lifelong viral persistence in the host (147,148). The lytic replication cycle (Figure 4) consists of four distinct phases: viral entry, DNA replication, assembly and maturation, and viral release (149). HCMV gains entry into host cells via glycoproteins on the viral envelope, which interact with specific host receptors, facilitating membrane fusion or endocytosis (150). Simultaneously, tegument proteins—primarily phosphoprotein (pp) 65 and pp71—are released into the cytoplasm, where they are targeted to distinct subcellular compartments. These proteins suppress early immune responses, enhance viral replication, and contribute to immune evasion (151). Once inside the cell, viral tegument proteins, which are tightly bound to the capsid, interact with host microtubules to transport viral capsids to the nuclear envelope. Here, the viral DNA is injected into the nucleus, initiating transcription, genome replication, and encapsidation (152). HCMV gene expression follows a sequential cascade, beginning with immediate early (IE) genes, which play a crucial role in initiating the viral replication cycle and modulating host cell functions to favor viral survival (153). Next, early (E) genes, primarily involved in metabolism and immune evasion, encode proteins essential for viral DNA replication (154). Viral DNA replication begins at the end of early gene expression. The expression of late (L) genes is dependent on successful viral DNA replication. Once

sufficient viral genomes have been synthesized, late genes are expressed, encoding structural proteins necessary for virion assembly and maturation within the nucleus (149). Following nuclear egress, nucleocapsids are transported to the cytoplasm, where they acquire their tegument and secondary envelope derived from the endoplasmic reticulum (ER), Golgi apparatus, and endosomal machinery (155–157). After approximately 72 hours, mature infectious virions—along with non-infectious particles known as dense bodies—are transported via secretory vesicles and released from the infected cell through exocytosis, enabling viral spread to neighboring cells (155,158).

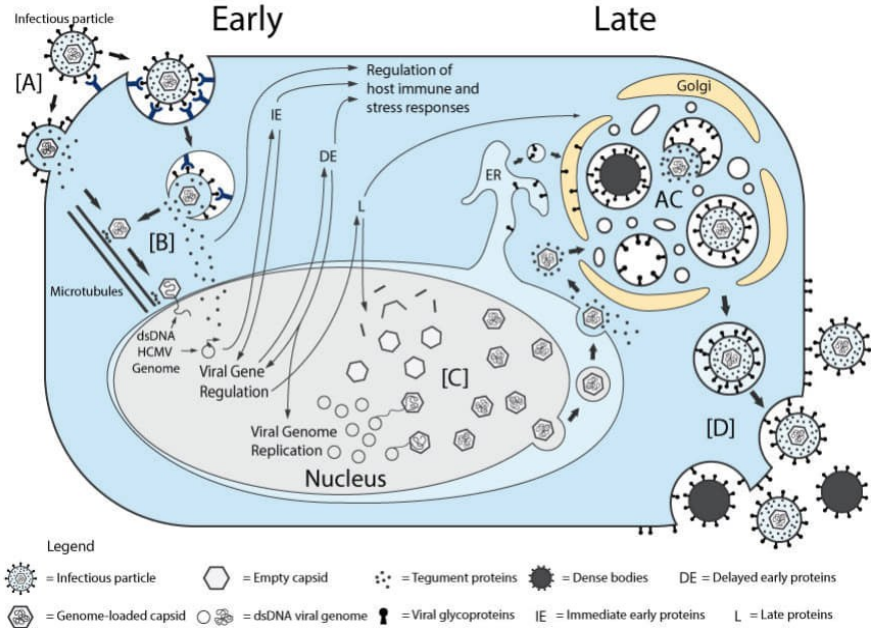

Figure 4: CMV replication cycle. (A) Infectious particles enter the host cell by binding specific receptors, delivering the capsid and tegument proteins into the cytoplasm. (B) The capsid is transported to the nucleus, where it releases and circularizes the viral genome. Tegument proteins modulate host responses and initiate the sequential expression of viral genes, starting with IE genes, followed by DE genes that drive genome replication, and finally L genes. (C) Late gene expression promotes capsid assembly in the nucleus, after which capsids enter the cytoplasm and associate with tegument proteins. They are then transported to the viral assembly complex (AC)-a network involving the ER, Golgi, and endosomal machinery-where they acquire additional tegument proteins and an envelope via budding into vesicles. (D) Finally, fully enveloped virions and non-infectious dense bodies are released from the cell. (Adapted from (159)).

1.2.2 Immune response to HCMV infection

HCMV is primarily transmitted through contact with infectious body fluids and initially invades epithelial cells of mucous membranes, particularly in the respiratory tract. The innate immune response is the first line of defense, recognizing viral PAMPs via pattern recognition receptors (PRRs), such as TLR-2, which detects HCMV glycoproteins and triggers NF-κB signaling, leading to the production of pro-inflammatory cytokines**,** mainly type I and type III IFNs (160–162). This response attracts immune cells-including macrophages, DCs, monocytes, neutrophils, and T cells-

to the infection site. Notably, during the perinatal period, when adaptive immunity is immature, innate immunity plays a dominant role in controlling the virus (163). A key component of HCMV immune sensing is the cyclic GMP-AMP synthase (cGAS)–stimulator of interferon genes (STING) pathway, which detects viral double-stranded (ds) DNA and leads to the activation of IRF3 and the induction of an antiviral state (161,164). However, HCMV employs mechanisms to evade this response, thereby allowing persistent infection. Nodular inflammatory foci (nIF), granuloma-like clusters of macrophages, DCs, and lymphocytes, develop in infected tissues such as the lungs, liver, and CNS, aiding viral containment but also contributing to tissue damage and fibrosis in chronic infections (165–167). NK cells play a crucial role by recognizing and killing infected cells, producing IFN-γ, granzymes, and perforin, and linking innate and adaptive immunity. Their cytokine production further supports T cell activation (168–170). Once primary infection is established, APCs process viral antigens and stimulate adaptive immunity, which is essential for controlling HCMV before the virus enters latency (149,171). The adaptive response is driven by HCMV-specific $CD4^+$ and $CD8^+$ T cells, with $CD8^+$ cytotoxic T cells eliminating infected cells and $CD4^+$ helper T cells supporting B cell-mediated antibody production (172,173). Antibodies targeting key viral envelope glycoproteins (gB, gH, gL) and non-structural proteins (IE1) contribute to viral control (174). HCMV elicits an unusually large memory T cell response, with HCMV-specific $CD8^+$ memory T cells constituting up to 30% of the total $CD8^+$ T cell pool in seropositive individuals, comparable to HIV-specific T cell responses in active infection (174,175). These cells maintain viral surveillance and prevent symptomatic reactivation in immunocompetent hosts. However, despite this strong immune response, HCMV is never fully eradicated and can reactivate under conditions of immunosuppression or advanced age (176,177).

1.3 *Mycobacterium tuberculosis*-HCMV coinfection

Epidemiological evidence indicates an association between HCMV and TB disease progression (101). This hypothesis is supported by studies demonstrating that HCMV prevalence is higher among TB patients compared to healthy controls, with greater HCMV exposure being associated with active TB disease and, according to some studies, with reduced antimycobacterial antibody levels (178–180). Moreover, subclinical or prior HCMV infection has been linked to an increased risk of TB in infants (181).

Both HCMV and *Mtb* are highly prevalent, particularly in low socioeconomic settings, and share key characteristics, such as targeting macrophages and dendritic cells, which are essential for immune defense and disease pathogenesis (78,105,182–184). Both pathogens employ immune evasion strategies—HCMV modulates immune cells and suppresses cellular immunity, while *Mtb* inhibits

macrophage activity and delays apoptosis (185). A notable parallel exists in the age distribution of disease progression for both pathogens. TB and HCMV infections peak during early childhood, decline during adolescence, and rise again in young adulthood, suggesting a period of heightened susceptibility (186). Both pathogens induce chronic inflammatory responses, which can exacerbate tissue damage and influence disease outcomes (167,187). *Mtb* cannot be fully cleared and remains latent in the host, capable of reactivation under specific conditions (60,188). Similarly, HCMV persists lifelong, with chronic antigenic exposure driving a prolonged expansion of HCMV-specific $CD8^+$ T cells—a phenomenon known as memory inflation—which can compromise immune responses against other infections, including *Mtb* (189,190). HCMV also dysregulates myeloid and T cell function, not only by suppressing antiviral immunity but also by creating an immune environment conducive to secondary infections (189,190).

One mechanism by which HCMV alters immunity is the latency-associated continuous production of IL-10, which has broad immunosuppressive effects (190,191). Beyond indirect IL-10-mediated suppression, HCMV directly impairs dendritic cell function and inhibits interferon-stimulated gene expression in macrophages, weakening antimicrobial defense (192,193). Given the central role of macrophages in TB immunopathogenesis, these disruptions may have severe consequences for *Mtb* containment (194,195). The lung serves as a reservoir for HCMV infection in both humans and mice and is a key site for viral reactivation (126,196–198). Pro-inflammatory cytokines such as TNF and IL-1β, which are rapidly upregulated in response to *Mtb* infection, have been implicated in triggering HCMV reactivation (199). Consequently, elevated HCMV antibody levels observed in TB patients may indicate viral reactivation rather than being a primary cause of *Mtb* replication.

Given the emerging evidence suggesting that HCMV coinfection may modulate immune responses during TB infection, further investigation is warranted to clarify its precise role in TB pathogenesis, as a direct causal relationship has yet to be proven. Since HCMV infection induces profound changes in immune cell populations crucial for *Mtb* control, and considering the emerging epidemiological link between HCMV seropositivity and TB, it is hypothesized that HCMV infection may contribute to TB disease progression. This hypothesis is increasingly supported by recent cohort studies and experimental data, although further research is needed to establish causality.

1.3.1 Mouse model

Understanding how MCMV coinfection influences TB disease progression necessitates a well-characterized and reproducible animal model. Different mouse strains respond uniquely to *Mtb* and MCMV, making the choice of an appropriate model critical for studying TB-CMV coinfection.

Animal models play a crucial role in understanding the progression of TB and the immune mechanisms involved in controlling *Mtb* infection. While no single model can fully replicate human TB, mouse models have been essential for studying key aspects of the disease. These models replicate essential features of human TB, including immune responses, and bacterial growth following aerosol infection in mice reflects the dynamics of infection progression observed in individual human TB cases (200,201).

Different mouse strains exhibit varying degrees of susceptibility to TB, largely due to their distinct genetic backgrounds. Based on survival, C57BL/6 and BALB/c mice are considered resistant, whereas C3HeB/FeJ, DBA/2, and 129/Sv mice are considered more susceptible (202). In both mice and humans, the lungs are the primary site of infection. However, a key distinction between the species lies in the dynamics of bacterial burden and disease progression (203). In humans, only 5–10% of infected individuals develop active TB, whereas in mice, *Mtb* infection typically leads to a chronic disease state characterized by slow bacterial growth and immune-mediated tissue damage, ultimately resulting in death (204,205). Consequently, latency, as observed in humans, does not occur in mice. Instead, mice tolerate a relatively high bacterial load in the lungs and other organs throughout infection; however, this bacterial load remains consistently high during the stationary phase and does not decrease (206). Beyond bacterial burden, further differences exist in the lung pathology of TB between humans and mice. Mice generally do not develop the highly stratified granulomas observed in humans in response to *Mtb* infection, nor do they exhibit necrosis and caseation, which are key factors in bacillary transmission (46,205). However, the extent of granuloma formation and other pathological features can vary depending on the mouse strain used (207). In humans, the adaptive immune response typically becomes active 5–6 weeks after *Mtb* infection, whereas in resistant mouse strains, bacterial growth is halted through adaptive immunity as early as day 12 (208,209). Nevertheless, despite these differences, the mouse model replicates many essential characteristics of TB found in humans. For example, studies using gene-deleted mice indicated that IFN-γ and IL-12p40 are essential for controlling *Mtb* infection in mice, which correlates with observations in humans (210–212). Although the mouse model does not perfectly replicate human responses to mycobacterial infection, it provides a living, breathing vertebrate lung model on a small scale, allowing for a large number of experiments with defined outcomes. Additionally, the mouse serves as a manipulable tool that reflects the complexity of the vertebrate immune response to *Mtb*, enabling detailed experimentation to isolate the critical components involved in both protection and pathogenesis (213). These models remain essential for preclinical research (214,215).

Cytomegaloviruses are highly species-specific, meaning that HCMV does not infect animals (216). However, murine cytomegalovirus (MCMV) serves as a well-established model for studying HCMV infection in mice, as it closely replicates key aspects of the human virus, including acute infection, latency, reactivation, and the expansion of memory T cells (217–219). Like HCMV, MCMV severity increases under immunosuppression, and both viruses respond to antiviral treatments such as ganciclovir (220,221). This makes MCMV an indispensable tool for investigating virus-host interactions and for developing therapeutic strategies. Among inbred mouse strains, BALB/c and C57BL/6 are commonly used to study MCMV pathogenesis (222) and these strains exhibit distinct immune responses to the virus. BALB/c mice are highly susceptible to MCMV infection, relying primarily on $CD8^+$ T cells for immune defense (220,223). Therefore, BALB/c mice are used as a model for viral pathogenesis and immunology (222). In contrast, C57BL/6 mice are naturally resistant due to their robust NK cell response, which is mediated by the Ly49H receptor recognizing the viral glycoprotein m157 on infected cells. This makes them a useful model to investigate NK cell-mediated control of MCMV (224–226). The absence of Ly49H in BALB/c mice renders them more vulnerable to infection, whereas the presence of this receptor in C57BL/6 mice allows them to efficiently control MCMV replication (222,227–229). However, this resistance can be overcome by using a modified virus strain, Δm157 MCMV, which lacks the ability to engage Ly49H (230). This prevents NK cells from recognizing infected cells, enabling productive viral infection even in otherwise resistant C57BL/6 mice.

Given these characteristics, the C57BL/6 strain provides a valuable platform for establishing a TB-CMV coinfection model. This strain is widely used in TB research due to its well-defined immune response, particularly its ability to control *Mtb* replication through T cell-mediated immunity. Using Δm157 MCMV in C57BL/6 mice, enables to study the effects of MCMV infection on TB disease progression in a controlled and reproducible manner. This approach allows the investigation of how chronic viral infection influences immune responses during TB, providing critical insights into coinfection dynamics and potential implications for human disease.

1.4 Objectives

Epidemiological evidence suggests a synergistic interaction between *Mtb* and HCMV, as coinfection is associated with worse disease progression in patients. While clinical observations are compelling, the immunological mechanisms underlying this interaction remain poorly understood. Current knowledge is largely derived from observational human cohort studies, which lack the resolution to mechanistically dissect how HCMV influences *Mtb* infection across different disease stages.
To address this gap, the present study investigates the outcome of *Mtb* infection during different phases of MCMV infection in C57BL/6 mice, with a focus on disease progression, inflammatory responses, lung tissue pathology, and immune cell infiltration.

The C57BL/6 mouse model is well established for investigating both TB and CMV infections, as it closely reflects key aspects of human immune responses. Using this model, the study addresses the following questions:

- **Does acute or latent MCMV infection alter TB disease progression?**

While viral infections are known to influence TB outcomes, the specific impact of MCMV coinfection at different stages of viral infection remains unclear. Determining whether acute or latent MCMV infection exacerbates TB could provide critical insights into the timing and nature of immunological changes.

- **Does *Mtb* infection trigger MCMV reactivation?**

Viral reactivation during coinfections has been documented in other models, but whether *Mtb*-driven inflammation directly induces CMV reactivation—and thereby amplifies immunosuppression—remains unclear.

- **How does MCMV coinfection affect immune cell migration during *Mtb* infection?**

HCMV modulates T and B cell subsets, dendritic cell activity, and myeloid cell function, but its impact on antimycobacterial immunity in a coinfection context is poorly understood. This question aims to dissect how MCMV reshapes immune cell infiltration during *Mtb* infection.

2 Material

2.1 Cells

Name	Description	Reference
10.1	Spontaneously immortalized murine embryonal fibroblasts isolated from BALB/c mice	(231)
Bone marrow-derived macrophages (BMDMs)	Primary bone marrow-derived macrophages isolated from female C57BL/6 mice	Research Center Borstel
M2-10B4	Murine bone marrow stromal cells	ATCC (CRL-1972)
L929	Murine fibroblast cell line	Research Center Borstel

2.2 Viruses

Name	Description	Reference
MCMV WT (Murine Cytomegalovirus wild type)	MCMV Smith strain pSM3fr-MCK-2fl	(232)
MCMV Δm157	MCMV Smith strain pSM3fr MCK-2fl with deletion of m157 as described in (230)	This work

2.3 Plasmids

Name	Description	Reference
pcDNA IE1	Quantitative polymerase chain reaction (qPCR) standard used for IE1 quantification	LIV
pcDNA Actin	qPCR standard used for Actin quantification	LIV
MCMV BAC HA-m117 (ZEO)	Template BAC for en passant mutagenesis, containing Zeocin resistance	(233) From LIV (unpublished)

2.4 Bacteria

Name	Description	Reference
E. coli GS1783	DH10BlcI857Δ(cro-bioA)<>araC-PBADI-sceI Growth at 30°C	(233)

2.5 Primers

Name	Sequence	Description
IE1_fw	ACTAGATGAGCGTGCCGCAT	Quantification of IE1 and Actin gene expression in qPCR
IE1_rv	TCCCCAGGCAATGAACAATC	
β-Actin_fw	AGAGGGAAATCGTGCGTGAC	
β-Actin_rv	CAATAGTGATGACCTGGCCGT	

MCMV delta m157_zeo_fw	CGTGGTCAAGCCGGTCGTGTTGTAC CAGAACTCGACTTCGGTCGCGTTCAT GTTGACAATTAATCATCGGCAT	Deletion of m157 from MCMV
MCMV delta m157_zeo_rv	CCTAGTAAAATTACTCTTGATTGTGTT TATCTCGGAACGTGCTGTAACAATCA GTCCTGCTCCTCGGCCA	
Seq-dm157 zeo_fw	CATCCCAAGGACGAAGTCAC	Sequencing m157 region
Seq-dm157 zeo_rv	TAGAGGATAATGATACAACC	

2.6 Antibodies

Antigen	**Application**	**Fluorophore**	**Clone**	**Isotype**	**Dilution**	**Reference**
Mouse CD4	Lymphocyte depletion	-	YTS 191	Rat IgG2b κ	-	Bio X Cell
Mouse CD8α		-	YTS 169.4	Rat IgG2b κ	-	Bio X Cell
Mouse NK1.1		-	PK136	Mouse IgG2a, κ	-	Bio X Cell
Mouse CD8α	Check for Lymphocyte depletion	FITC	53-6.7	Rat IgG2a κ	1:400	Biolegend
Mouse NK1.1		BV421	PK136	Mouse IgG2a, κ	1:100	Biolegend
Mouse CD4		PE-Cy7	GK1.5	Rat IgG2a κ	1:640	Biolegend
Mouse CD3		PE	17A2	Rat IgG2a κ	1:1200	Biolegend

Mouse CD45		APC-Cy7	30-F11	Rat IgG2a κ	1:1500	Biolegend
Mouse CD16/CD32		-	93	Rat IgG2a λ	1:100	Biolegend
Mtb Mpt64	mIF	Opal 690	Polyclonal	Rabbit IgG	1:1000	Cusabio
Mouse CD68		Opal 520	Polyclonal	Rabbit IgG	1:250	Abcam
Mouse CD3		Opal 570	SP7	Rabbit IgG	1:200	Zytomed
Mouse CD19		Opal 780	EPR23174-145	Rabbit IgG	1:200	Abcam

2.7 Chemicals and reagents

2.7.1 Antibiotics

Name	**Application**	**Final concentration**	**Reference**
Chloramphenicol	Selection of bacteria	15 µg/mL	Carl Roth GmbH & Co. KG
Streptomycin	Cell culture supplement	100 µg/mL	PAA
Zeocin	Selection of bacteria	50 µg/mL	Thermo Fisher Scientific Inc.

2.7.2 Enzymes

Name	**Reference**
Fast Digest restriction enzymes and buffer	Thermo Fisher Scientific Inc.

PowerTrack™ SYBR Green Master Mix (Including Taq Polymerase)	Thermo Fisher Scientific Inc.
PRECISOR DNA polymerase and buffer	BioCat
RNAse A	Thermo Fisher Scientific Inc.

2.7.3 Molecular mass standards

Name	**Reference**
GeneRuler™ DNA Ladder Mix	Thermo Fisher Scientific Inc.

2.7.4 Other reagents and chemicals

Substance	**Company**
Acetic acid	Carl Roth GmbH & Co. KG
Albumin bovine fraction V, protease-free (BSA)	SERVA Electrophoresis GmbH
Aqua B. Braun	B.Braun
Aqua destillata (dH_2O)	Water purification system for deionized water at the Research Center Borstel
BBL Seven H11 agar base	Becton Dickinson GmbH
Boric acid	Sigma Aldrich
Calcium acetate	Carl Roth GmbH & Co. KG
Chloroform	Carl Roth GmbH & Co. KG
Dimethylsulfoxid (DMSO)	Carl Roth GmbH & Co. KG

Dulbecco's Modified Eagle Medium (DMEM) w: 4.5 g/L Glucose, w/o: L-Glutamine, w: Sodium pyruvate, w: 3.7 g/L NaHCO3	PANTM-Biotech GmbH
Dulbecco´s Phosphate Buffered Saline (PBS) w/o Calcium & Magnesium	PANTM-Biotech GmbH
EDTA-free Protease Inhibitor Cocktail	Sigma Aldrich
Eosin	Merck KGaA
Ethanol (EtOH)	Merck KGaA
Ethylenediaminetetraacetic acid (EDTA)	Carl Roth GmbH & Co. KG
Fetal calf serum (FCS)	Biochrom AG
Glycerol	Carl Roth GmbH & Co. KG
Guanidin-thiocyanat	Sigma Aldrich
2-[4-(2-hydroxyethyl)piperazin-1-yl]ethanesulfonic acid (HEPES)	Sigma Aldrich
Hematoxylin	Merck KGaA
Hydrochloric acid 37% (HCL)	Carl Roth GmbH & Co. KG
H_2O_2	Carl Roth GmbH & Co. KG
Isopropanol	Carl Roth GmbH &T Co. KG
Potassium chloride (KCl)	Sigma-Aldrich
Ketamine Ketamidor®	WDT
Potassium bicarbonate ($KHCO_3$)	Sigma-Aldrich
L929 cell culture supernatant	produced in-house (filtered)

L-Glutamine (200 mM)	PANTM-Biotech GmbH
Minimum Essential Medium (MEM) (10 x), no glutamine	Thermo Fisher Scientific Inc.
Methanol (MeOH)	Carl Roth GmbH & Co. KG
Methylcellulose viscosity: 4,000 cP, 2.5% in water (20 °C)	Merck KGaA
Middlebrook 7H11 agar	Difco/BD Bioscience
Sodium chloride (NaCl)	Carl Roth GmbH & Co. KG
Ethylenedinitrilotetraacetic acid disodium salt dihydrate (Na_2EDTA)	Sigma Aldrich
Sodium bicarbonate ($NaHCO_3$)	Sigma Aldrich
Sodium azide ($NaN_{3)}$	Merck KGaA
Sodium hydroxide (NaOH)	Carl Roth GmbH & Co. KG
Oleic Albumin Dextrose Catalase (OADC)	Sigma-Aldrich
Paraformaldehyde (PFA)	Carl Roth GmbH & Co. KG
Penicillin-Streptomycin, Solution stabilized, with 10,000 units penicillin and 10 mg streptomycin/mL, 0.1 µm filtered	Merck KGaA
Propidium Iodide Solution	Miltenyi Biotec
Sodium citrate	Sigma-Aldrich
Sodium Hydrogencarbonate ($NaHCO_3$)	Carl Roth GmbH & Co. KG
Sodium pyruvate	Thermo Fisher Scientific Inc.

Sucrose	Carl Roth GmbH & Co. KG
Sodium dodecyl sulfate (SDS)	Carl Roth GmbH & Co. KG
TRI Reagent	Zymo Research
Tris(hydroxymethyl)aminomethane (TRIS)	Carl Roth GmbH & Co. KG
TRIzol LS Reagent®	Thermo Fisher Scientific Inc.
Trichloromethane	Carl Roth GmbH & Co. KG
Triton X-100	Carl Roth GmbH & Co. KG
Trypan blue, 10 g	Carl Roth GmbH & Co. KG
Trypsin 0,25%/ EDTA 0,02%	Merck KGaA
Tween 20	Sigma-Aldrich
Tween 80	Sigma-Aldrich
Xylazin Xylavet®	WDT
Xylene	WALTER CMP GmbH & Co. KG

2.8 Medium

2.8.1 Cell Culture media

Cells	**Component**
BMDM (Culture medium)	65% (v/v) DMEM
	10% (v/v) FCS (heat-inactivated)
	20% (v/v) L929 cell culture supernatant (filtered)
	5% (v/v) Horse serum

	2 mM L-Glutamine
	1 mM Sodium pyruvate
	10 mM HEPES in DMEM
BMDM (Freezing medium)	70% BMDM medium
	20% (v/v) FCS (heat-inactivated)
	10% (v/v) DMSO in BMDM medium
M2-10B4/10.1 (Culture medium)	88% DMEM
	10% (v/v) FCS (heat-inactivated)
	1% (v/v) Penicillin/streptomycin (100×)
	1% (v/v) L-Glutamine
M2-10B4 (for Plaque Assay)	95% DMEM
	3% (v/v) FCS (heat-inactivated)
	1% (v/v) L-Glutamine
	1% (v/v) Penicillin/streptomycin (100×)

2.8.2 Methylcellulose overlay

Component	**Amount**
10×MEM	40 mL
FCS (heat-inactivated)	16 mL
L-Glutamine (200 mM)	5 mL
Methylcellulose 2% (m/v)	360 mL

$NaHCO_3$ (1M)	15 mL
Penicillin/streptomycin (100×)	4 mL

2.8.3 Bacteria Media

Name	**Component**
7H11 agar medium	1.9% (w/v) 7H11 agar
	0.5% (v/v) Glycerin
	10% (v/v) Bovine serum in dH_2O
Mtb H37Rv grow medium	Middlebrook 7H9 broth
	10% v/v OADC
	0.2% (v/v) Glycerin
	0,05% (v/v) Tween 80

2.9 Buffers

Name	**Components**	**pH**
4% Paraformaldehyde (PFA)	4% (w/v) PFA in 1 x PBS	-
50 × TAE buffer (Used 1× for pouring agarose gel and running buffer)	2M Tris-HCl	8.0
	50 mM EDTA	8.0
	5.7% (v/v) acetic acid	-
Back extraction buffer (BEB)	4 M Guanidine Thiocyanate	-
	50 mM Sodium Citrate	-

	1 M Tris, fill up to 250 mL with dH_20	-
Cell lysis buffer	0.5% (v/v) Triton X-100 in ddH_2O	-
Decolorizer solution	92,3% EtOH (v/v)	-
	4,7% (v/v) MeOH	-
	3% (v/v) HCl	-
Fluorescence-activated cell sorting (FACS) buffer	3% (v/v) FCS (heat-inactivated)	-
	0.1% (w/v) NaN3	-
	2 mM EDTA in 1 x PBS	-
Fc blocking buffer	1% (v/v) Rat serum	-
	1% (v/v) Mouse serum	-
	1% (v/v) Hamster serum	-
	1% (v/v) Anti-CD16/32 in FACS-buffer	-
S1 Buffer	50 mM Tris-HCl	8.0
	100 µg/mL RNAse A	
	10 mM EDTA	
S2 Buffer	200 mM NaOH	-
	1% (v/v) SDS	-
S3 Buffer	2.8 M calcium acetate	5.2

Tris-borate-EDTA (TBE) electrophoresis buffer (10×) (Used 0.5 × for pouring agarose gel and running buffer)	1M Tris-HCl	-
	0.02 M EDTA	-
	1 M boric acid	-
Tris-buffered saline with Tween20 (TBST)	50 mM Tris	7.6
	0.05% Tween-20	
Tris-EDTA (TE) buffer	10 mM Tris-HCl	8.0
	1 mM EDTA	-
Tris-HCl	10 mM Tris	8.0
Trypan blue solution	1:10 of 0.5% stock solution in 1 x PBS	-
VSB-Sucrose	50 mM (v/v) TrisHCl	-
	12 mM (v/v) KCl	-
	5 mM (v/v) Na_2EDTA	-
	15% (w/v) Sucrose	-
Wash buffer	0.05% Tween 20 in 1 x PBS	-
Wilkins-Chalgren Anaerobic (WTA) buffer	1% (w/v) BSA	-
	1% (v/v) Tween 80 in dH_2O	-
	1% (v/v) Tween 80 in dH2O	

2.10 Kits

Name	Reference
innuPREP DNA mini kit	Analytik Jena
LEGENDplex™ Mouse Inflammation Panel	Biolegend
LEGENDplex™ Mouse Proinflammatory Chemokine Panel	Biolegend
NucleoSpin Gel and PCR Clean-up Kit	Macherey-Nagel
NucleoBond Xtra Midi Kit	Macherey-Nagel
Opal 3-Plex Anti-Rb Manual Detection Kit	Akoya Biosciences
PolyFect Transfection Reagent	Qiagen

2.10.1 Consumables

Material	Company
BD DiscarditTM II Syringes 5 mL, 10 mL, 20 mL	Becton Dickinson GmbH
BD PlastipakTM Syringe 1 mL	Becton Dickinson GmbH
BD Microlance 3 (23G, 0,6 x 10 mm; 26G, 0,45 x 10 mm)	Becton Dickinson GmbH
Biosphere® Safe Seal Tube 1.5 mL	Sarstedt AG & Co. KG
Biosphere® plus DNA-, DNase, RNase-free filter tips (200 µL, 20 L, 10 µL)	Sarstedt AG & Co. KG
Bottles, PC Widemouth 250ML (PKG - 6)	Beckman Coulter Life Sciences
Corning® 25 cm^2 rectangular canted neck TC-treated culture flask with Plug Seal cap	Corning Inc.

Costar® 6-well Cell Culture Plates	Corning Inc.
Costar® 24-well Cell Culture Plates	Corning Inc.
Costar® 48-well Cell Culture Plates	Corning Inc.
Costar® 96-well Cell Culture Plates (flat bottom,round bottom)	Corning Inc.
Deep Well MegaBlock®, 2.2 mL, PP	Sarstedt AG & Co. KG
Dissection utensils	Hammer
Electroporation Cuvettes, 0.2 cm	Bio-Rad
Ethidium bromide (Etbr)	Thermo Fisher Scientific Inc.
Gloves, nitrile, powder free	Ansell
Measuring cylinder	Vitlab
MicroAmp™ Optical 96-Well Reaction Plate	Applied Biosystems
MicroAmp™ optical adhesive film	Applied Biosystems
Microtome Leica SM 2000 R	Leica Biosystems
Screw cap micro tube, 2 mL	Sarstedt AG & Co. KG
Parafilm®	Bemis Company, Inc.
Petri dish, 92 x 16 mm, transparent, with cams	Sarstedt AG & Co. KG
Petri dish, 35 x 10 mm, transparent, with venting cams	Sarstedt AG & Co. KG
Tissue culture dish, (ØxH): 150 x 20 mm, surface: Standard	Sarstedt AG & Co. KG

Pipette tips (10 µL, 200 µL, 1000 µL)	Sarstedt AG & Co. KG
Rotilabo® glass rods	Carl Roth GmbH & Co. KG
Rubber policeman, 7×25 mm	Glaswarenfabrik Karl Hecht GmbH & Co. KG
Rubber policeman, 35×25×32 mm	Glaswarenfabrik Karl Hecht GmbH & Co. KG
Reaction tube, 1.5 mL & 2 mL, PP	Sarstedt AG & Co. KG
Sarstedt Screw cab tube, 15 mL, PP with conical base, sterile	Sarstedt AG & Co. KG
Sarstedt Screw cab tube, 50 mL, PP with conical base, sterile	Sarstedt AG & Co. KG
Schülke mikrozid®	Schülke & Mayr GmbH
Stericup Quick Release 500 mL	Merck KGaA
Sterican blunt cannula 27G 25 x 0.40mm	Braun
StripetteTM Serological Pipets 1 mL, 5 mL, 10 mL, 25 mL	Corning Inc.
Syringe filter, Filtropur S plus, pore size 0.2 µm	Sarstedt AG & Co. KG
Tissue culture dish, 100 x 20 mm	Sarstedt AG & Co. KG

2.10.2 Instruments

Equipment	**Company**
-20 °C Comfort freezer	Liebherr-Hausgeräte GmbH
-80 °C HERA FREEZE HFU 400 BV	Thermo Fisher Scientific Inc.
Aerosol cages	Marine & Industrie Technik

Beckman Optima L-70 Ultracentrifuge	Beckman Coulter Life Sciences
Biometra T3000 thermal cycler	Analytik Jena
Cell Counting Chamber Neubauer improved, depth 0.1 mm, 0.0025 mm^2	Paul Marienfeld GmbH & Co KG
Eppendorf Centrifuge 5415 R	Eppendorf SE
Eppendorf Multipette Stream	Eppendorf SE
FastPrep-24™ 5G	MP Biomedicals
Finnpipette™ (20 µL, 100 µL, 200 µL, 1000 µL)	Thermo Fisher Scientific Inc.
Fridge	Liebherr-Hausgeräte GmbH
Fridge	Robert Bosch GmbH
Gene Pulser XCell	BioRad
Grant bio-PMS 1000 microplate shaker	Keison Products
Heraeus Multifuge X1R Centrifuge	Thermo Fisher Scientific Inc.
Heraeus Pico 17 Centrifuge	Thermo Fisher Scientific Inc.
Incubator BD 53	Binder GmbH
Incubator Heratherm	Thermo Fisher Scientific Inc.
Light microscope Olympus BX41	Olympus
MACSQuant® Analyzer 10 flow cytometer	Miltenyi Biotec B.V. & Co. KG
MSC-Advantage™ Class II Biological Safety Cabinets	Thermo Fisher Scientific Inc.
Multi-channel Transferpette® S -8 (200 µL)	Brand GmbH + Co KG

NanoDrop™ 1000	Thermo Fisher Scientific Inc.
Nikon A1+ confocal laser scanning microscope	Nikon
Nikon Eclipse Ti	Nikon
Nikon Eclipse TS100	Nikon
Pipetus	Hirschmann Laborgeräte GmbH & Co. KG
QuantStudio™ 3 Real-Time PCR system	Thermo Fisher Scientific Inc.
Sorvall RC 6 Plus Superspeed-centrifuge	Thermo Fisher Scientific Inc.
Sterile Working Bench Safe 2020	Thermo Fisher Scientific Inc.
Sunrise Reader	TECAN Sunrise™
TC20 automated cell counter	Bio-Rad
TC™ Automated cell counter	Bio-Rad
Thermomixer comfort 5355	Eppendorf SE
Tissue Stainer TST 44 C	Medite
Vortexer IKA MS 3 basic	IKA-Werke GmbH & CO. KG
Water Bath Aqualine AL 5	Lauda Dr. R. Wobserr Gm bH & Co. KG

2.10.3 Sera

Serum	**Company**
Bovine Serum (heat-inactivated)	BIOWEST SAS
FCS (heat-inactivated)	Biochrom AG
Mouse Serum	PANTM-Biotech GmbH

Rat Serum	PANTM-Biotech GmbH
Hamster Serum	PANTM-Biotech GmbH

2.10.4 Software and Websites

Name	**Company**
CLC Main Workbench 7 (Version 7.9.1)	QIAGEN
Design & Analysis Software (Version 2.7.0)	Thermo Fisher Scientific Inc.
FCS Express 4 flow cytometry (Version 7.12.0020)	DeNovo™ Software
GraphPad Prism® (Version 9)	GraphPad Software
Image Lab software (Version 2.0.1)	Bio-Rad Laboratories
InForm software	Akoya Biosciences
LEGENDplex™ software (Version 2024-06-15)	Biolegend
Microsoft Word/Excel/Powerpoint LTSC Professional Plus 2021 (Version 2108)	Microsoft Corporation
Phenochart (Version 1.1.0)	Akoya Biosciences
Qu-Path (Version 0.5.1)	Pathomation

3 Methods

3.1 Bacteria and virus

3.1.1 *Mycobacterium tuberculosis* (*Mtb*)

Mtb H37Rv was grown in Middlebrook 7H9 broth (BD Biosciences) supplemented with 10% v/v OADC (Oleic Albumin Dextrose Catalase) enrichment medium (BD Bioscience), 0.2% v/v glycerol and 0,05% v/v Tween 80 to logarithmic growth phase (OD600 0.2 - 0.4) and bacterial aliquots were frozen at -80 °C (grown by Martina Ackermann, kindly provided by the Molecular and Experimental Mycobacteriology group, Research Center Borstel). Viable cell number in thawed aliquots were determined as described in 3.5.1.

3.1.2 Murine Cytomegalovirus (MCMV)

The MCMV-Δm157 virus used in this study was based on the pSM3fr-MCK-2-fl BAC (232) and modified to delete m157 as described in (230). For this, en passant mutagenesis, a site-directed technique that can introduce a variety of mutations, was used which is further described under 3.2.1. MCMV stock production is described under 3.3.4.

3.2 Molecular biology methods

3.2.1 En passant mutagenesis

En passant mutagenesis is a precise genetic engineering technique that enables targeted mutations, deletions, or insertions into large DNA molecules such as bacterial artificial chromosomes (BACs) via homologous recombination in bacteria. In this study, the BAC was mutated using en passant mutagenesis as described by Tischer and colleagues (233). First the zeocin resistance gene with its promoter EM7, was amplified using oligonucleotides containing homology sequences that bind upstream and downstream of MCMV m157 gene in addition to the specific sequence for the annealing to the zeocin cassette. Zeocin will be used to select for the mutated bacteria later in the process. The PCR product was then digested by DpnI to remove the BAC and loaded on a TAE agarose gel. The correct size of ~543 bp fragment was cut from the gel and purified by NucleoSpin Gel and PCR clean up kit. 150ng of the purified PCR product was transformed to E. coli GS1783 electrocompetent bacteria carrying MCMV BAC. Transformed bacteria were then plated on LB agar plates containing chloramphenicol and zeocin in order to select for the clones where the homologous recombination was efficient and the m157 gene replaced by the zeocin cassette. After overnight incubation at 30 °C, 10 colonies were picked up and incubated in LB-Broth medium containing chloramphenicol and zeocin for overnight incubation with continuous shaking at 30 °C. BAC DNA from the overnight culture was extracted and digested with XbaI. The DNA fragments

were analyzed by running a TBE agarose gel overnight. Based on the TBE agarose gel, two positive clones were selected, plated onto LB plates containing zeocin and chloramphenicol via stripping dilution, and incubated overnight at 30 °C. Clones were picked from single-clone plate and incubated in LB containing zeocin and chloramphenicol for BAC DNA extraction. Finally, a PCR was performed to check if the insertion of zeocin was correct and that no unexpected mutations happened in the region. PCR products were load on a TAE gel and the correct fragment was purified from Gel and prepared for sequencing. After confirmation of the sequencing, 2 selected positive clones were incubated in LB broth containing chloramphenicol for Midi-preps for reconstituting the virus in murine fibroblasts. In parallel glycerol stocks of the chosen clones were prepared.

3.2.2 Polymerase Chain Reaction (PCR)

PCR was performed by using PRECISOR High-Fidelity DNA polymerase according to the manufacturer's protocol. The PRECISOR polymerase was used for cloning and mutagenesis since it has low error rates and amplifies accurately and efficiently. In all PCR-based assays, negative controls without template DNA were included to verify assay performance.

Table 1: Reaction Setup PCR.

Component	**Amount**
Template pEPkan-S	1 µL
Reaction buffer (5 x)	10 µL
Deoxynucleotide triphosphate (dNTPs) (10 µM)	1.5 µL
Primer fw/rv (10 µM each)	2 µL
DMSO	1.5 µL
PRECISOR Polymerase	1 µL
H_2O	31 µL

Table 2: Cycling conditions PCR.

Step	**Temperature**	**Time**	**Cycles**
Pre-incubation/ Denaturation	95 °C	2 min	1
Amplification	95 °C	30 sec	35
	58.2 °C	30 sec	35
	72 °C	60 sec	35
Final extension	72 °C	2 min	1
Hold	4 °C	∞	∞

3.2.3 Restriction digestion of DNA

DNA digestion was performed by using FastDigest restriction enzymes according to the manufacturer's instructions.

Table 3: Reaction set up and digestion conditions.

Component	**Amount**
10 x FastDigest Green Buffer	5.5 µL
PCR product	50 µL
DpnI	1 µL
37 °C for 60 min	
10 x FastDigest Green Buffer	

3.2.4 Agarose gel electrophoresis

PCR products or digested DNA were loaded on a 0.8%-1% (w/v) TAE agarose gel and run at 120-130 V for 1 hour. The BAC DNA fragments were loaded on a 0.6% (w/v) TBE agarose gel and run at 50 V overnight. Both TAE and TBE gels contain 0.5 µg/mL ethidium bromide. The GeneRuler DNA Ladder

Mix was loaded on the gel as a size ladder. The sizes of DNA fragments were visualized with GelDoc XR+(BioRad). The pictures of the gels were taken using a GelDoc XR+(BIO-RAD) and analyzed with the Image Lab software.

3.2.5 Purification of DNA fragments

The DNA fragments with the correct size were cut from TAE gels and purified using the NucleoSpin Gel and PCR Clean-up kit, following the manufacturer's instructions. The concentration and quality of the purified DNA were assessed using NanoDrop-1000. The DNA was then stored at -20 °C for future use.

3.2.6 Bacterial transformation

Electrocompetent bacteria were transformed via electroporation. First, 50 µL of *E. coli* GS1783 was thawed on ice and combined with 150 ng of linear PCR-amplified DNA. The mixtures were then transferred to 2 mm electroporation cuvettes and subjected to a pulse using the Gene Pulser XCell (BioRad) with the following settings: 2500 V, 25 µF, and 200 Ω. Immediately after the pulse, 900 µL of warm LB broth was added to the bacteria. *E. coli* GS1783 was incubated, shaking at 30 °C for 1 hour. The cells were then centrifuged at 2000 × g for 2 minutes, resuspended, and plated on LB agar plates containing chloramphenicol and zeocin. The plates were incubated overnight at 30 °C in a bacterial incubator.

3.2.7 Extraction of BAC DNA (Mini prep)

Single colonies were selected from an LB agar plate and inoculated into 5 mL of LB broth medium containing chloramphenicol and zeocin for overnight shaking incubation at 30 °C. The overnight culture was centrifuged at 6000 × g for 2 minutes at 4 °C, and the bacteria pellet was resuspended in 300 µL of ice-cold S1 buffer. Next, 300 µL of ice-cold S2 buffer was added, and the mixture was gently inverted 3-5 times. After a 4-minute incubation at room temperature, 300 µL of ice-cold S3 buffer was added, and the solution was gently inverted 3-5 times. The samples were then incubated on ice for an additional 7 minutes before being centrifuged at 11.000 × g for 20 minutes at 4 °C. The clear supernatant was transferred to a new tube and mixed with 0.8× volume of isopropanol. After gently inverting the tube 3 times, it was centrifuged at 11.000 × g for 45 minutes at 4 °C. The resulting pellet was washed with 400 µL of 70% ethanol and centrifuged again at 11.000 × g for 5 minutes at 4 °C. The DNA pellet was air-dried and then dissolved in 50 µL of 10 mM Tris-HCl (pH 8) through gentle shaking. Digestion of 20 µL isolated DNA was performed as described in 0 but XbaI was used instead of DpnI. Digested DNA was load on a TBE agarose gel as previously described 0 and positive clones were plated onto LB plates containing zeocin and chloramphenicol via stripping

dilution so that single bacterial colonies can be obtained on the plate the next day. Plates were incubated over night at 30 °C. Single clones were picked and incubated in LB medium containing chloramphenicol and zeocin for BAC DNA extraction.

3.2.8 Extraction of BAC DNA (Midi prep)

Bacteria were grown overnight in 200 mL of LB broth medium with chloramphenicol and zeocin, shaken continuously at 30 °C. BAC DNA was extracted using the NucleoBond Midi Xtra Kit according to the manufacturer's low copy protocol instructions. The resulting DNA pellet was dissolved in Tris-HCl buffer (pH 8.0) and stored at -20 °C. For final confirmation of the successful insertion of zeocin, again a PCR was performed using again PRECISOR polymerase. Instead of 1 µL template, 3 µL BAC DNA were used. Beside this difference, reaction setup and cycling conditions were equal.

3.2.9 Storage of bacteria

600 µl of an overnight culture was mixed with 300 µl of autoclaved 86% glycerol and stored at -80 °C.

3.2.10 DNA Sequencing

MCMV virus DNA and BACs were sequenced by the NGS facility at the LIV. PCR products were sequenced by SEQLAB Sequence Laboratories (Maschmühlenweg 36, 37081, Göttingen, Germany).

3.2.11 Determination of the viral load (qPCR)

Quantitative PCR was used to determine the number of viral genome copies. Total DNA was extracted from organ homogenates diluted 1:3 in TRIZOL LS following the protocol from van de Rijn Laboratory in Stanford, USA. The DNA concentration and purity were determined using a NanoDropTM 1000 (Thermo Fisher Scientific Inc.). qPCR targeting the MCMV IE1 gene was performed using the QuantStudio™3 Real-Time PCR system. Serial dilutions ranging from 10^{10} to 10^{3} copies of pcDNA expressing MCMV IE1 or beta-actin were used as standards. Analysis of the absolute quantification was performed using the QuantStudio Design and Analysis Software (version 2.7.0, Thermo Fisher Scientific Inc.). All quantifications were normalized to the beta-actin copies number.

Table 4: Reaction setup qPCR.

Component	**Amount**
Template DNA	~ 100 ng
PowerTrack™ SYBR Green Master Mix	5 µL
Primer fw/rv (10 µM each)	0.5 µL
H_2O	Fill up to 10 µL

Table 5: Cycling conditions qPCR.

Step	**Temperature**	**Time**	**Cycles**
Pre-incubation	50 °C	2 min	1
Denaturation	95 °C	10 min	1
Amplification	96 °C	15 sec	40
	60 °C	60 sec	∞
	4 °C	∞	∞

3.3 Cell biology methods

3.3.1 Cell culture

All cells were cultured at 37 °C in a Hera Cell incubator with 80% relative humidity and 5% CO_2. All cell culture procedures were conducted within a laminar flow hood (HeraSafe, Heraeus).

M2-10B4 (CRL-1972) cells were obtained from the American Type Culture Collection. Murine 10.1 fibroblasts are spontaneously immortalized mouse embryonic fibroblasts (MEFs) from BALB/c mice obtained from Thomas Shenk (Princeton University, USA) (231). M2-10B4 and 10.1 cells were cultured in complete Dulbecco's modified Eagle medium (DMEM) supplemented with 10% fetal calf serum, 100 U/mL penicillin, and 100 µg/mL streptomycin in 25 cm^2 culture flasks. When the cells reached approximately 90% confluence, they were washed with PBS and detached using a 0.25% Trypsin-EDTA solution at 37 °C. The trypsin was neutralized by adding growth medium containing FCS (heat-inactivated), and the cells were then split at a ratio of 1:10. For cell counting, 10 µL of the

cell suspension was diluted with 90 µL trypanblue and loaded onto a Neubauer cell counting chamber (Paul Marienfeld GmbH & Co KG).

Bone marrow-derived macrophages (BMDM) were generated from bone marrow isolated from female C57BL/6 mice provided by the animal facility of Research Center Borstel. After euthanasia, the mice were disinfected with 70% ethanol and the tibia and femur were removed, cleaned of tissue, and the marrow was flushed into a 50 mL conical tube using a 23-G syringe with 20 mL of cold BMDM medium per leg. Cells were centrifuged at 250 x g for 5 minutes at 4 °C, and the supernatant was discarded. Cells were resuspended in BMDM medium, seeded in petri dishes (6 dishes per mouse) and incubated at 37 °C and 5% CO_2 for 6-7 days, with 5 mL additional medium added after 3 days. After differentiation, BMDMs were detached from the culture dish using cold PBS and a sterile rubber policeman. The cells were then collected and resuspended in fresh BMDM medium for subsequent experiments.

3.3.2 Cryopreservation

For cryopreservation, the cell suspension was centrifuged at 250 × g for 10 minutes. The cell pellet was resuspended in FCS (heat-inactivated) containing 10% DMSO and aliquoted into cryotubes. The cells were immediately placed in a freezing container ("Mr. Frosty”- Thermo Fisher Scientific Inc.) at -80 °C overnight before being transferred to liquid nitrogen. To thaw the cells, an aliquot of frozen cells was retrieved from liquid nitrogen and quickly thawed through gentle shaking in a 37 °C water bath. The thawed cells were then transferred into a 50 mL falcon tube containing 10 mL of growth medium and centrifuged at 250 x g for 5 minutes. The cell pellet was resuspended in 10 mL of growth medium and transferred to a 10 cm² culture dish.

3.3.3 Transfection of BAC DNA

MCMV BAC DNA was transfected into 10.1 murine fibroblasts using the Polyfect transfection reagent to reconstitute MCMV viruses. The day before transfection, 1×10^5 cells were seeded in a 6-well plate. On the day of transfection, 3 µg of MCMV BAC DNA was added to 100 µL of DMEM without supplements and 15 µL of Polyfect. The BAC DNA and Polyfect solutions were mixed and incubated at room temperature for 15 minutes. Subsequently, 600 µL of growth medium was added to the mixture, which was then transferred to the cells and gently distributed over the entire well. Six hours post transfection, 1.5 mL media of each well were removed and 600 µL fresh DMEM with 10% FCS (heat-inactivated) were added to each well. After a gentle mix the plate was incubated at 37 °C. Once the cells reached confluence, they were transferred to a 15 cm² cell culture dish.

Reconstitution of MCMV was monitored by observing cytopathic effects (CPE). The supernatant from the infected cells was collected for virus stock preparation.

3.3.4 Infection of cells and preparation of MCMV stock

For the production of a viral stock, murine 10.1 fibroblasts were infected in 15 cm² petri dishes at a multiplicity of infection (MOI) of 0.025, based on the titer of the viral stock. The needed amount was calculated as follows:

$$volume\ of\ virus\ stock\ (mL) = \frac{number\ of\ cells\ x\ MOI}{PFU/mL}$$

The calculated amount of virus was diluted in the growth medium and added to infect the cells. Three days post-infection, the supernatant was collected, and fresh medium was added to the cells to allow for an additional harvest two days later, aiming to increase yield. The supernatant collected on day 3 was stored at 4 °C. On day 5, the supernatant was collected again, combined with the day 3 supernatant, and centrifuged at 6000 x g for 15 minutes at 4 °C to remove cellular debris. The supernatant was then transferred to fresh centrifuge tubes and centrifuged at 27000 x g for 3.5 hours at 4 °C to pellet the virus. After centrifugation, the supernatant was discarded, and the viral pellet was resuspended in 2 mL of medium and allowed to dissolve overnight on ice at 4 °C. The next day, the resuspended pellet was carefully transferred into ultracentrifuge tubes containing 18 mL of a sucrose cushion, where the virus formed a layer above the sucrose cushion. Ultracentrifugation was performed at 70000 x g for 1.5 hours at 4 °C using a L70 Ultracentrifuge. The viral pellet was then dissolved in 300 µL of PBS (for in vivo experiments) overnight at 4 °C. The virus stock was aliquoted into 20 µL per tube and stored at -80 °C.

3.4 Animal experiments

Animal experiments were in accordance with the German Animal Protection Law and approved by the Ethics Committee for Animal Experiments of the Ministry of Agriculture, Rural Areas, European Affairs and Consumer Protection of the State of Schleswig-Holstein (approval number 85-9/20). All mice used were purchased from Janvier Labs and maintained under specific barrier conditions in the BSL-3 facility at the Research Center Borstel. Female C57BL/6 mice aged between 10-13 weeks were used.

3.4.1 *Mtb* infection

Infection of the mice was performed in special mesh steel cages via the respiratory route by using a Glas-Col aerosol chamber (Glas-Col, Terre-Haute). *Mtb* stocks were diluted in sterile distilled water at a concentration providing an uptake of 100 viable bacilli per lung. For infection, a frozen

Mtb H37Rv stock was thawed and resuspended ten times with a 27-G cannula to separate the mycobacteria aggregates. The suspension was then diluted in sterile Braun water to a total volume of 6 mL, of which 5.5 mL were transferred into a nebulisation vessel, and the system was started. After a warm-up time of 900 seconds, the system was run for 2400 seconds. After nebulisation for 2400 seconds, suction for 2400 seconds, and decontamination for 900 seconds, the mice were transferred back into their individually ventilated cages (IVC). The remaining 500 µL of the bacterial suspension was plated on 7H11 agar plates with bovine serum at dilutions ranging from 10^{-2} to 10^{-5} to assess the bacteria count in the inoculum. The plates were incubated at 37 °C for 3 to 4 weeks. One day after infection, lungs of infected mice were harvested to determine the actual bacterial uptake. After harvest, the lungs were homogenized in 1 mL of PBS twice for 45 seconds using the FastPrep system. Between the first and second steps, the samples were kept on ice. The undiluted lysates were distributed on six 7H11 agar plates with bovine serum. After 3 to 4 weeks of incubation at 37 °C, the colonies were counted.

3.4.2 MCMV infection

Female WT C57BL/6 mice were infected intranasally with 2×10^5 PFU MCMV-Δm157 in PBS per mouse. The mice were anesthetized with a mixture of 12.5% ketamine and 1.25% xylazine in 1 x PBS (200 µL/20 g body weight), and the inoculum was slowly and evenly administered, 20 µL per nostril.

3.4.3 Assessment of the health status of infected animals

The health status, severity of disease and disease progression of infected animals was assessed using a clinical score. Animals were scored in terms of general behaviour, activity, feeding habits, and weight gain or loss. Each of the criteria is assigned score points from 1 to 5 with 1 being the best and 5 the worst. The mean of the score points represents the overall score for an animal. Animals with severe symptoms (reaching a clinical score of ≥3.5) were euthanized to avoid unnecessary suffering, and the time-point was recorded as the end point of survival for that individual mouse.

Table 6: Scoring criteria for infected mice.

Score	Activity	Body weight	Body condition	Behaviour
1	Very active	No change or increase	Shiny and groomed fur; clear eyes; clean body orifices	Normal
2	Active	Reduction <10%	Fur defects (less or excessive grooming)	Slight deviation
3	Less active	Reduction 10-20%	Dull/greasy and ruffled fur, decreased grooming, body orifices not well cleaned, increased muscle tone	Unusual; impaired motor functions or hyperkinetic
4	Barely active	Reduction 20-30%	Dirty fur; sticky or damp body orifices; hunched; high muscle tone; dull eyes	Isolation from peers; lethargy; hyperkinetic; stereotypies; coordinative dysfunctions
5	Lethargic	Reduction >30%	Cramps; paralysis (trunk musculature, limbs); respiratory sounds; cold body	Vocalization of pain when grabbing; selfamputation (autoaggressive behavior)

3.4.4 Organ harvest and homogenization

Mice were euthanized by CO_2 on respective days for organ harvest. After opening the abdominal wall, the blood was taken from the inferior vena cava using a syringe and 27-G cannula and transferred to an Eppendorf tube. The blood was centrifuged at 5724 x g or 10 min and 4 °C and the serum stored at -80 °C for later analyzes. For histological examinations of the lungs, the right

upper lung lobe was removed at chosen time points from some animals and stored in 4% PFA for 24 h at 4 °C. The residual lung, mLN, salivary gland (SG) and spleen were taken and homogenized in 1 x PBS (mixture of 1.4 mm and 2.8 mm ceramic beads, Bertin Technologies; Minilys ®, Bertin Technologies). The lung, spleen and SG were homogenized twice at 1817 x g for 50 seconds, the mLN once for 50 seconds. Between step one and two, the organs were kept on ice. The homogenates were distributed for respective analyzes such as bacterial load, viral load and inflammatory mediators. Homogenates were stored at -80 °C.

3.5 Microbiological methods

3.5.1 Determination of the bacterial load

Tenfold serial dilutions ranging from 10^{-2} to 10^{-5} of the organ homogenates or cell lysates in WTA buffer were plated onto Middlebrook 7H11 agar plates supplemented with 10% v/v heat-inactivated bovine serum. The plates were incubated at 37 °C, and colonies were enumerated after 3-4 weeks.

3.5.2 Determination of the viral load

Titers of infectious virus were determined as plaque forming units (PFU) using a plaque assay on M2-10B4 cells. In this standard virological method, serial dilutions of the virus-containing samples are added to a monolayer of susceptible cells. Each infectious virus particle forms a visible area of cell destruction, known as a plaque. By counting these plaques, the number of infectious particles in the sample—the viral titer—can be calculated.

A total of 4×10^4 M2-10B4 cells were seeded per well in 400 µL of M2-10B4 medium in 48-well plates, 24 hours prior to infection. On the following day, serial dilutions of the samples were prepared in 1 mL of 3% FCS (heat-inactivated) growth medium for each sample. Organ homogenates or supernatants of infected BMDMs were titrated in duplicates, with dilutions ranging from 10^{-1} to 10^{-4}, and virus stocks (cell supernatants) in 4 independent serial dilutions with dilutions ranging from 10^{-3} to 10^{-10}. From each well, 300 µL of M2-10B4 medium were removed and 100 µL from each virus dilution was added to the respective wells. Following a 3-hour incubation period at 37 °C, 300 µL of methylcellulose were added to each well. After five to six days of incubation, plaques were counted, and the viral titer was calculated as described by Zurbach et al. (234). In addition, qPCR was used to overcome the detection limit of the Plaque Assay, allowing for the detection of low viral loads as described in 3.2.11.

3.6 Immunological methods

3.6.1 Lymphocyte depletion

Depletion of CD8α, NK1.1, and CD4 lymphocyte populations in C57BL/6 mice was achieved via intraperitoneal (i.p.) administration of anti-mouse CD8α, anti-mouse NK1.1, and anti-mouse CD4 antibodies, using a 26-G syringe. A dose of 150 µg per antibody was used, with each mouse receiving 100 µL of the antibody cocktail.

3.6.2 Flow cytometry

Flow cytometry is a technique that enables the rapid analysis of the physical and chemical characteristics of cells or particles as they flow in a fluid stream through a beam of light. It is commonly used to identify and quantify distinct cell populations based on the expression of specific markers. Successful lymphocyte depletion was confirmed by flow cytometry. A drop of blood was collected from the tail of the mouse using a 26-G syringe and transferred into an EDTA tube. After adding 50 µL of blocking buffer, the blood was resuspended and incubated at room temperature for 10 minutes. Then, 50 µL of fluorescently-coupled antibody mix was added, resuspended, and incubated in the dark for an additional 30 minutes at room temperature. The cells were diluted with 300 µL of FACS buffer and stored in aluminium foil at 4 °C until analysis on the MACSQuant® Analyzer 10 flow cytometer (MQ10). For each flow cytometry experiment, appropriate isotype controls and unstained samples were included to ensure specificity and accuracy of antibody staining.

3.6.3 Quantification of chemokines/cytokines by multiplex bead-based immunoassays

Multiplex immunoassays enable the simultaneous measurement of multiple cytokines or chemokines in a single sample. The LEGENDplex system (BioLegend) uses antibody-coated beads, enabling the detection of several target proteins at once by flow cytometry. For this study, cytokine concentrations (Mouse Inflammation panel, Biolegend) and chemokine concentrations (Mouse Proinflammatory Chemokine Panel, Biolegend) in lung homogenates were quantified by LEGENDplex™ multiplex immunoassay. Lung homogenates were centrifuged (8.000 x g, 5 min, 4 °C) and the supernatants were processed according to the manufacturer's instructions. Data acquisition was performed on a MACSQuant® Analyzer 10 (Miltenyi Biotec), and results were analyzed using LEGENDplex™ software (BioLegend).

3.6.4 TNF Quantification

TNF levels in cell supernatants were quantified using the TNF-α ELISA MAX™ kit (BioLegend), following the manufacturer's protocol. Absorbance was measured at 450 nm using a microplate

reader. TNF concentrations were calculated based on a standard curve generated from known concentrations of TNF standards.

3.7 Histopathological analyzes

3.7.1 Tissue fixation, embedding and sectioning

Embedding and processing of lung tissue were carried out by the Histology Core Unit at the Research Center Borstel under the supervision of Prof. Dr. Torsten Goldmann. Superior lung lobes from infected mice and naïve controls were fixed with 4% w/v paraformaldehyde for 24 h, embedded in paraffin, and sectioned (4 µm). Embedding, sectioning as well as Hematoxylin and Eosin staining of the sections, were performed by Christian Rosero and Jasmin Tiebach. Christian Rosero and Dr. Sebastian Marwitz conducted the multiplex immunofluorescence staining and analysis.

3.7.2 Hematoxylin and Eosin (H&E) staining

Hematoxylin and Eosin (H&E) staining was performed using a linear stainer (Tissue Stainer TST 44 C) by the Histology Core Unit. The procedure involved the following steps: Paraffin-embedded tissue sections were first deparaffinized by immersing them twice in xylene for 1 minute each. Rehydration was then carried out through a graded series of ethanol solutions: 100% ethanol for 1 minute, 96% ethanol for 1 minute, and 70% ethanol for 1 minute. This was followed by immersion in distilled water for 1 minute to complete the rehydration process. The rehydrated sections were stained with Mayer's hematoxylin solution for 3 minutes, and this step was repeated once to enhance nuclear staining, resulting in 6 minutes of hematoxylin exposure. Excess stain was removed by washing the slides in tap water for 1 minute. To achieve optimal nuclear bluing, the sections were immersed in a 1% calcium acetate solution for 1 minute, followed by another wash in tap water for 1 minute. For cytoplasmic staining, the sections were immersed in 0.2% eosin solution for 2 minutes. The slides were then dehydrated through a graded series of ethanol concentrations: 80% ethanol for 15 seconds, 96% ethanol for 30 seconds, and twice in 100% ethanol for 1 minute each. Clearing was performed by immersing the sections twice in xylene for 1 minute each. Finally, the slides were coverslipped using a suitable mounting medium for microscopic examination.

3.7.3 Multiplex-immunofluorescence (mIF) staining

Multiplex-immunofluorescence (miF) staining was performed by Christian Rosero from the Histology Core Unit. Formalin-fixed, paraffin-embedded (FFPE) samples of mouse lung tissues were deparaffinized by immersion into xylene (2 x 10 min) and rehydrated by graded series of ethanol (2 x 2 min 100%, 2 min 96%, 2 min 90%, 2 min 80%, 2 min 70%, 2 min distilled water). Rehydrated

samples were transferred to 1 x TBST (50 mM Tris, pH 7.6, 0.05% Tween-20) and subsequently forwarded to mIF staining. The Opal 3-Plex Anti-Rb Manual Detection Kit (Akoya Biosciences, Marlborough, USA, NEL840001KT) was used with additional fluorophores as indicated in 2.6. Overall, mIF staining consisted of several, subsequent cycles of IF staining targeting one antigen per time: Before antigen detection, endogenous peroxidases were blocked once by incubation for 10 min at RT in 3% H_2O_2 followed by 3 x 2 washing with 1 x TBST. One IF cycle consisted of 10 min protein blocking using antibody diluent (Akoya Biosciences, Marlborough, USA) followed by 3 x 2 min washing with 1 x TBST. Primary antibodies were diluted using antibody diluent (Akoya Biosciences, Marlborough, USA) and incubated for 45 min at RT followed by 3 x 3 min washing with 1 x TBST. Primary antibodies were detected by incubation for 10 min with HRP-Polymer (Akoya Biosciences, Marlborough, USA) and subsequent TBST washing for 3 x 3 min. Signals were visualized by OPAL-TSA reaction for 10 min at RT and stopped by washing 3 x for 3 min with 1 x TBST. An antigen-retrieval (AR) step by heating in citric acid buffer pH6 (Akoya Biosciences, Marlborough, USA) for 1 min at 1000 W followed by simmering for 10 min at 100 W was used to remove primary antibodies and HRP polymer before entering the next staining cycle. Finally, nuclei were stained using spectral DAPI (Akoya Biosciences, Marlborough, USA) and slides were mounted with cover slips using ProLong Gold (Invitrogen, Carlsbad, USA).

3.7.4 Quantitative assessment of lung lesions and associated immune cell subsets

The quantitative analysis of inflammatory area was conducted by determination of whole lung area and inflammatory area for H&E-stained sections using the software QuPath (235).

Whole-slide imaging (WSI) was performed using a PhenoImager HT multi-spectral slide scanner (Akoya Biosciences, Marlborough, USA) at 20 x magnification (0.5 µm/pixel) with exposure times held constant for all analyzed samples (DAPI: 1.1 ms, Opal 690: 30 ms, Opal 520: 35 ms, Opal 570: 43.12 ms, Opal 780: 25 ms). Phenochart software 1.1.0 (Akoya Biosciences, Marlborough, USA) was used to select regions of interest for generation of image analysis algorithms as well as batch analyzes across all tissues. For this, an analysis algorithm was built using InForm software 2.6.0 (Akoya Biosciences, Marlborough, USA) with two representative regions from each tissue. The image analysis algorithm consisted of several steps including spectral unmixing based on proprietary spectral libraries of designated fluorochromes as supplied by Akoya Biosciences, Marlborough, USA, pixel-based tissue segmentation, cell segmentation, and cell classification. Tissue segmentation was tested on randomly selected WSIs and retrained on areas where initial tissue segmentation failed to correctly identify designated areas. Representative regions from WSIs were imported into InForm software, spectrally unmixed, and forwarded to user-guided, machine-

learning tissue segmentation based on manual annotation for areas consisting either of empty glass/no tissue, B cell enriched tissue, and tissue without B cell enrichment. Once tissue segmentation reached a satisfactory level, individual cells were segmented based on their DAPI signal and accessory information from antibody staining. A cell classification algorithm was trained to identify each antigen in a binary approach (antigen positive vs negative).

Two representative regions from each WSI were forwarded to batch analysis. All resulting images were individually reviewed, and areas containing imaging artifacts (dust, fibers, tissue folds, out-of-focus regions) as well as pleura with excess autofluorescence were removed by manually drawing regions of disinterest. Samples with insufficient tissue segmentation results were excluded from downstream analyzes. Resulting cell segmentation files of 128 images from 64 WSIs were merged and consolidated into a single data file using the R package phenoptr reports 0.3.3. Phenoptr reports was further used to determine the cell density (cells/mm²) of two images/WSI for selected combinations of detected antigens across the complete tissue of each animal. The slides were analyzed in a blinded manner.

3.8 Statistics

All data were analyzed and graphs generated using GraphPad Prism 10 (GraphPad Software, La Jolla, USA). Statistical tests are indicated in the individual figure legends. An ordinary 2-way ANOVA (comparison of 3 or more groups) was performed with a Tukey's (for comparisons involving three or more groups to assess all possible pairwise differences) or Sidak's (for comparisons involving only two groups to control for multiple testing with fewer comparisons) multiple comparisons test (95 % confidence interval). The survival curve analysis was performed using the log rank (Mantel-Cox) test. Unless otherwise defined, the differences were considered significant if p-values were ≤ 0.05 and are specified and marked with stars as the following: * $p \leq 0.05$; ** $p \leq 0.01$; *** $p \leq 0.001$; **** $p \leq 0.0001$. Data is shown as means with the corresponding standard deviation (SD).

4 Results

HCMV has been implicated in TB pathogenesis, with epidemiological evidence supporting an association between HCMV and TB disease progression (178–181,236,237). To investigate the impact of CMV infection on TB disease progression, a murine coinfection model was employed using C57BL/6 mice. The following experiments aimed to assess clinical outcomes, bacterial/viral burden, and viral reactivation dynamics in the context of *Mtb* infection, with or without pre-existing MCMV infection. The results presented here provide experimental insight into the interaction between these two pathogens and its influence on host disease outcomes.

4.1 Latent MCMV modifies TB outcomes in coinfected mice following *Mtb* infection

For reference:

- *Day 14 post-Mtb corresponds to 194 days post-MCMV infection*
- *Day 150 post-Mtb corresponds to 330 days post-MCMV infection*

The C57BL/6 mouse strain is a well-established model for studying both *Mtb* and MCMV infections. Although it is susceptible to infection with virulent *Mtb*, it is considered relatively resistant due to its ability to control bacterial replication, limit lung pathology, and survive long-term following low-dose *Mtb* exposure (214). Importantly, the immune response of C57BL/6 mice to MCMV is well-characterized and closely resembles key aspects of the human immune response to HCMV, making it a valuable model for studying human infection processes (238). This mouse strain is however MCMV-resistant due to NK cell activation via the viral glycoprotein m157 (239,240). But this resistance can be prevented by using an m157-deficient MCMV mutant (Δm157 MCMV) unable to bind to the NK cell receptor Ly49H (241).

In order evaluate the impact of latent MCMV infection on the outcome of *Mtb* infection, the disease progression was examined in a murine coinfection model. Previous studies have shown that MCMV establishes latency in the lungs following mucosal infection, one important natural transmission route of CMV (242). Therefore, female C57BL/6 mice were intranasally infected with 2×10^5 plaque-forming units (PFU) of MCMV-Δm157 (Figure 5).

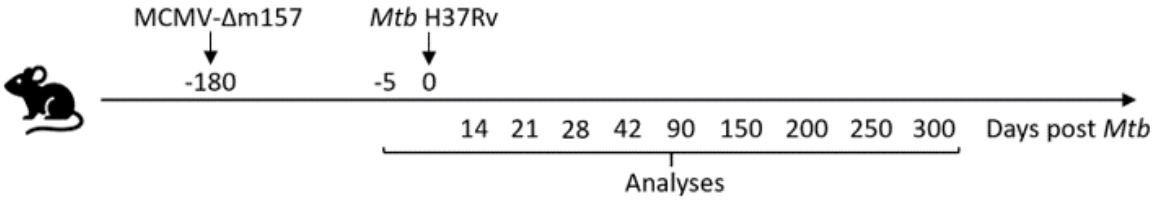

Figure 5: Timeline. C57BL/6 mice were infected i.n. with 2x10^5 PFU MCMV-Δm157 and 180 days later with a low dose of *Mtb* H37Rv.

Following infection, mice were housed in a Biosafety Level 3 (BSL-3) facility for six months to allow the establishment of latent MCMV infection, characterized by the absence of detectable replicating virus in multiple tissues while the viral genome persists in certain cell types, such as monocytes or endothelial cells (243). During this phase, viral gene expression is highly restricted, with only a few transcripts detectable, and reactivation typically requires specific triggers such as cytokine signalling or cellular differentiation (244). Six months post infection, viral genome loads were quantified in the lungs and salivary glands using qPCR (Figure 6). Viral genomes were detected in the majority of samples 175 days after MCMV infection, in the lung and in the salivary gland, which is the primary site of MCMV latency (219). For comparison, Oduro et al. reported a median of approximately 12,000 viral genomes per 10^6 cells six months after intranasal MCMV infection in a mouse strain with higher susceptibility to MCMV than C57BL/6 mice (242). In the current study, the median viral load was lower under similar experimental conditions. Some samples remained below the quantification limit, indicating that the viral burden in these samples was too low to be reliably detected and quantified; these samples are therefore considered as not detectable.

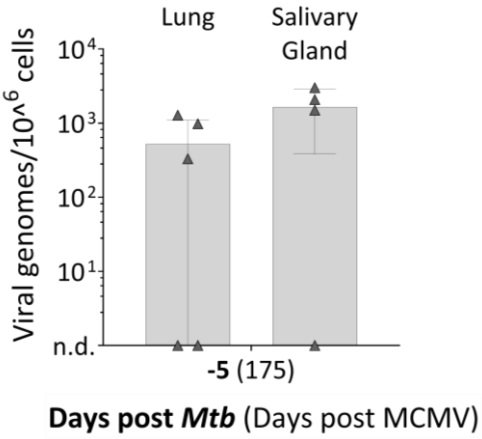

Figure 6: Quantification of viral genomes by qPCR in lung and salivary gland tissue. Organs were collected 5 days before *Mtb* coinfection. Viral genome levels were normalized to β-actin. The qPCR limit of detection was defined as 10 genome copies per 10^6 cells. Data represent pooled results from two independent experiments (n=4–5; n.d. = not detectable). Values are presented as mean ± SD. Each data point corresponds to an individual mouse. Statistical significance was assessed using an unpaired t-test. No statistically significant differences were detected ($p > 0.05$).

Next, mice were coinfected with a low dose of *Mtb* H37Rv via the aerosol route (Figure 5) and monitored in order to assess disease progression in the presence and absence of latent MCMV infection. Clinical scores started to rise in all three groups 150 days after *Mtb* infection (Figure 7A). Mice infected with MCMV alone exhibited minimal symptoms throughout the observation period, maintaining consistently low clinical scores. Unexpectedly, the clinical score was highest in the group of mice infected with *Mtb* alone and significantly lower in the presence of MCMV. Consequently, 4 out of 10 *Mtb*-only infected mice reached the defined humane endpoint and were euthanized, compared to only 1 out of 10 coinfected mice (Figure 7B), suggesting that latent MCMV infection mitigates disease progression. The health status of the animals and their euthanasia were conducted in accordance with the criteria established by the state of Schleswig-Holstein and Ministry for Energy Transition, Agriculture, Environment, Nature, and Digitalization. Mice with a total score of ≥3.5 were classified as experiencing severe suffering, promptly removed from the experiment, and euthanized in compliance with animal welfare regulations, limiting severe suffering to a maximum of 1 day.

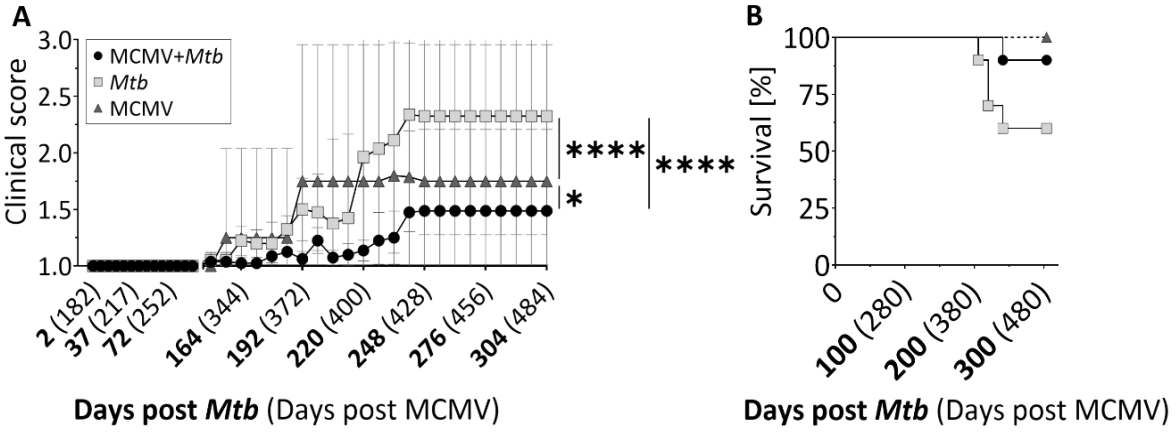

Figure 7: Latent MCMV infection modulates disease progression and survival in coinfected mice. (A) Clinical scores and (B) survival rates were monitored until day 304 post-*Mtb* infection. Data represent results from one experiment (n=7–10). Values are presented as mean ± SD. Each data point corresponds to an individual mouse. Statistical significance was assessed using (A) two-way ANOVA with Tukey's multiple comparison test and (B) the log-rank (Mantel-Cox) test. Significance levels: *p ≤ 0.05, ****p ≤ 0.0001. No statistically significant differences were detected in (B) (p > 0.05).

To determine whether the improved condition of coinfected mice was associated with enhanced bacterial control, organs of interest were collected at defined time points throughout the observation period to assess *Mtb* burden. However, bacterial loads in the lungs, mediastinal lymph nodes and spleen were comparable between *Mtb*-only and coinfected mice (Figure 8A-C), indicating that the observed differences in disease outcome were independent of bacterial replication control.

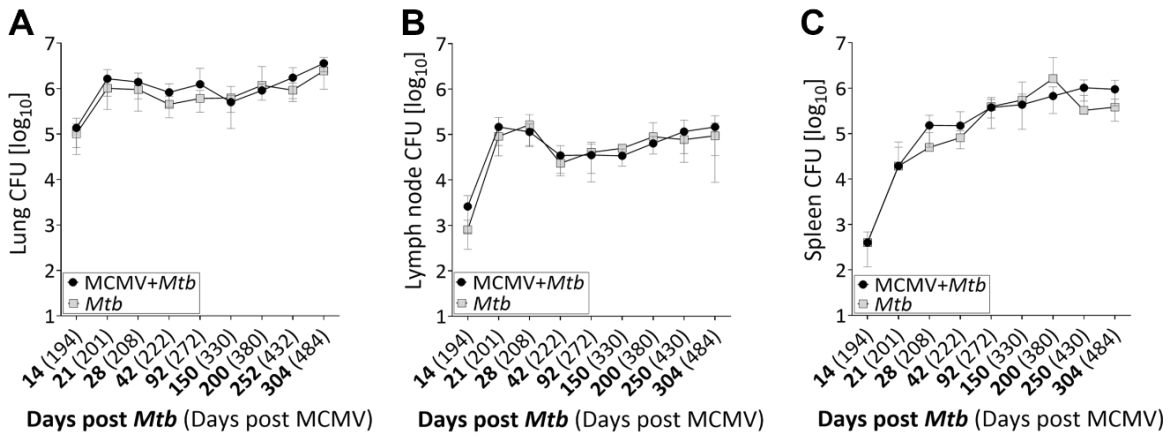

Figure 8: Bacterial burden (CFU) in *Mtb*-infected mice with and without latent MCMV infection. At the indicated time points, bacterial burden in (A) the lung, (B) lymph node, and (C) spleen was determined. Data represent pooled results from two independent experiments (n=6–9). Values are presented as mean ± SD. Each data point corresponds to the mean value of all mice in the respective group at each time point. Statistical significance was assessed using (A-C) two-way ANOVA followed by Sidak's multiple comparison test. No statistically significant differences were detected in (A-C) ($p > 0.05$).

As the lung is not only a reservoir of latent MCMV infection but also a site of virus reactivation (245) it was investigated whether reactivation was triggered by *Mtb* coinfection. To analyze this, viral genome levels were quantified in the lungs 14 days after *Mtb* infection (Figure 9A). The analysis showed that viral genome loads remained stable before and after *Mtb* infection, with some samples even falling below the detection limit. These findings indicate that under these conditions, *Mtb* infection does not induce MCMV reactivation.

To confirm that MCMV reactivation is generally possible in this model, lymphocyte depletion was carried out in a selected group of latently MCMV-infected mice - an established protocol to induce immunosuppression in mice, known to reactivate latent MCMV. $CD4^+$ and $CD8^+$ T cells, as well as NK cells, were depleted using a single dose of specific antibodies, as described by Brizić et al., 2018 (246). Lymphocyte depletion was confirmed 48 hours after depletion via flow cytometry using blood collected from the tail veins of naïve and depleted mice (Figure 9B).

In contrast, to evaluate whether immunosuppression triggered viral reactivation, MCMV genome loads in the lungs were quantified 14 days after lymphocyte depletion (Figure 9A). The results imply a potential increase in viral genome levels in lymphocyte-depleted mice compared to untreated controls, suggesting that lymphocyte depletion may facilitate conditions conducive to MCMV reactivation in this model. While statistical significance was not reached, the observed trend highlights the need for further investigations to better understand the mechanisms underlying MCMV reactivation.

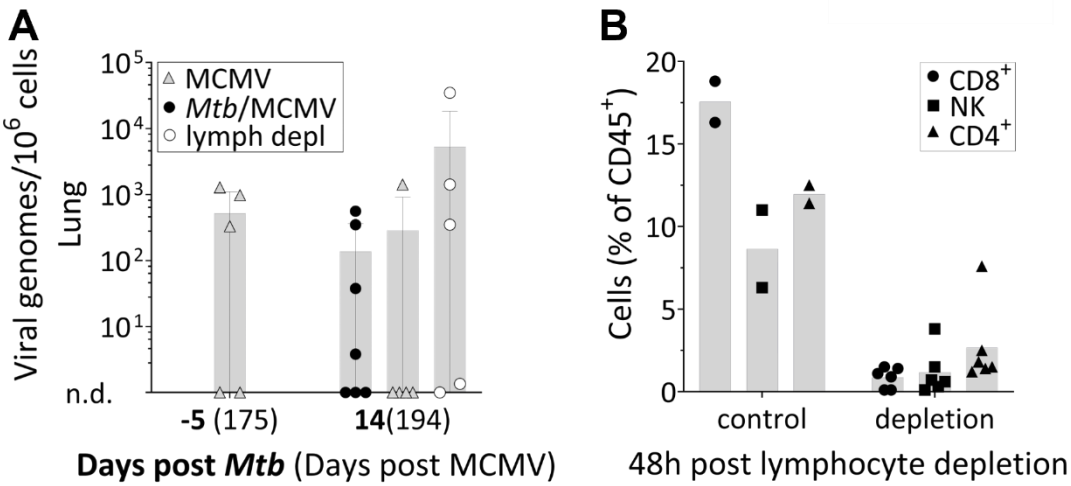

Figure 9: Viral genomes in the lungs of MCMV-infected mice following *Mtb* coinfection or lymphocyte depletion. (A) Quantification of NK^+, $CD4^+$, and $CD8^+$ cells after lymphocyte depletion by flow cytometry. (B) Quantification of viral genomes by qPCR in lung tissue collected 14 days post-*Mtb* infection or 14 days post-lymphocyte depletion. Viral genome levels were normalized to β-actin. The qPCR limit of detection was defined as 10 genome copies per 10^6 cells. Data represent pooled results from two independent experiments (n=4–7; n.d. = not detectable). Values are presented as mean ± SD. Each data point corresponds to an individual mouse. Statistical significance (A) was assessed using Mann-Whitney test. No statistically significant differences were detected in (A) ($p > 0.05$).

Together, these data suggest, contrary to the initial hypothesis, that latent MCMV infection exerts a beneficial effect in coinfected animals, which displayed improved disease outcomes compared to those infected with *Mtb* alone.

4.1 Summary of key findings:

- In this coinfection model, mice latently infected with MCMV before *Mtb* infection showed lower clinical scores and improved survival compared to *Mtb*-only infected mice.
- MCMV coinfection ameliorated disease severity but did not affect *Mtb* bacterial loads in the lungs, lymph nodes or spleen.
- *Mtb* infection did not trigger MCMV reactivation.

4.2 Coinfected animals exhibit elevated levels of inflammatory cytokines and chemokines in the lungs

For reference:

- *Day 21 post-Mtb corresponds to 194 days post-MCMV infection*
- *Day 150 post-Mtb corresponds to 330 days post-MCMV infection*
- *Day 252 post-Mtb corresponds to 432 days post-MCMV infection*

The data presented suggest that the increased disease tolerance observed in coinfected animals, compared to those infected with *Mtb* alone, cannot be attributed to better pathogen control. To investigate potential alterations in the inflammatory environment in coinfected and singly infected mice, the levels of inflammatory cytokines and chemokines known to play a role in *Mtb* infection were quantified using a multiplex immunoassay. For this analysis, lung homogenates from infected animals from three representative time points were used: early day 21 post-*Mtb* represents the time were adaptive immunity to *Mtb* is usually established, mid-infection day 150 post-*Mtb* is shortly before clinical scores increased, and late day 252 post-*Mtb* is the time point when differences in clinical scores were most apparent. This approach allowed a comprehensive assessment of cytokine and chemokine dynamics over the course of infection.

The heat maps in Figure 10 provide an overview of cytokine levels measured in lung homogenates at various time points post *Mtb* infection and corresponding days post MCMV infection. Among the cytokines measured, IL-1α exhibited the highest expression levels in both coinfected and *Mtb*-only infected animals, while its levels remained low in MCMV-only infected mice at all measured time points (Figure 10A-C).

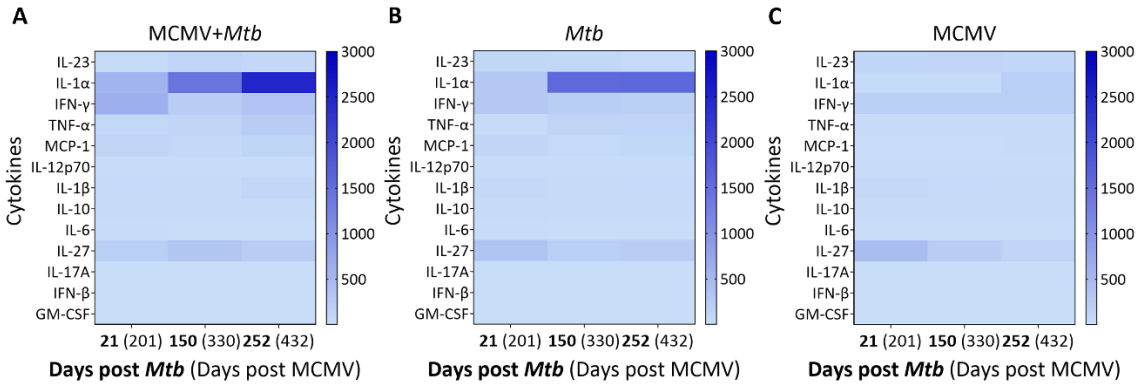

Figure 10: Overview of cytokine levels measured in lung tissue at different time points post *Mtb* coinfection. Heat maps of cytokine levels in lung homogenates from (A) coinfected, (B) *Mtb*-infected or (C) MCMV-infected mice, showing the mean concentration for each cytokine. Data represent pooled results from two independent experiments (n=6–7). Cytokine concentrations are presented in pg/mL, with color intensity reflecting cytokine levels (scale: 0–3000 pg/mL).

A closer examination of the heat maps revealed that, in addition to IL-1α, other cytokines also displayed notable differences between coinfected and singly infected mice. Similar to IL-1α, IL-1β and TNF concentrations progressively increased throughout the infection period, reaching significantly higher levels in coinfected mice at day 252 post-*Mtb* infection (Figure 11A-C), which coincided with the time point when differences in clinical scores between groups were most pronounced (Figure 7A). This difference was particularly evident for IL-1α, which demonstrated the highest concentration in the coinfected group (Figure 11A).

In contrast, IFN-γ expression followed a temporal pattern that diverged from the other cytokines analyzed (Figure 11D). IFN-γ demonstrated an early peak at day 21 post-*Mtb* infection, with approximately 2-fold higher concentrations in coinfected animals compared to *Mtb*-only infected mice. In contrast, the IFN-γ levels in MCMV-only infected animals remained near the detection limit across all examined time points, showing no significant increase in expression.
IFN-γ levels declined markedly in coinfected and *Mtb*-only infected mice by day 150 post-*Mtb* infection and remained low through day 252, with minimal differences between experimental groups at these later time points. This observation suggests that while MCMV infection alone was insufficient to induce substantial proinflammatory cytokine responses in the lung, it significantly enhanced *Mtb*-mediated inflammatory reactions when present as a coinfection.

IL-27 and IL-23, cytokines linked to long-term *Mtb* control and B cell follicle formation, exhibited similar expression patterns across experimental groups (Figure 11E, F). At day 21 post-*Mtb* infection, both cytokines were significantly lower in coinfected mice compared to MCMV-only infected animals, while showing comparable levels to *Mtb*-only infected mice at this early time point. Over time, IL-23 and IL-27 levels increased in coinfected mice, peaking at day 150 post-*Mtb* infection, with IL-23 being significantly higher compared to *Mtb*-only infected mice (Figure 11F). This divergence between coinfected and *Mtb*-only groups was particularly pronounced for IL-23, suggesting a potential synergistic effect of dual infection on this cytokine's expression at the intermediate phase. By day 252 post-*Mtb* infection, while no significant differences were observed between groups, IL-23 levels remained highest in coinfected and MCMV-only infected mice compared to the *Mtb*-only group, which displayed a decrease in IL-23 expression during this late phase of infection. The remaining cytokines exhibited comparable levels across all groups and time points and are thus not shown individually.

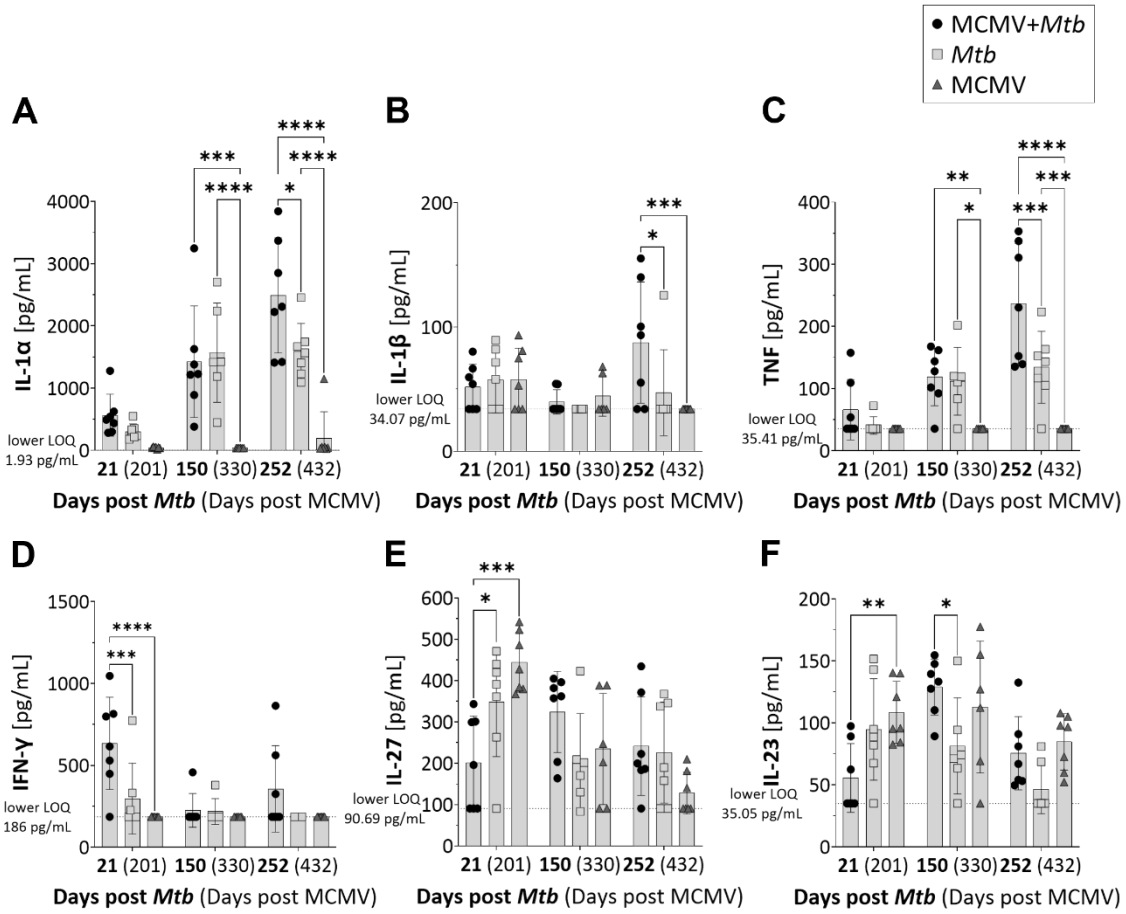

Figure 11: Altered pulmonary cytokine responses in coinfected mice. Concentration of selected cytokines (A-F) at representative time points. Data represent pooled results from two independent experiments (n=6–7; LOQ = Limit of Quantification). Values are presented as mean ± SD. Each data point corresponds to an individual mouse. Statistical significance was assessed using (A-F) two-way ANOVA followed by Tukey's multiple-comparison test. Significance levels: *p ≤ 0.05; **p ≤ 0.01; ***p ≤ 0.001; ****p ≤ 0.0001.

In addition to cytokines, several chemokines were upregulated in both singly and coinfected animals. Upon initial examination of the heatmaps summarizing the chemokine expression profiles in *Mtb*-only and coinfected mice (Figure 12A, B), it becomes evident that there is no discernible difference in the chemokine expression patterns between coinfected animals and those infected with *Mtb* alone, despite the presence of concurrent viral infection in the former group. The heatmap representing MCMV-only infected animals exhibits less chemokine induction compared to *Mtb*-infected mice across all measured time points, suggesting a limited inflammatory response to MCMV infection in this experimental model (Figure 12C).

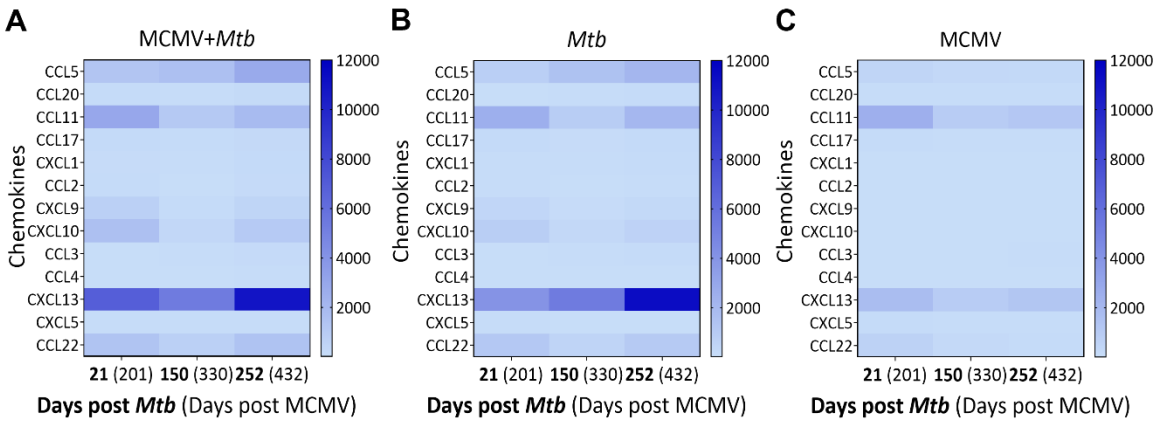

Figure 12: Overview of chemokine levels measured in lung tissue at different time points post-*Mtb* coinfection. Heat maps of chemokine levels in lung homogenates from (A) coinfected, (B) *Mtb*-infected or (C) MCMV-infected mice, showing the mean concentration for each chemokine. Data represent pooled results from two independent experiments (n=6–7). Chemokine concentrations are presented in pg/mL, with color intensity reflecting chemokine levels (scale: 0–12000 pg/mL).

However, closer examination of individual chemokines revealed that CXCL9, CXCL10, and CCL2 were significantly higher in coinfected mice as early as day 21 post-*Mtb* infection, whereas their levels were lower in MCMV-only infected mice (Figure 13A-C). During the mid-infection phase (day 150 post-*Mtb*), CXCL9, CXCL10 and CCL2 levels (Figure 13A-C) were comparable between co- and *Mtb*-only infected animals, while their levels in MCMV-only infected mice remained below the detection limit. In the late infection phase (day 252 post-*Mtb*), CXCL9, CXCL10, and CCL2 concentrations rose again in both *Mtb*-only and coinfected mice, with significantly higher levels observed in the latter. This biphasic pattern, with enhanced chemokine expression in coinfected animals at both early and late time points but not during the intermediate phase, suggests a temporal regulation of chemokine responses in the context of MCMV and *Mtb* coinfection.

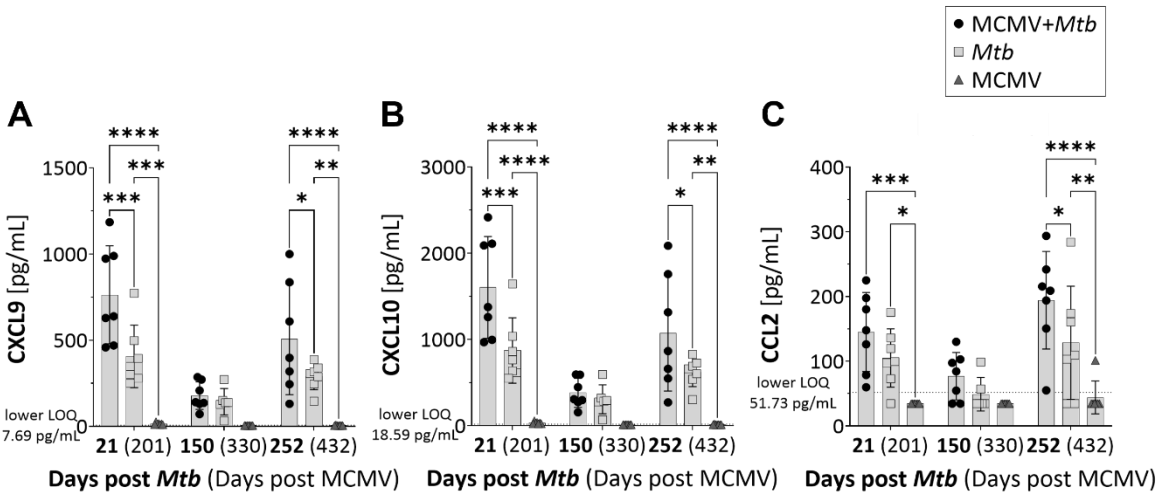

Figure 13: Altered pulmonary chemokine responses in coinfected mice. Concentration of (A) CXCL9, (B) CXCL10 and (C) CCL2 at representative time points. Data represent pooled results from two independent experiments (n=6–7; LOQ = Limit of Quantification). Values are presented as mean ± SD. Each data point corresponds to an individual mouse. Statistical significance was assessed (A-C) using two-way ANOVA followed by Tukey's multiple-comparison test. Significance levels: *p ≤ 0.05; **p ≤ 0.01; ***p ≤ 0.001; ****p ≤ 0.0001.

The remaining chemokines exhibited comparable levels across all groups and time points and are thus not shown individually. Overall, these findings reveal discernible variations in cytokine and chemokine profiles in the lungs of coinfected mice, especially during the early and late phases of infection. These immune signatures are associated with improved clinical outcomes, suggesting a potential mechanistic link between the inflammatory milieu and enhanced disease tolerance in coinfected animals.

4.2 Summary of key findings:

- Pulmonary levels of IL-1α, IL-1β, and TNF increased over time, peaking in coinfected mice during late-stage infection, whereas IFN-γ levels were highest in coinfected mice early in the course of infection.
- IL-27 and IL-23 were significantly reduced in coinfected compared to MCMV-infected mice on day 21 but increased in coinfected lungs over time.
- CXCL9, CXCL10, and CCL2 were significantly elevated in coinfected mice, particularly during early and late infection, but remained low in MCMV-only infected mice.

4.3 Histopathological changes in lung tissue in the presence and absence of latent MCMV

For reference:

- *Day 150 post-Mtb corresponds to 330 days post-MCMV infection*
- *Day 252 post-Mtb corresponds to 432 days post-MCMV infection*

In order to investigate if the differences observed in the inflammatory response are reflected in lung pathology, one lung lobe from each mouse per group - *Mtb*-only, MCMV-only, and coinfected mice - was processed for histological analysis. Overall tissue pathology was assessed using Hematoxylin & Eosin (H&E) staining, a standard method for visualizing tissue architecture, cellular composition, and inflammatory infiltrates. This technique allows for the identification of structural alterations, such as immune cell infiltration and tissue damage, which are crucial for evaluating infection-induced pathology. Histopathological examination of lung tissue was performed at day 150 and day 252 post-*Mtb* infection, corresponding to mid- and late-infection stages.

Histopathological imaging provides an initial overview of tissue architecture and allows for the identification of structural changes. In this study, visual examination of the histological sections (Figure 14) revealed differences between the experimental groups. At day 150 post-*Mtb* infection, the lungs of coinfected mice displayed granulomatous lesions with irregular borders and a diffuse pattern of inflammation throughout the lung parenchyma (Figure 14, d150 post-*Mtb*). These lesions coalesced in certain areas, forming extensive consolidated regions. In contrast, *Mtb*-only infected mice exhibited more distinct, circumscribed granulomatous lesions that were fewer in number but showed more intense violet-blue staining, indicative of dense lymphocyte and macrophage infiltration (Figure 14, d150 post-*Mtb*).

By day 252 post-*Mtb* infection, both *Mtb*-only and coinfected lungs exhibited progressive pathology with larger granulomatous lesions (Figure 14, d252 post-*Mtb*). In coinfected mice, dark-blue regions—characterized by intense hematoxylin staining and indicative of high nuclear density—were more prominent within granulomas compared to day 150 post-*Mtb* infection. These areas may reflect dense accumulations of cells, such as lymphocyte infiltrates or lymphoid tissues, including germinal centers.

MCMV-only infected lungs exhibited minimal pathological changes at mid-infection day 150 post-*Mtb* infection, revealing smaller areas of inflammatory infiltration compared to *Mtb*-infected lungs (Figure 14, d150 post-*Mtb*). However, by day 252 post-*Mtb*, larger areas of consolidation became apparent in MCMV-only infected lungs, with mild violet staining indicative of low lymphocyte

infiltration primarily located in perivascular and peribronchiolar regions (Figure 14, d252 post-*Mtb*). This pathology was distinct from the granulomatous lesions observed in *Mtb*-infected lungs.

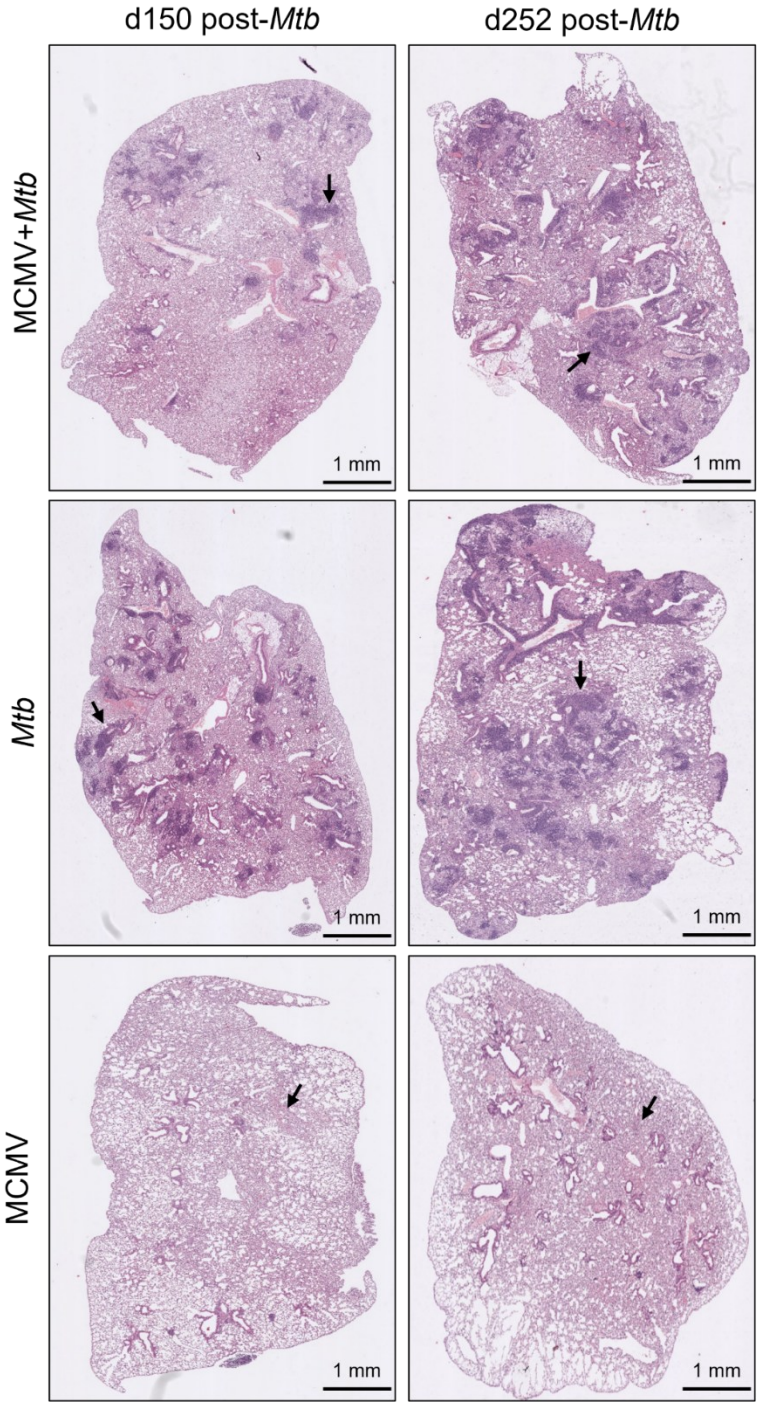

Figure 14: HE-stained lung sections reveal tissue pathology in MCMV-*Mtb* coinfection. Lungs were collected at day 150 and day 252 post-*Mtb* infection, PFA-fixed and paraffin embedded. Tissue sections were stained with H&E. Representative micrographs from lungs of one mouse per group are shown. Group sizes were as follows: day 150 –MCMV+*Mtb* n=7, *Mtb*-only n=6, MCMV-only n=6; day 252 – MCMV+*Mtb* n=7, *Mtb*-only n=7, MCMV-only n=7. Scale bar = 1 mm. Black arrows indicate granulomatous lesions as an exemplary pathological feature.

Quantification of the inflammatory area in lungs of singly and coinfected mice provides an objective complement to the histological observations. Although differences in the proportion of affected lung tissue between *Mtb*-only and coinfected groups were not statistically significant at either time point examined, the visual trends observed warranted further investigation (Figure 15).

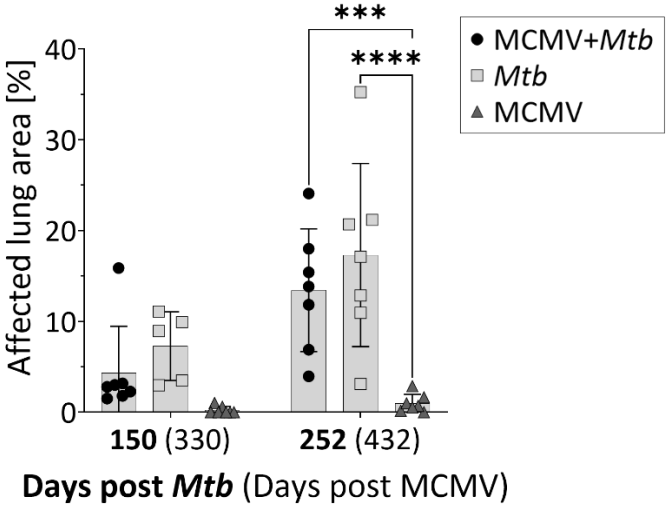

Figure 15: Quantification of inflammatory areas in singly and coinfected lungs. Quantitative analysis of inflammatory areas in lung tissue sections after H&E staining, as shown in Fig.14, was performed using QuPath. Data represent results from one experiment (n=5–7). Values are presented as mean ± SD. Each data point corresponds to an individual mouse. Statistical significance was assessed using two-way ANOVA followed by Tukey's multiple-comparison test: ***p ≤ 0.001; ****p ≤ 0.0001.

To better understand these differences observed between groups and to identify immune cell populations involved in the inflammatory response and disease progression during *Mtb* infection (195,247,248), multiplex immunohistochemistry (mIF) for the detection of $CD19^+$ B cells, $CD3^+$ T cells, and $CD68^+$ monocytes/macrophages was performed (Figure 16). This approach allowed a more closely examination of immune cell infiltrates within the inflammatory regions identified by H&E staining. Visual evaluation of mIF-stained sections revealed different immune cell infiltration among *Mtb*-only, coinfected, and MCMV-only infected mice at both days 150 and 252 post-*Mtb* infection. In the *Mtb*-infected lungs (Figure 16, d150 post-*Mtb*, middle column), well-defined cellular aggregates are visible, characterized by a high density of $CD19^+$ B cells (blue), which form organized structures, particularly pronounced at day 150 post-*Mtb*. In contrast, the coinfected lungs (Figure 16, d150 post-*Mtb*, left column) exhibit a diffuse immune cell distribution with less distinct aggregates and reduced B cell abundance. By day 252 post-*Mtb*, both *Mtb*-infected groups show expanded areas of immune cell infiltration; however, the *Mtb*-only group (Figure 16, d252 post-*Mtb*, middle column), retains more organized granulomas with a higher presence of B cells (blue) and $CD3^+$ T cells (magenta), while the coinfected group (Figure 16, d252 post-*Mtb*, left

column), demonstrates an increased abundance of $CD68^+$ macrophages/monocytes (green). In MCMV-only infected mice, were, compared to *Mtb*-infected lungs, only few immune cell infiltrates detectable at either time point, with minimal or no visible aggregates of $CD19^+$ B cells, $CD3^+$ T cells, or $CD68^+$ macrophages/monocytes observed in the lung sections (Figure 16, right column).

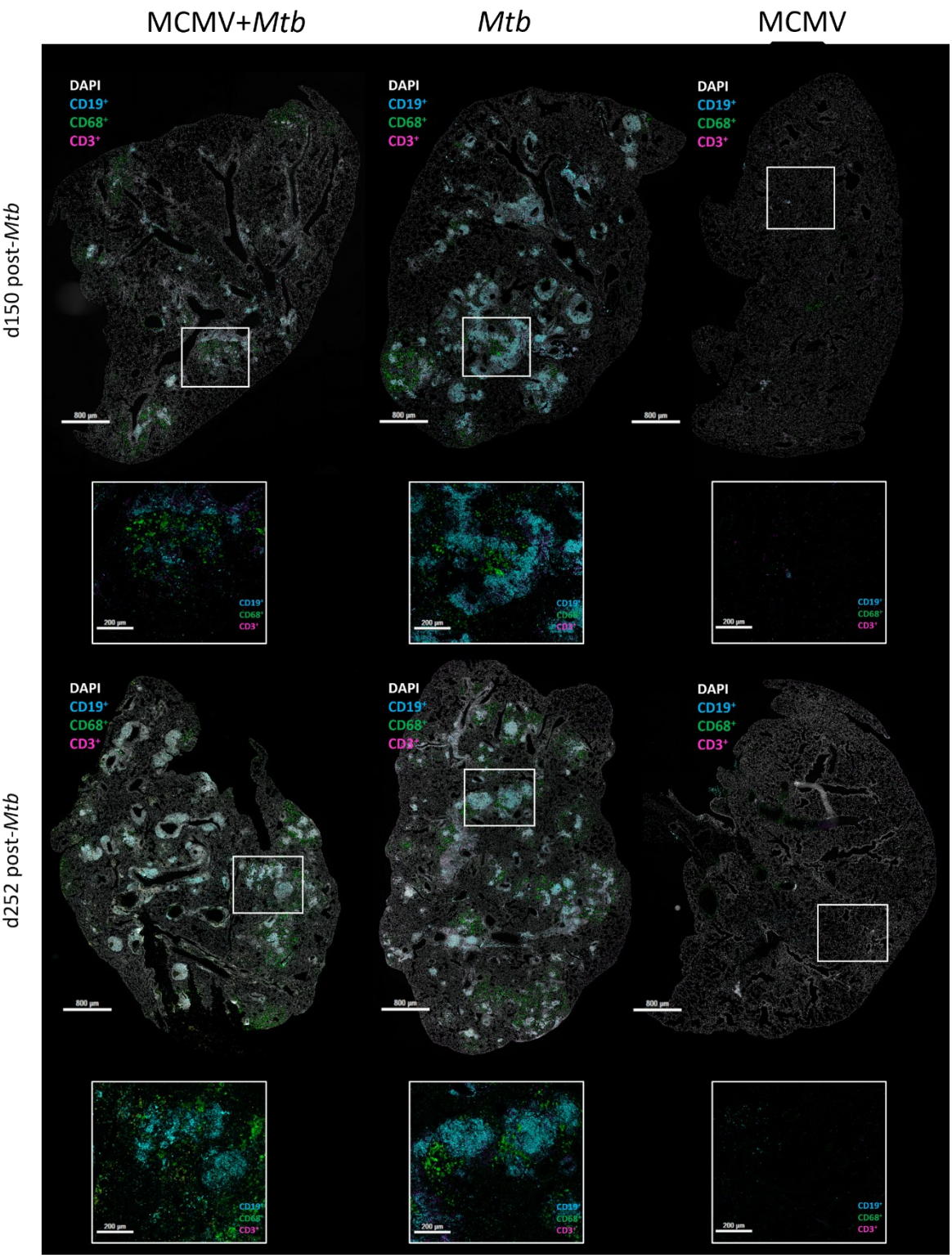

Figure 16: MCMV coinfection modulates the spatial distribution of immune cell populations within the *Mtb*-infected lung. Lungs were collected at day 150 and day 252 post *Mtb* infection, PFA-fixed and paraffin embedded. Representative micrographs from lungs of one mouse per group are shown. Group sizes were as follows: day 150 –MCMV+*Mtb* n=7, *Mtb*-only n=6, MCMV-only n=6; day 252 –MCMV+*Mtb* n=7, *Mtb*-only n=7, MCMV-only n=7., stained with antibodies to detect B cells ($CD19^+$), T cells ($CD3^+$), and macrophages ($CD68^+$); Bar = 800 µm; micrographs in detail bar = 200 µm.

Quantification of CD19⁺ B cells, CD3⁺ T cells and CD68⁺ macrophages per mm² lung area confirmed these visual observations, revealing a high density of CD19⁺ B cells during the mid and late phases of *Mtb* infection (days 150 and 252 post-*Mtb*), which was reduced in coinfected mice and reached statistical significance at day 150 post-*Mtb* (Figure 17A). Similarly, the density of CD3⁺ T cells was highest in the lungs of *Mtb*-only infected mice, particularly on day 252 post-*Mtb* infection (Figure 17B). In contrast, no significant differences were observed in the density of CD68⁺ macrophages between the two groups, although there was a trend towards higher numbers of CD68⁺ macrophages in coinfected mice at day 252 post-*Mtb* (Figure 17C). This trend is reflected in a significantly higher CD68⁺ macrophage to CD3⁺ T cell-ratio in the lungs of coinfected mice (Figure 17D). This is consistent with findings of increased production of the monocyte-attracting chemokine CCL2 in coinfected mice (Figure 13C). This also aligns with the elevated levels of IL-1α, IL-1β, and TNF, produced by multiple myeloid cell populations including CD68⁺ inflammatory monocytes and macrophages (Figure 11A-C).

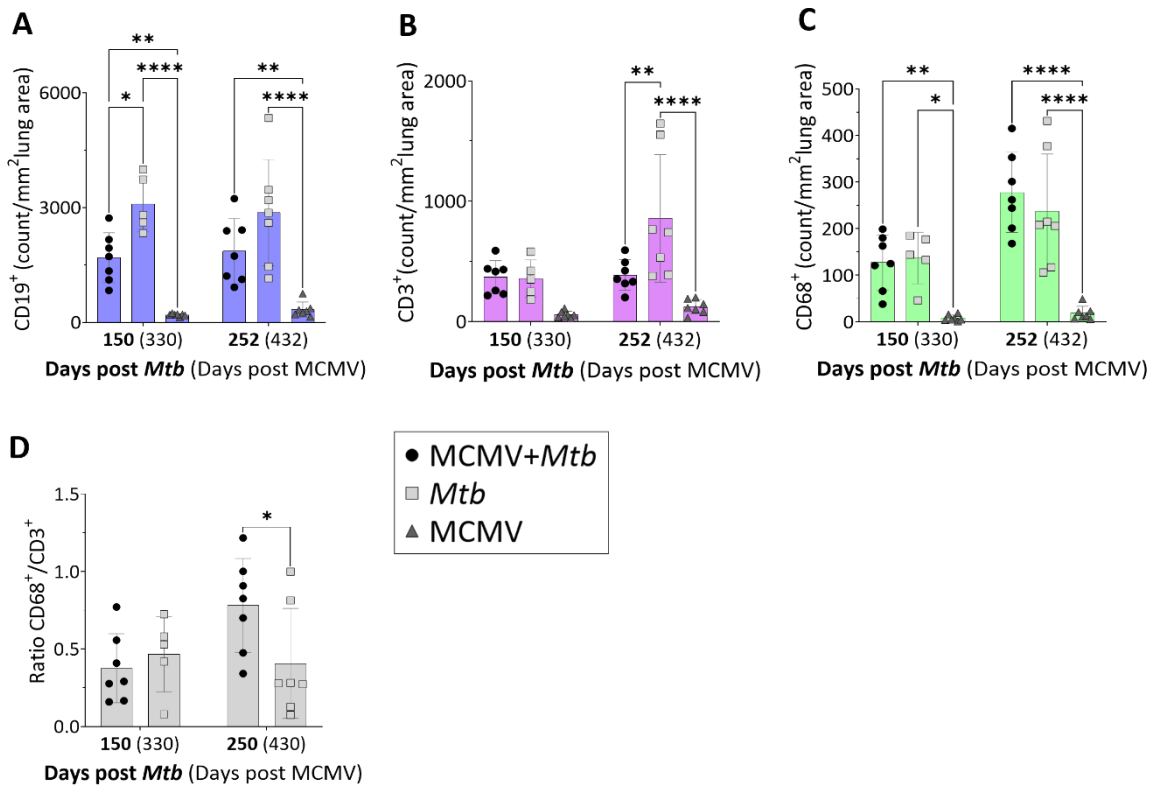

Figure 17: Quantitative analysis of immune cell densities in singly and coinfected mice. (A-C) Quantification is based on the mean of two images/Whole-Slide Image as shown in Figure 16. The bar colors correspond to the fluorescent labels for each cell population in the mIF images—blue for CD19⁺ B cells, magenta for CD3⁺ T cells, and green for CD68⁺ macrophages/monocytes—to facilitate direct comparison between the quantitative analysis and the visualized immune cell distributions. (D) Ratio of CD68⁺ macrophages to CD3⁺ T cells. Data represent results from one experiment (n=5–7). Values are presented as mean ± SD. Each data point corresponds to an individual mouse. Statistical significance

was assessed using (A-C) two-way ANOVA followed by Tukey's multiple-comparison test and (D) Pearson correlation with simple linear regression. Significance levels: *p ≤ 0.05; **p ≤ 0.01; ****p ≤ 0.0001.

Additionally, analysis of mpt64-positive CD68$^+$ monocytes/macrophages was conducted, as mpt64 is a secreted virulence-associated antigen of *Mtb* and serves as an established marker for actively *Mtb*-infected cells (249,250). Quantification of CD68$^+$mpt64$^+$ cells at days 150 and 252 post-*Mtb* infection demonstrated that, while cell numbers were low and comparable across all groups at day 150 post-*Mtb*, there was a marked increase in the number of these cells in the coinfected group at day 252 post-*Mtb* (Figure 18). At this later time point, coinfected mice exhibited significantly higher counts of CD68$^+$mpt64$^+$ cells compared to both the *Mtb*-only and MCMV-only groups. No significant differences were observed between the *Mtb*-only and MCMV-only groups at either time point. This difference was also visually evident in the stained lung sections (Figure 19).

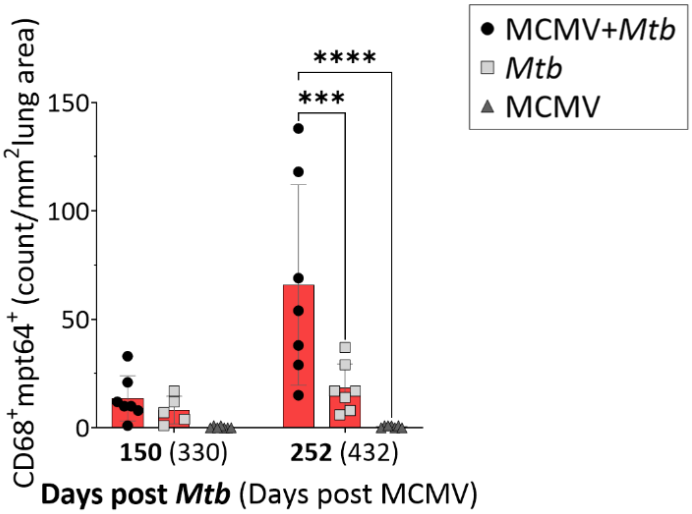

Figure 18: Quantitative analysis of CD68$^+$mpt64$^+$ macrophage/monocyte density in coinfected and *Mtb*-only infected mice. Quantitative analysis of CD68$^+$mpt64$^+$cells is based on the mean of two images/Whole-Slide Image as shown in Figure 19. The bar color corresponds to the fluorescent label for mpt64$^+$ CD68$^+$ macrophages/monocytes in the mIF images to facilitate direct comparison between the quantitative analysis and the visualized immune cell distributions. Data represent results from one experiment (n=5–7). Values are presented as mean ± SD. Each data point corresponds to an individual mouse. Statistical significance was assessed using two-way ANOVA followed by Tukey's multiple-comparison test. Significance levels: p ≤ 0.001 ***; ****p ≤ 0.0001.

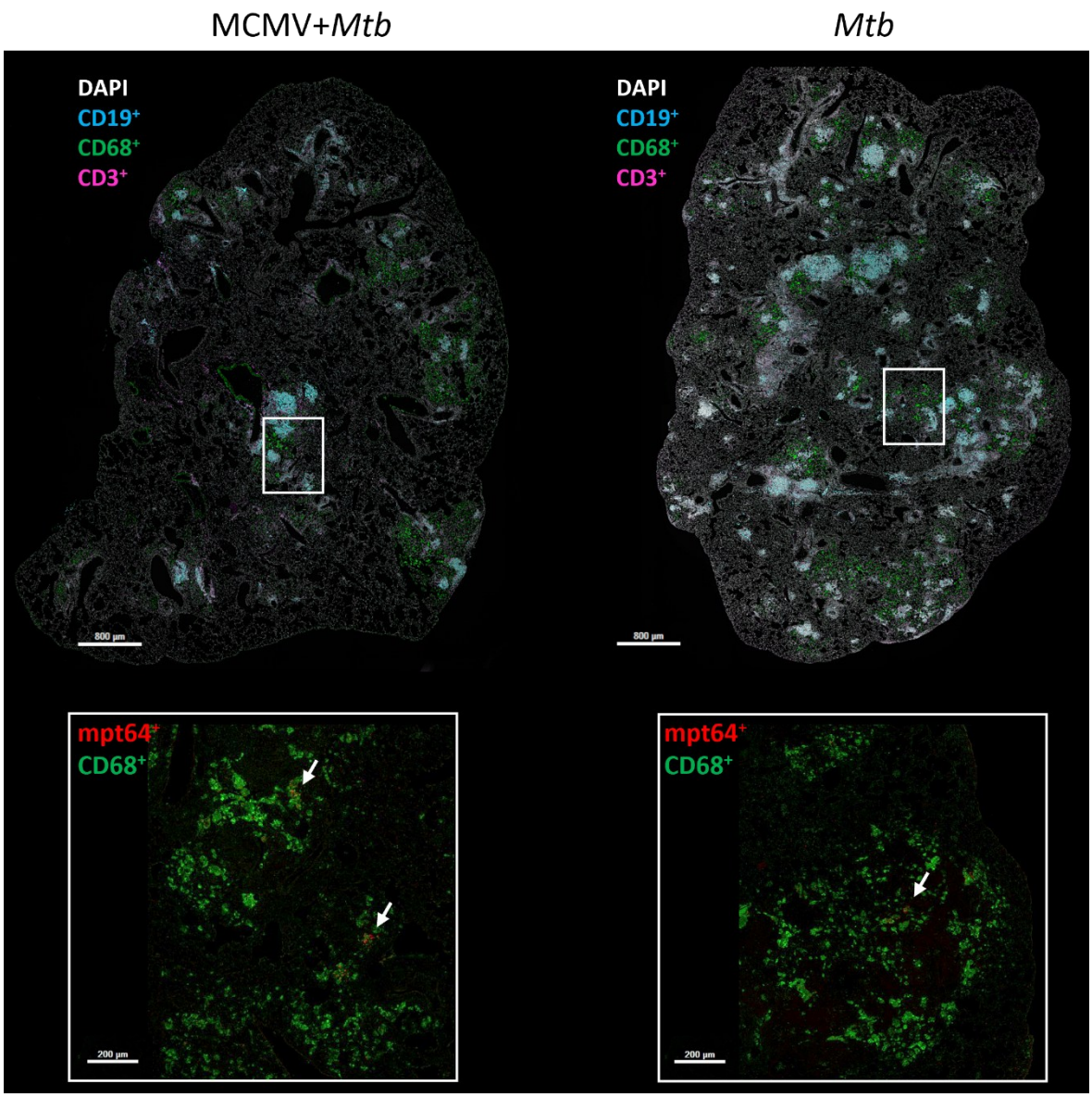

Figure 19: Immunohistochemical detection of mpt64 in lung sections. Lungs were collected at day 252 days post *Mtb* infection (432 days post MCMV), PFA-fixed and paraffin embedded. Representative micrographs from lungs of one mouse per group are shown (out of n=7), stained with antibodies to detect mpt64$^+$ macrophages (CD68$^+$); Bar = 800 µm; micrographs in detail bar = 200 µm. White arrows indicate mpt64 as an exemplary pathological feature.

Overall, histological characterization of murine lungs revealed that MCMV coinfection alters the lung pathology during TB, with coinfected animals showing reduced B and T cell infiltration, and a higher macrophage-to-T cell ratio compared to *Mtb*-only infected mice.

4.3 Summary of key findings:

- Histological analysis revealed differences in immune cell infiltration between coinfected and singly infected mice.
- *Mtb*-only infected mice exhibited significantly higher levels of $CD19^+$ B cells during the mid and late infection phases, alongside increased $CD3^+$ T cell levels, particularly at day 252.
- Coinfected mice demonstrated a higher proportion of $CD68^+$ macrophages compared to singly infected mice, reflected by a significantly elevated ratio of $CD68^+/CD3^+$ cells at the late stage of infection.
- Coinfection was associated with increased detection of mpt64 antigen at the late stage of infection.

4.4 Impact of MCMV and *Mtb* coinfection on macrophage function

For reference:

- *2 hours post-Mtb corresponds to 26 hours post-MCMV infection*
- *24 hours post-Mtb corresponds to 48 hours post-MCMV infection*
- *48 hours post-Mtb corresponds to 72 hours post-MCMV infection*

To investigate how MCMV coinfection affects macrophage responses to *Mtb*, bone marrow-derived macrophages (BMDMs) from female C57BL/6 mice were infected with MCMV-Δm157 (MOI 1), followed by *Mtb* H37Rv (MOI 0.3) 24 hours later (Figure 20). The effects described below were consistently observed across two independent experiments.

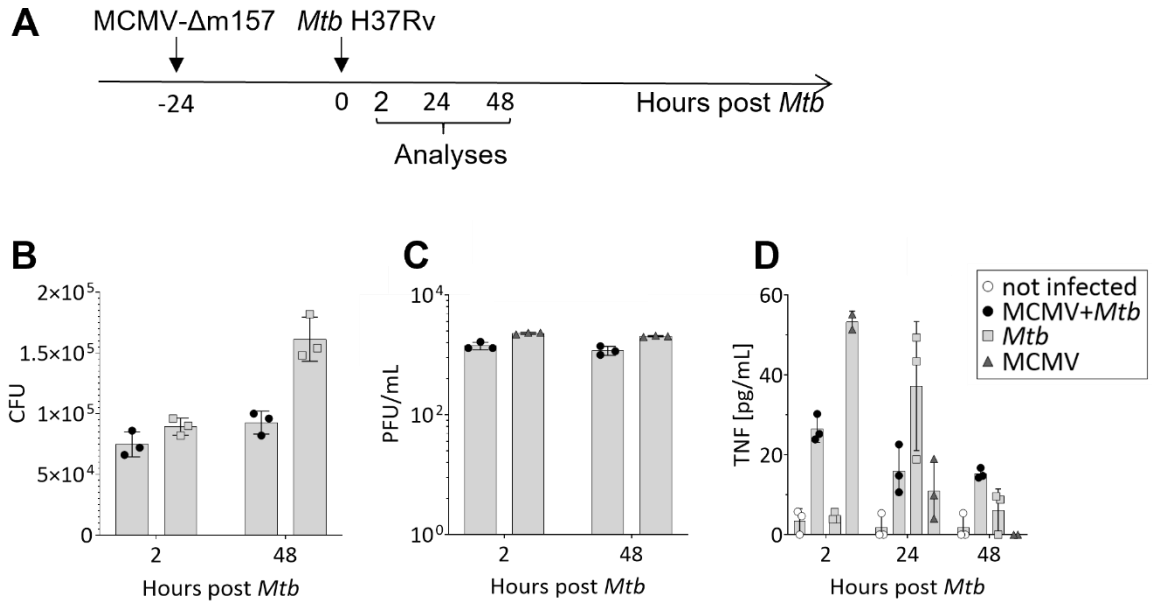

Figure 20: Impact of MCMV coinfection on macrophage activation and bacterial control. (A) Timeline. BMDMs isolated from C57BL/6 mice were infected with MCMV-Δm157-WT MOI 1 and one day later coinfected with an MOI of 0.3 *Mtb* H37Rv. (B) At the indicated time points, serial dilutions were plated onto Middlebrook 7H11 agar plates for CFU determination. (C) Serial dilutions of cell culture supernatants were plated on M2-10B4 cells to determine the plaque forming units (PFU) per mL. (D) TNF production was determined in the cell supernatant at the indicated time points. Values are presented as mean ± SD from technical triplicates and are representative of two independent experiments.

To assess initial bacterial uptake, *Mtb* loads were quantified 2 hours post-infection. At this early stage, bacterial numbers were comparable between *Mtb*-only and coinfected BMDMs, indicating that prior MCMV infection did not impair macrophage phagocytosis (Figure 20B). After 48 hours, CFU counts were 1.5-fold higher in *Mtb*-only infected BMDMs compared to coinfected cells, indicating a trend towards enhanced control in macrophages previously infected with MCMV. Viral titers in infected macrophages were assessed by plaque assay (Figure 20C). Quantified viral loads

were comparable between MCMV-only infected BMDMs at both 2 and 48 hours post-*Mtb* infection compared to those infected with *Mtb*.

To evaluate macrophage activation during (co)infection, TNF, a key cytokine released by macrophages upon activation, was quantified in cell culture supernatants. At 2 hours post-*Mtb* infection, TNF levels (Figure 20D) in the supernatant of *Mtb*-only infected macrophages were comparable to those in uninfected controls. In contrast, cells previously infected with MCMV exhibited higher TNF levels at this time point. By 24 hours post-*Mtb* infection, TNF levels in MCMV-infected macrophages declined, whereas those in *Mtb*-only infected macrophages increased. At 48 hours, TNF levels were low and comparable between coinfected and *Mtb*-only infected macrophages.

In conclusion, MCMV coinfection did not impair macrophage phagocytosis of *Mtb* but resulted in lower *Mtb* loads at 48 hours post-infection compared to *Mtb*-only infected macrophages, suggesting enhanced control in macrophages previously infected with MCMV. Additionally, MCMV infection triggered early TNF production.

4.4 Summary of key findings:

- Bacterial loads were initially comparable between *Mtb*-only and coinfected BMDMs, but lower in coinfected BMDMs after 48 hours.
- Prior MCMV infection resulted in an early TNF release in *Mtb*-infected macrophages, in contrast to singly infected cells.
- Viral loads were comparable between coinfected and MCMV-only infected BMDMs.

4.5 MCMV coinfection shows beneficial effects only in latency

For reference:

- *Day 280 post-Mtb corresponds to 230 days post-MCMV infection*
- *Day 350 post-Mtb corresponds to 300 days post-MCMV infection*

The sequence and timing of coinfections play a crucial role in shaping disease outcomes (101). Having observed the positive impact of a preceding latent MCMV infection on disease progression during subsequent *Mtb* infection, it was investigated whether MCMV infection occurring only when chronic *Mtb* infection was already established would have a similar effect.

To do so, mice were infected with a low dose *Mtb* H37Rv and, 50 days later - when TB enters a chronic but controlled phase - MCMV-Δm157 was administered i.n. (Figure 21).

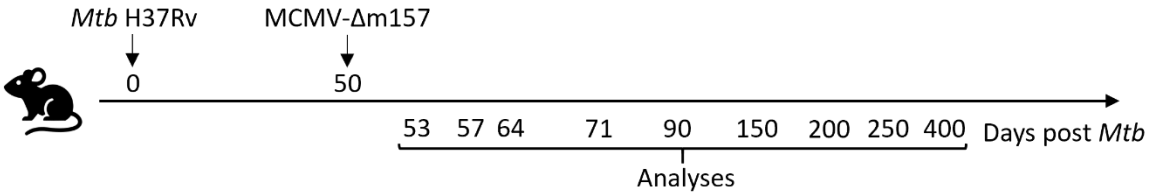

Figure 21: Timeline. C57BL/6 mice were infected with a low dose of *Mtb* H37Rv and 50 days later i.n. infected with $2x10^5$ PFU MCMV-Δm157.

Again, disease progression was monitored, and bacterial loads in the lungs, mediastinal lymph nodes, and spleen were quantified at defined time points, along with viral loads in the lungs. Early analyzes (53, 57 and 64 days post-*Mtb* infection) were conducted to investigate whether an acute MCMV infection during the initial phase of coinfection influences *Mtb* control and to assess the potential impact of *Mtb* infection on viral clearance. Later time points (71, 90, 150, 200, 250 and 400 days post-*Mtb* infection) were analyzed to assess the long-term effects of MCMV coinfection on *Mtb* disease progression. Overall, the disease burden observed in these animals was classified as moderate (Figure 22A). Clinical scores in coinfected mice began to increase around 280 days post-*Mtb* infection (230 days after MCMV coinfection), whereas *Mtb*-only mice developed symptoms 70 days later (350 days post-*Mtb*). Notably, coinfected mice displayed significantly higher clinical scores compared to both *Mtb*-only and MCMV-only groups, with the latter maintaining consistently low scores throughout the observation period. One coinfected mouse reached the predefined endpoint (as described in 4.1) and required euthanasia before the end of the observation period (Figure 22B). In contrast, all remaining mice survived the full observation period.

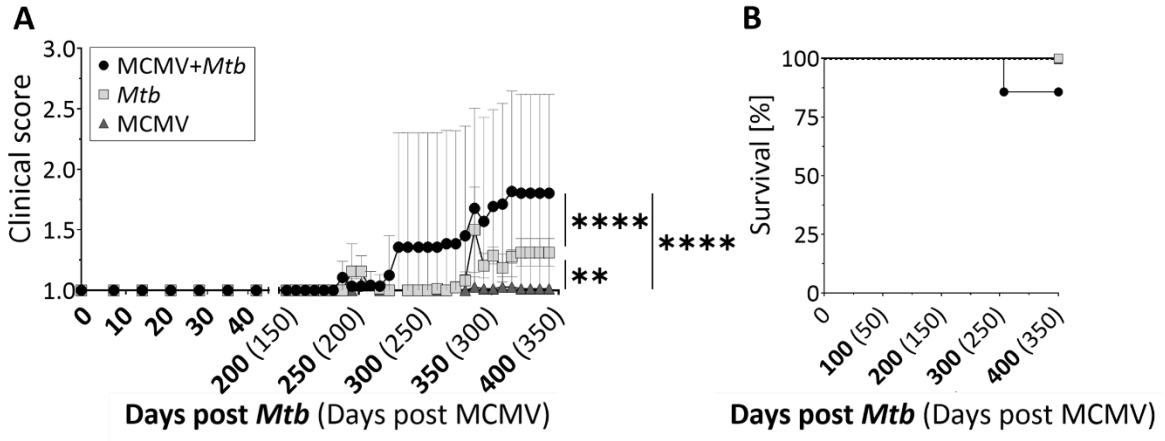

Figure 22: Timing of MCMV coinfection determines disease outcome in MCMV/*Mtb*-infected mice. (A) Clinical scores and (B) survival rates were monitored until day 400 post-Mtb infection. Data represent results from one experiment (n=7–9). Values are presented as mean ± SD. Each data point corresponds to an individual mouse. Statistical significance was assessed using (A) two-way ANOVA with Tukey's

multiple comparison test and (B) the log-rank (Mantel-Cox) test. Significance levels: **p ≤ 0.01; ****p ≤ 0.0001. No statistically significant differences were detected in (B) (p > 0.05).

Despite higher clinical scores observed in coinfected mice, bacterial loads in the lungs, mediastinal lymph nodes, and spleen remained comparable throughout the infection between the *Mtb*-only and coinfected groups. This suggests that the observed clinical deterioration was not a result of uncontrolled bacterial replication (Figure 23A-C).

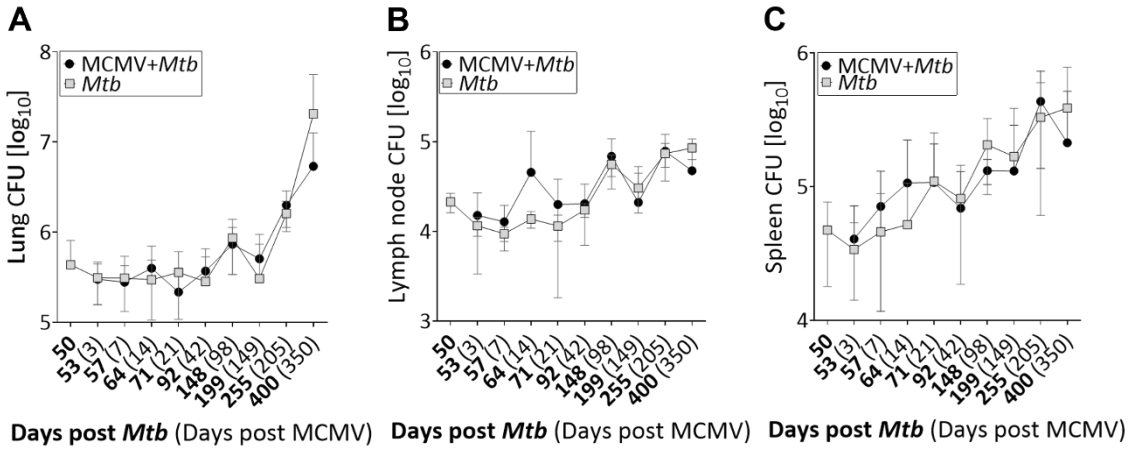

Figure 23: Bacterial burden (CFU) in *Mtb*-infected mice following MCMV coinfection. At the indicated time points, bacterial burden in (A) the lung, (B) lymph node, and (C) spleen was determined. Data represent pooled results from three independent experiments (n=6–12). Values are presented as mean ± SD. Each data point corresponds to the mean value of all mice in the respective group at each time point. Statistical significance was assessed using (A-C) two-way ANOVA followed by Sidak's multiple comparison test. No statistically significant differences were detected in (A-C) (p > 0.05).

To assess potential links between impaired viral clearance and accelerated disease progression in coinfected mice, MCMV genome levels in lung tissue were quantified. Viral loads showed no significant differences overall, though a minor reduction in genome copies was observed in coinfected mice at day 3 post-MCMV infection (Figure 24).

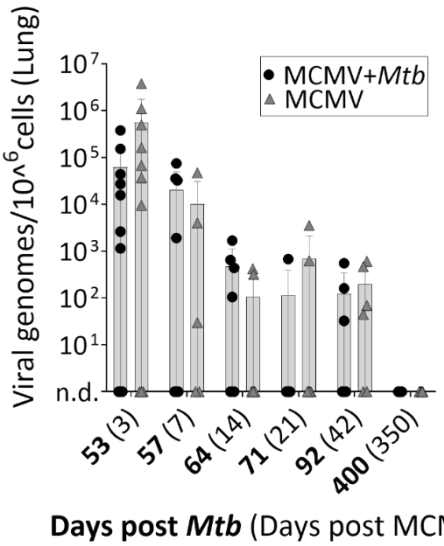

Figure 24: Viral genome quantification in lung tissue capturing acute phase of MCMV infection. Quantification of viral genomes by qPCR in lung tissue collected at the indicated time points. Viral genome levels were normalized to β-actin. The qPCR limit of detection was defined as 10 genome copies per 10^6 cells. Data represent pooled results from two independent experiments (n=5–10; n.d. = not detectable). Values are presented as mean ± SD. Each data point corresponds to an individual mouse. Statistical significance was assessed using an unpaired t-test. No statistically significant differences were detected ($p > 0.05$).

These results suggest that MCMV infection does not inherently confer a beneficial effect in the context of coinfections. Instead, the sequence and timing of infection play a decisive role.

4.5 Summary of key findings:

- While survival was not significantly affected, MCMV coinfection following *Mtb* infection led to marked differences in clinical scores.
- MCMV-only infected mice maintained consistently low clinical score.
- Despite increased clinical scores, bacterial loads were comparable between *Mtb*-only and coinfected groups.
- Viral load was comparable between MCMV and coinfected mice and not detectable at late stages of infection.

4.6 Sequence of infection matters: Limited effects of MCMV after *Mtb* infection

For reference:

- *Day 53 post-Mtb corresponds to 3 days post-MCMV infection*
- *Day 200 post-Mtb corresponds to 150 days post-MCMV infection*
- *Day 400 post-Mtb corresponds to 350 days post-MCMV infection*

Since a preceding latent MCMV infection altered the production of several cytokines and chemokines during subsequent *Mtb* infection (4.2), the question arose how MCMV modulates the immunological environment in the lungs when administered during the chronic stage of *Mtb* infection. To this end, multiplex analysis was performed as described previously (3.6.3). This approach aimed to determine whether the observed changes in immune cell infiltration were specific to latent MCMV infection or if similar alterations occurred when MCMV was introduced after chronic *Mtb* infection. To address this, three representative time points were selected - 53-, 200-, and 400-days post *Mtb* infection. These time points were chosen to capture key phases of disease: an early stage shortly after MCMV infection (day 53 *post-Mtb* infection), a mid-phase of chronic infection (day 200 post-*Mtb* infection), and a late stage when long-term effects could be assessed (day 400 post-*Mtb* infection. The heat maps in Figure 25 provide a comparative overview of cytokine levels in lung homogenates across the three experimental groups at various time points. After initial observation, it is noticeable that among the cytokines measured, IL-1α exhibited the highest expression levels in both coinfected and *Mtb*-only infected animals, consistent with its elevated levels previously observed in the latent MCMV infection model (Figure 25A, B). In contrast, its levels remained low in MCMV-only infected mice at all time points (Figure 25C).

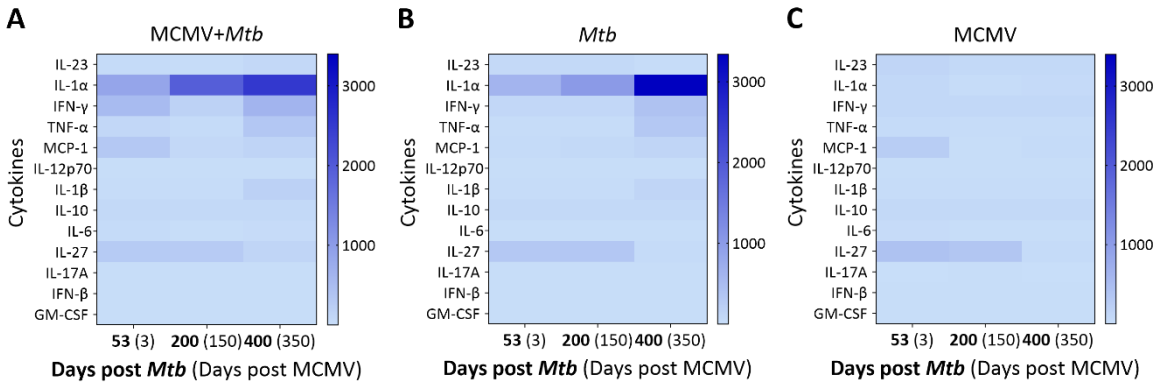

Figure 25: Overview of cytokine levels measured in lung tissue at different time points post-MCMV coinfection. Heat maps of cytokine levels in lung homogenates from (A) coinfected, (B) Mtb-infected or (C) MCMV-infected mice, showing the mean concentration for each cytokine. Data represent pooled results from two independent experiments (n=6–10). Cytokine concentrations are presented in pg/mL, with color intensity reflecting cytokine levels (scale: 0–3200 pg/mL).

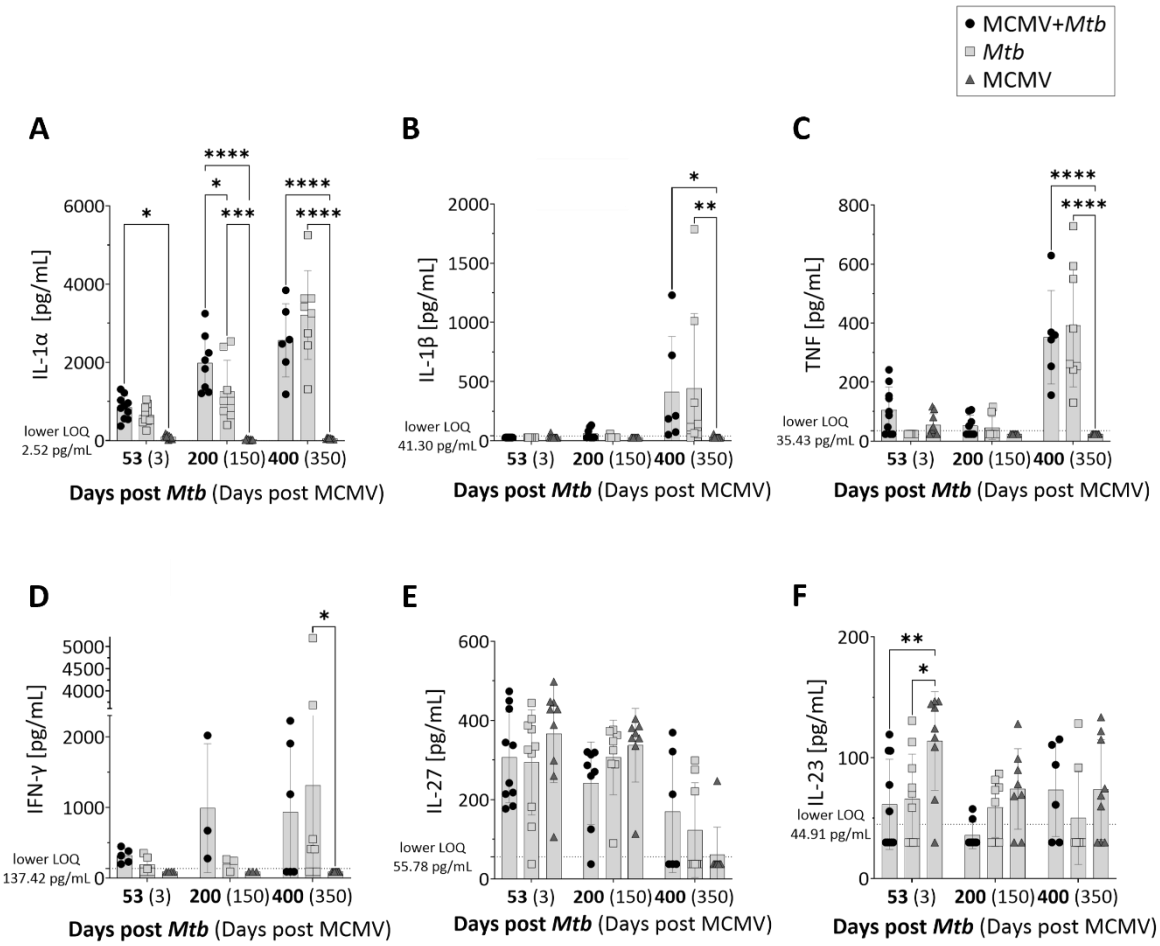

Figure 26: Cytokine responses in lungs of *Mtb*-infected mice with or without subsequent MCMV coinfection. Concentration of selected cytokines (A-F) at representative time points. Data represent pooled results from two independent experiments (n=6–10; LOQ = Limit of Quantification). Values are presented as mean ± SD. Each data point corresponds to an individual mouse. Statistical significance was assessed using (A-F) two-way ANOVA followed by Tukey's multiple-comparison test. Significance levels: *p ≤ 0.05; **p ≤ 0.01; ****p ≤ 0.0001.

A closer examination of the heat maps revealed that IL-1 α steadily increased in both groups over time, showing significantly higher levels in coinfected lungs compared to *Mtb* infected lungs on day 200 post-*Mtb* infection (Figure 26A). In contrast, IL-1β levels (Figure 26B) remained consistently low across all groups until day 400 post-*Mtb* infection, when it increased in some of the *Mtb*-only and coinfected mice. At this stage, IL-1β concentrations were comparable between these groups.

TNF levels (Figure 26C) increased late during infection in both groups, following an initial increase in coinfected mice 53 days after *Mtb* infection (day 53 post-*Mtb*). Similarly, IFN-γ exhibited a small increase on day 53 post-*Mtb* infection (Figure 26D) and remained low throughout the mid and late phases, except for a few outliers with elevated levels observed in both the *Mtb*-only and coinfected groups. In contrast, the level of all four cytokines remained low in MCMV-only infected mice throughout the observation time. Unlike the steady increase observed in the aforementioned

cytokines, IL-27 levels peaked early after MCMV infection in all three groups (Figure 26E) and declined over the course of the experiment, with no significant differences between the groups. IL-23 was significantly elevated 3 days after MCMV infection in MCMV-only infected mice but remained at low levels thereafter, with no significant differences between groups at later time points (Figure 26F). The remaining cytokines exhibited comparable levels across all groups and time points and are thus not shown individually.

As for the chemokines, the heat maps illustrate that *Mtb*-infected animals exhibited an increase in chemokine levels at day 400 post-*Mtb* infection, corresponding to the late phase of infection (Figure 27A, B). In contrast, MCMV-only mice showed moderate elevations in a few chemokines at the final time point analyzed but, consistent with findings from the latency phase, overall chemokine levels remained largely unchanged in MCMV-only infected mice (Figure 27C).

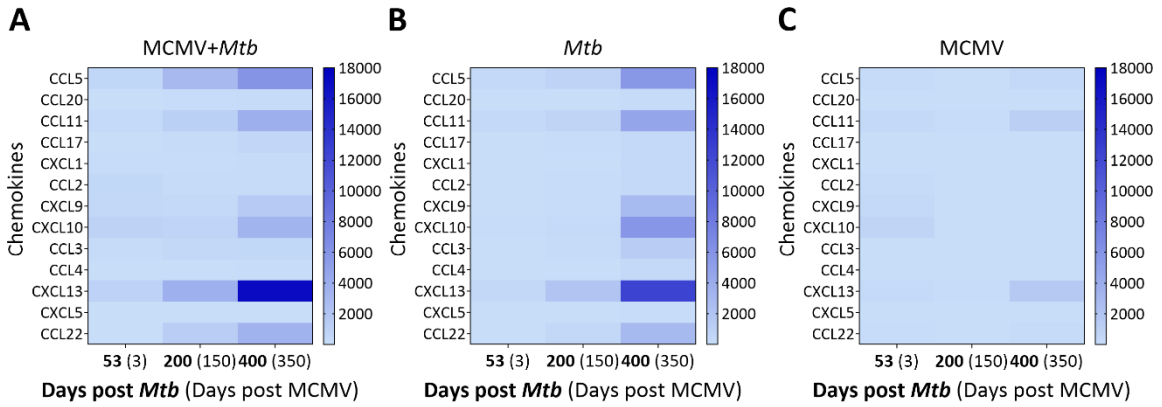

Figure 27: Heat maps of Chemokine expression following MCMV coinfection. Heat maps of chemokine levels in lung homogenates from (A) coinfected, (B) *Mtb*-infected or (C) MCMV-infected mice, showing the mean concentration for each chemokine. Data represent pooled results from two independent experiments (n=6–10). Chemokine concentrations are presented in pg/mL, with color intensity reflecting chemokine levels (scale: 0–18,000 pg/mL).

A closer examination of chemokine levels showed that CXCL9 and CXCL10 only increased significantly during the late stages of *Mtb* infection, and the MCMV coinfection had no significant impact on their production (Figure 28A, B). In contrast, CCL2 levels rose immediately after MCMV coinfection (day 53 post-*Mtb* infection; Figure 28C), reaching significantly higher levels in coinfected compared to *Mtb* infected mice. Over time, the levels decreased, with no difference observed between *Mtb*-only and coinfected animals. The levels of all three chemokines remained low in the MCMV-only infected animals. The remaining chemokines exhibited comparable levels across all groups and time points and are thus not shown individually.

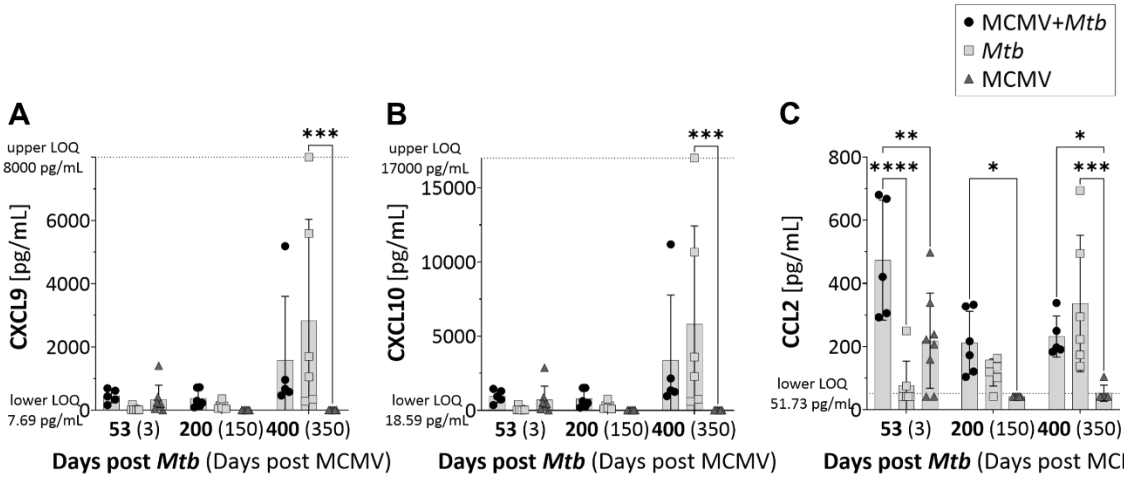

Figure 28: Quantitative analysis of selected chemokines after MCMV coinfection. Concentration of (A) CXCL9, (B) CXCL10 and (C) CCL2 at representative time points. Data represent pooled results from two independent experiments (n=5–8; LOQ = Limit of Quantification). Values are presented as mean ± SD. Each data point corresponds to an individual mouse. Statistical significance was assessed (A-C) using two-way ANOVA followed by Tukey's multiple-comparison test. Significance levels: *p ≤ 0.05; **p ≤ 0.01; ***p ≤ 0.001; ****p ≤ 0.0001.

In summary, overall cytokine and chemokine levels remained largely comparable between coinfected and singly infected mice, suggesting that MCMV has minimal impact on the cytokine and chemokine landscape once *Mtb* infection has reached its chronic phase.

4.6 Summary of key findings:

- Post-*Mtb* MCMV infection had minimal impact on cytokine and chemokine responses.
- IL-1α increased over time in all groups, with slightly higher levels in coinfected mice at day 200.
- TNF and IFN-γ peaked early in coinfected mice, but remained low thereafter.
- CXCL9 and CXCL10 increased during late-stage *Mtb* infection, independent of coinfection.
- CCL2 showed an early peak in coinfected mice, later reaching levels comparable to *Mtb*-only.

5 Discussion

Epidemiological studies indicate that HCMV infection is associated with an increased risk of progression from latent to active TB (101,178–181,185,236,237). Nevertheless, it remains unclear which aspects of host immunity are influenced by HCMV during *Mtb* infection. Building on these observations, this study employed a murine coinfection model to investigate the immunopathological interplay between MCMV coinfection and TB disease progression, revealing unexpected beneficial interactions that challenge conventional paradigms of viral-bacterial coinfection.

5.1 Impact of latent MCMV on TB disease progression in coinfected mice

In the latency model, confirming the presence of latent MCMV was essential to ensure that observed effects were attributable to viral latency; however, this task proved exceptionally challenging. Despite repeated testing, latent MCMV genomes were inconsistently detected in MCMV-infected mice. Furthermore, clinical scores in the MCMV-only group remained unchanged throughout the experiment. These findings raise questions about (i) the reliability of the latent MCMV detection method and (ii) whether mice with undetectable viral DNA were truly infected, especially in the absence of clinical symptoms such as weight loss or behavioural changes. The validity of the infection model must therefore be critically assessed.

One possible explanation for the inconsistent detection of latent MCMV genomes in the infection model employed in this study may lie in the use of the intranasal infection route. In this study, MCMV infection was established via the intranasal route, which closely mimics the natural transmission pathway of cytomegaloviruses in both mice and humans (251). While most experimental studies employ parenteral routes such as intraperitoneal, subcutaneous, or intravenous injection for reasons of efficiency and control, the intranasal route offers greater physiological relevance by targeting the respiratory mucosa, the natural portal of entry (252). However, this approach presents unique challenges, including lower efficiency and increased variability in infection outcomes. For instance, parenteral routes (e.g., intraperitoneal) deliver a standardized viral inoculum directly into systemic circulation, ensuring consistent dissemination, whereas intranasal administration inherently introduces variability due to mucosal barriers, mucociliary clearance, and uneven deposition in the respiratory tract (251). These factors can lead to significant mouse-to-mouse differences in initial viral uptake, potentially contributing to the variable detection of latent MCMV genomes observed in the current study.

Previous studies have shown that latent CMV persists in reservoir tissues such as the lungs and salivary glands without detectable viral replication under immunocompetent conditions (242,253,254). Further, it was shown that reactivation typically occurs only under immunosuppression or systemic inflammation, which can trigger viral gene expression and transition from latency to productive infection (198,255).

However, quantifying latent MCMV is inherently challenging due to its non-replicative state, and distinguishing true latency from low-level chronic replication remains difficult. If genome copy numbers fall below detection limits, it is unclear whether the virus has been cleared or persists at undetectable levels. While viral load measurements were not performed directly after MCMV infection in the latency-focused cohort, analysis in the infection model with reversed infection sequence—where MCMV was administered after *Mtb* infection (Figure 24)—detected viral genomes in the lung at both 3 and 7 days post-MCMV infection. These early measurements provide a useful baseline for acute-phase viral replication, which may help to interpret later findings and, in principle, allow for a distinction between active replication, low-level persistence, and true latency at later time points, such as six months post-infection. Since all infection parameters, including virus strain, dose, and route, were identical in both infection models, it is reasonable to assume that the initial infection dynamics were comparable across experiments. This interpretation is further supported by established models (11), which indicate that MCMV latency is typically established by six months post-infection under these conditions. Therefore, although some uncertainty remains, it appears likely that the observed effects in the coinfection cohort are attributable to latent MCMV infection.

Future studies could address detection limitations by employing more sensitive techniques such as digital droplet PCR (ddPCR) for absolute genome quantification, or in situ hybridization for single-cell visualization of viral DNA or transcripts (158,256). Chromatin immunoprecipitation (ChIP) targeting histone modifications associated with viral genome silencing (257) and targeted genome enrichment with deep sequencing (258) may further clarify transcriptional activity during latency.
The absence of overt disease symptoms in C57BL/6 mice following MCMV-Δm157 infection does not compromise the validity of the model. Rather, it reflects the strain's intrinsic resistance and the subclinical infection dose (2×10^5 PFU) administered intranasally. C57BL/6 mice are known to mount effective antiviral responses against MCMV, even in the absence of Ly49H$^+$ NK cell recognition, as demonstrated by studies using the Δm157 mutant. This compensatory immunity is driven by robust IFN-γ–mediated responses and heightened CD8$^+$ T cell activation, which suppress

viral replication and pathology, even in the absence of Ly49H (259–262). This phenotype parallels HCMV infection, where viral genomes persist asymptomatically in immunocompetent humans. The absence of reactivation in immunocompetent C57BL/6 mice mirrors the clinical stability of HCMV latency, where immune pressure prevents viral recrudescence unless immunosuppression occurs (263,264).

Clinical presentation varies between mouse strains: BALB/c mice develop severe symptoms after MCMV infection (265,266), while C57BL/6 mice remain asymptomatic under standard infection protocols ($\leq 10^5$ PFU, intranasal/i.p.) due to Ly49H$^+$-NK cell and/or CD8$^+$ T cell-mediated control. Higher infection doses of MCMV-Δm157 ($\geq 10^6$ PFU i.p.) can induce transient weight loss and hepatic pathology in C57BL/6 mice, but without systemic clinical scores. Susceptibility also varies between strains, as shown by Oduro et al. (242), where the same MCMV strain and inoculum as used in the present study, delivered intranasally, resulted in significantly higher viral loads in the lungs after six months in 129/Sv mice (a more susceptible background). Thus, a consistently low clinical score in MCMV-only infected mice in the current model should not be interpreted as evidence of absent infection, but rather as an outcome of host resistance and viral control below the threshold of clinical detection.

Contrary to initial expectations, latent MCMV infection did not exacerbate TB progression but instead improved disease outcomes, reducing mortality without affecting bacterial loads. This suggests that latent MCMV enhances disease tolerance rather than bacterial control, contrary to the exacerbated disease severity reported in viral-bacterial coinfections.

No evidence of MCMV reactivation was observed following *Mtb* infection, as viral genome loads remained low in lung tissues. This contrasts with human studies, where CMV reactivation in TB patients is typically reported in the context of extrinsic immunosuppressive factors, such as immunosuppressive therapies (e.g., corticosteroids, TNF inhibitors) (185,255,267). Further investigation is needed to explore whether transient reactivation events occurred undetected due to the timing of analysis. Since *Mtb*-induced immune modulation evolves gradually, the chosen time points in this thesis may not have captured potential reactivation events (268). Future studies should explore later time points to fully assess the impact of *Mtb* infection on MCMV latency. Furthermore, longitudinal harvesting of lungs and salivary glands at defined intervals during the latency phase (e.g., monthly over six months) would provide valuable insights into the dynamics of latent viral reservoirs and their interaction with host immunity prior to *Mtb* coinfection. Such data could clarify whether fluctuations in viral genome detection reflect true latency or low-level chronic

replication. These findings reinforce the idea that while MCMV remained latent in this coinfection model, the potential for reactivation still exists under immunocompromised conditions.

The exclusive use of female C57BL/6 mice in this study was a deliberate choice, driven by practical considerations such as reduced aggression during group housing. In addition, the use of female mice is consistent with the majority of published studies investigating *Mtb* H37Rv and MCMV infection in this model (102,269–271). This approach enhances the comparability of our results and provided a controlled experimental framework to investigate the immunomodulatory effects of MCMV infection on *Mtb* disease progression. Female mice, with stronger Th1-driven immunity and a more pronounced type I interferon response, may better reveal protective or detrimental effects of latent MCMV. In males, these effects could be less pronounced due to testosterone-driven immunosuppression and a weaker type I IFN response (272–274). Sex differences in CMV susceptibility further underscore the relevance of this model. In murine studies, male mice exhibit greater resistance to systemic MCMV infection. This resistance is linked to higher TLR9 expression, stronger neutrophil recruitment, and reduced liver inflammation compared to females (275). The sex bias in MCMV susceptibility is TLR9-dependent, as TLR9-deficient mice show no sex differences (275). In humans, latent CMV infection drives larger pro-inflammatory T-cell responses in males, while females are more susceptible to tissue-invasive CMV disease post-transplantation (276). These findings are similar to what is seen in TB, where enhanced type I IFN and Th1 responses in females improve pathogen control but may increase immunopathology risk (277).

Including male cohorts in future studies would enhance translational relevance, given the male-biased TB incidence in humans (278) and the interplay between CMV-driven sex differences and hormonal-immune cross-talk. For instance, testosterone-mediated suppression of IFN-γ and IL-12 pathways might attenuate the protective effects of latent MCMV, while heightened IL-1β/TNF responses could exacerbate immunopathology, as observed in sex-stratified inflammatory models (279). Exploring these differences would clarify how hormonal versus chromosomal factors shape immune interactions in coinfection and improve the clinical applicability of findings (280).

While HCMV infection in humans is often linked to immunosenescence and increased susceptibility to infections (281), emerging evidence suggests that its impact on immune function is more complex and may vary throughout the lifespan (282–285). Although persistent viral infections are generally regarded as detrimental, certain aspects of latency-driven immune remodelling might confer advantages in specific pathogen encounters. For example, herpesviruses such as CMV and Epstein-Barr virus (EBV) have been shown to modulate immune responses in ways that could explain such protective effects. For instance, Sandalova et al. demonstrated that during acute

hepatitis B virus (HBV) infection, CMV- and EBV-specific $CD8^+$ T cells contributed significantly to the expansion of the activated $CD8^+$ T cell pool in humans (285). These virus-specific T cells exhibited heightened activation and increased IFN-γ production in response to HBV infection, suggesting an enhanced effector functionality.

These observations align with murine studies demonstrating that prior MCMV infection protects against heterologous pathogens (40,41), highlighting the potential of latency-driven immune modulation to reshape host defense strategies. Importantly, it was shown that this protective effect is not restricted to viral infections but also extends to bacterial pathogens. For instance, latent MCMV infection has been shown to provide protection against *Listeria monocytogenes* and *Yersinia pestis*, mediated by the sustained activation of macrophages and prolonged production of IFN-γ and TNF (286). This led to a notable decrease in bacterial load, emphasizing the potential of latency-driven immune modulation to enhance host defence in animal models.

In this study, improved TB outcomes were observed in the absence of reduced bacterial loads, indicating that latent MCMV enhances the host's ability to tolerate *Mtb* infection through immune modulation rather than by directly limiting pathogen burden. These findings add to a growing body of evidence that persistent viral infections can, under certain conditions, confer beneficial effects by reshaping immune dynamics and promoting disease tolerance.

5.2 The impact of coinfection on the inflammatory environment in the lungs

The observation that improved disease outcomes in coinfected animals occurred without differences in bacterial or viral loads suggests that the protective effects of latent MCMV infection are mediated by immune modulation rather than direct pathogen control. Elevated levels of proinflammatory cytokines such as IL-1α, IL-1β, and TNF in coinfected mice indicate heightened macrophage activation and enhanced inflammasome signaling, potentially driven by immune priming through latent MCMV infection (287,288). These cytokines are critical for granuloma formation and pathogen containment (289–291) but can also contribute to immunopathology when dysregulated (287). Interestingly, delayed upregulation of IL-1β during the late phase of infection (d252 post-*Mtb*; 432 days post-MCMV) suggests temporal regulation of inflammatory responses, potentially contributing to improved disease tolerance rather (292,293). Whether this upregulation results from direct MCMV-driven immune modulation or altered immune cell composition in the lung remains unclear. Further studies are needed to clarify these mechanisms.

Cytokine levels in coinfected animals may be optimally regulated to balance protective inflammation with tissue preservation. For instance, early elevation of IFN-γ may have enhanced

TNF and IL-1 production, promoting effective immune responses and granuloma formation. TNF is pivotal in coordinating the chemokine response in the *Mtb*-infected lung, working synergistically with IFN-γ to enhance macrophage activation and facilitate protective granulomatous responses (294,295)—a phenomenon also described in viral-bacterial coinfections, where prior viral pathogen exposure primes monocytes and macrophages for heightened responsiveness to subsequent bacterial challenge (286). IFN-γ may also mitigate immunopathology through mechanisms such as Indoleamine-2,3-dioxygenase (IDO) induction and regulatory T cell (Treg) expansion (81,296–299). IDO, triggered by IFN-γ in dendritic cells (DCs), depletes tryptophan and generates immunosuppressive metabolites that promote FoxP3$^+$ Treg development while suppressing effector T cell responses (300–304). These processes dampen excessive T cell activation and favor tissue preservation over destructive inflammation. A similar effect was observed by Gbedande et al., where MCMV-induced IFN-γ provided cross-protection against Plasmodium chabaudi by promoting CD8α$^+$ dendritic cell expansion and IL-12 production, enabling a robust adaptive immune response during secondary infections.

Regulatory T cells (Tregs) likely play a complementary role in modulating the immune response during coinfection. Latent MCMV infection has been shown to expand Treg populations, which are critical for maintaining viral latency and controlling excessive inflammation (305). Although not directly assessed in this study, Tregs may contribute to restraining hyperinflammatory responses through IL-2 sequestration, CTLA-4-mediated suppression of dendritic cell activation, and secretion of tissue-protective factors such as amphiregulin and IL-10. These mechanisms could synergize with IFN-γ-driven tolerance pathways to sustain a balanced inflammatory response that supports granuloma integrity while preventing tissue damage (255,306).

Delayed IL-1β upregulation may reflect a secondary wave of immune regulation, preserving granuloma integrity while limiting bacterial dissemination. While early inflammasome activity was likely restrained by IFN-γ-induced S-nitrosylation of NLRP3 (307–309), the subsequent release of this inhibition during late infection may have allowed for a controlled increase in IL-1β production (287).

Chemokines such as CXCL9, CXCL10, and CCL2 were also elevated in coinfected animals and likely played a role in recruiting monocytes and T cells to the lung (287,310–312). CXCL9 and CXCL10 are induced by IFN-γ and TNF and recruit CXCR3$^+$ effector cells to sites of infection (310,311). This chemokine-driven recruitment may enhance granuloma stability and pathogen containment without triggering excessive inflammation (311). Similarly, CCL2 facilitates the recruitment of CCR2$^+$

monocytes, which are essential for phagocytosis and bacterial control (287,288). The sustained elevation of these chemokines suggests that MCMV-induced immune imprinting creates a microenvironment optimized for cellular crosstalk during *Mtb* infection.

The expression patterns of IL-23 and IL-27 further illustrate how prior MCMV infection modulates immune responses. Early elevations of these cytokines in MCMV-only infected mice suggest virus-driven modulation that tempers inflammation (313). Both cytokines are known to play dual roles in TB pathogenesis: IL-27 regulates Th1 responses by promoting early IFN-γ production before shifting to immunosuppressive functions that curb excessive inflammation (313,314), while IL-23 sustains CCL2-mediated monocyte recruitment and granuloma stabilization (315,316).
Notably, coinfected animals exhibited a delayed IL-23/IL-27 peak, indicating a temporal shift in immune dynamics that aligns with sustained immune activation. This delayed increase may indicate MCMV-induced imprinting for regulated, long-term cytokine production. The persistence of IL-23 in both MCMV-only and coinfected mice supports a microenvironment conducive to balancing inflammation and bacterial containment. IL-23 has been implicated in maintaining CCL2 production and granuloma stability during chronic *Mtb* infection, which aligns with its delayed elevation in coinfected animals (315,316). In contrast, *Mtb*-only infected mice showed lower IL-23 levels, underscoring the unique immune adaptability conferred by prior MCMV infection—a phenomenon that likely contributes to the improved survival observed in coinfected animals.
These findings align with broader evidence of immune imprinting, such as during the COVID-19 pandemic, where prior exposure shaped responses to subsequent strains (317). Similarly, MCMV-induced imprinting may enhance the host's capacity to regulate inflammation during *Mtb* coinfection, promoting disease tolerance without compromising pathogen control.

Overall, prior MCMV infection establishes a distinct immunological baseline characterized by heightened but regulated inflammation, enhancing disease tolerance rather than directly influencing bacterial clearance. However, the precise mechanisms—whether due to direct immune reprogramming or secondary effects—require further investigation.

5.3 Prior MCMV infection alters pulmonary pathology in coinfected mice

To determine whether cytokine and chemokine differences were reflected in lung pathology, H&E and mIF staining were performed. Increased cytokine and chemokine expression in coinfected mice suggested heightened immune cell infiltration and inflammation. Paradoxically, T cell-recruiting

chemokines were elevated, while T and B cell abundance was reduced in coinfected mice, raising questions about how prior viral infection reshapes host immunity.

This reduction may result from suppressed recruitment, altered trafficking, or functional changes in T and B cells due to persistent viral-driven modulation (318,319). Given that *Mtb*-only infected mice showed significantly higher levels of $CD3^+$ T cells in the late phase and $CD19^+$ B cells during mid- and late infection, the reduced abundance of these cells in coinfected animals underscores the potential long-term effects of MCMV latency on adaptive immunity.

Several mechanisms could contribute to this phenomenon. Chronic viral infections, like CMV, have been shown to induce profound and long-lasting alterations in the adaptive immune system, including T cell exhaustion, redistribution, or sequestration in non-lymphoid tissues (318). Additionally, MCMV infection may induce a competitive immune environment where virus-specific T cells undergo expansion at the expense of *Mtb*-specific T cells, effectively diluting the pool of available effector cells capable of responding to *Mtb* infection (319).

Early immune priming through IFN-γ during the initial phase of coinfection (day 21 post-*Mtb*; 201 days post-MCMV) may also contribute to this shift by reinforcing an innate immune strategy over an adaptive one. IFN-γ is a potent macrophage activator that suppresses neutrophil recruitment by inhibiting IL-17 production (320,321). While neutrophils play a dual role in TB—contributing to early pathogen clearance but exacerbating tissue damage when dysregulated—IFN-γ-driven suppression may favor monocyte and macrophage accumulation at infection sites (322). This is consistent with findings by Kim et al., who demonstrated that IFN-γ promotes monocyte differentiation and enhances macrophage accumulation at sites of infection (182). Neutrophils — although not examined in this study — could be an intriguing focus for future investigations.

Latent viral infections are known to induce epigenetic reprogramming via histone modifications in myeloid cells, enhancing antimicrobial functions (323). Although not directly assessed here, such mechanisms could explain the lasting effects of MCMV-induced imprinting on macrophage activation.

Supporting this hypothesis, coinfected mice exhibited a significantly increased $CD68^+$ macrophage-to-$CD3^+$ T cell ratio during late infection stages (day 252 post-*Mtb*; equivalent to 432 days post-MCMV suggesting a shift toward macrophage-oriented immune response. The elevated ratio was paralleled by an increased number of $CD68^+$ macrophages and higher levels of CCL2, a key monocyte chemoattractant known to promote macrophage recruitment and differentiation (287,288,310). These findings are consistent with previous studies highlighting the role of macrophages in bacterial containment within granulomas, where they limit pathogen

dissemination and help mitigate immunopathology (45,55). The increase in $CD68^{+}mpt64^{+}$ macrophages observed in the coinfected group at the late infection timepoint (day 252 post-*Mtb*) may reflect altered immune cell infiltration or increased antigen exposure in the lung microenvironment. This accumulation of macrophages with *Mtb*-antigen contact could be consistent with a sustained or potentially reactivated immune response against *Mtb* in the presence of pre-existing MCMV infection, although alternative explanations cannot be excluded. The lower cell counts in both singly infected groups (*Mtb*-only and MCMV-only) suggest that this effect may be related to the coinfection state, but the substantial variability within the coinfected group, as indicated by the wide range of data points, may reflect individual differences in immune response or disease stage. While these findings are in line with the hypothesis that MCMV infection can influence immune cell composition and activation during *Mtb* infection, the functional significance of this observation remains uncertain. It should also be considered that MPT64 is a secreted antigen and its detection in macrophages does not necessarily indicate direct bacterial infection, as it may also result from uptake of extracellular antigen or debris from infected cells (249,250). Without additional data on macrophage function, bacterial burden, or disease outcomes, it is difficult to determine whether this shift reflects enhanced antimycobacterial activity, impaired bacterial control, or other changes in lung pathology. Further studies are needed to clarify the functional implications of these observations.

The interplay between macrophage recruitment, bacterial containment, and reduced adaptive immune responses in coinfected mice raises questions regarding immune tolerance and host-pathogen interactions. While T cells are typically essential for mounting an effective immune response against *Mtb*, excessive or dysregulated T cell activity has been associated with severe immunopathology (324). It is possible that the reduction in T cell infiltration observed represents an adaptive mechanism where MCMV-induced immune modulation prevents excessive T cell-mediated inflammation, thereby reducing tissue damage (167). This notion aligns with findings from Almanan et al., who demonstrated that latent MCMV infection increases regulatory T cells (Tregs) in tissues as the salivary glands, leading to suppressed effector T cell responses (305). While this has been observed in other tissues, it remains unclear whether a similar mechanism occurs in the lungs during MCMV-*Mtb* coinfection.

The broader implications of these findings extend beyond TB pathogenesis. Chronic viral infections can induce durable changes through immune imprinting that alters responses to subsequent infections (318,325). In this context, latent MCMV infection may establish a immune environment where macrophage-driven regulation takes precedence over conventional T cell-driven responses.

Similar observations have been made during HCMV infections where latently infected monocytes modulate innate immunity by inhibiting neutrophil recruitment through downregulation of S100A8/S100A9 expression (326). If similar mechanisms occur here, they could explain preferential recruitment of monocyte-derived macrophages observed during coinfection.

Collectively, these findings suggest that coinfection influences immunity to promote effective *Mtb* control while minimizing immunopathology during persistent infection. The increased macrophage-to-T cell ratio driven by CCL2-mediated monocyte recruitment and IFN-γ priming indicates how latent viral infections reprogram host defenses against bacterial pathogens. Understanding how viral latency modulates immunity could inform host-directed therapies aimed at optimizing responses while minimizing tissue damage. Future studies should assess molecular mechanisms underlying this remodeling—particularly viral imprinting's role—and evaluate neutrophil dynamics alongside macrophage activation states for deeper insights into MCMV's impact on TB immunity.

5.4 MCMV-*Mtb* coinfection at the macrophage level

Macrophages are key target cells for both *Mtb* and MCMV (327,328), making them central to understanding how prior MCMV infection modulates the immune response during *Mtb* coinfection. While CMV has been reported to impair macrophage functions such as phagocytosis and TNF production (329), this study suggests a more nuanced interaction. MCMV-infected macrophages retained phagocytic capacity for *Mtb*, comparable to naïve macrophages, indicating that viral infection does not universally suppress bacterial uptake.

However, the distinct kinetic profile of TNF expression observed in MCMV-infected macrophages emphasizes the dynamic interplay between viruses and bacteria. TNF levels were elevated early in MCMV-infected macrophages but declined 24 hours later, suggesting a rapid but transient TNF response, while *Mtb* infection leads to a delayed and more sustained TNF production in *Mtb*-only infected BMDMs. In coinfected macrophages, TNF levels at early timepoints are higher than in *Mtb*-only infected cells but do not reach the peak observed with MCMV-only infection. This transient TNF response may reflect early macrophage activation followed by MCMV-mediated immune evasion. Viral proteins that interfere with NF-κB signaling and inflammasome activation (330–332) likely contribute to this suppression, while anti-inflammatory cytokines such as IL-10 may further dampen prolonged inflammation (333,334). Interestingly, *Mtb* itself employs virulence factors like lipoarabinomannan (LAM) to suppress TNF via SOCS-mediated pathways (335), potentially exacerbating the immunosuppressive environment created by MCMV.

Notably, the timing and multiplicity of infection (MOI) likely play critical roles. In the experimental model employed here, *Mtb* was introduced 24 hours after MCMV infection at a low MOI of 0.3. This setup may capture an early activation phase of macrophages prior to the onset of extensive viral immune evasion. Low MOI infections are known to stimulate macrophage activation without inducing excessive stress or cell death, allowing them to initiate proinflammatory responses (336). Furthermore, the 24-hour gap between MCMV and *Mtb* infection may allow macrophages to enter a preactivated state before MCMV-mediated immune suppression becomes fully effective (337–339).

The slow intracellular replication cycle of *Mtb* compared to other pathogens like Legionella pneumophila may provide a temporal window for macrophages to mount antimicrobial defenses before viral suppression becomes dominant (340–343).

Macrophages are major producers of TNF and are also highly responsive to it, so early TNF induction in MCMV-infected and coinfected macrophages may not only reflect a state of preactivation, but it could also contribute to enhanced bacterial control in an autocrine manner. TNF promotes antimicrobial activity by facilitating phagolysosome maturation, reactive oxygen species (ROS) production, and apoptosis of infected cells—particularly when synergizing with IFN-γ, another key macrophage activator (344,345). Whether IFN-γ signaling is altered during coinfection was not investigated in this thesis, but future studies should directly address this axis, given the importance of TNF and IFN-γ synergy in *Mtb* control (294).

Future studies should explore whether MCMV-induced immune imprinting alters long-term macrophage activation states or promotes epigenetic reprogramming that enhances bacterial containment. Additionally, evaluating the role of neutrophil dynamics and regulatory cytokines like IL-10 in shaping the immune environment during coinfection could provide critical insights into how pathogens co-opt host responses for persistence.

5.5 Timing matters: MCMV coinfection benefits are limited to latency

Having observed the beneficial effects of latent MCMV on subsequent *Mtb* infection, it was next investigated whether reversing the infection sequence would alter disease outcomes.

Interestingly, this infection resulted in exacerbated disease progression in coinfected mice, despite comparable bacterial and viral loads. This suggests that the observed effects are not merely a consequence of pathogen burden but rather reflect broader immune modulation triggered by MCMV.

Similar findings have been reported in other models, where coinfections modulate disease severity through immune-mediated mechanisms rather than direct effects on pathogen replication. For

instance, Gonzalez et al. demonstrated that coinfection with rhinovirus or murine coronavirus attenuates influenza A virus severity by modulating immune signaling pathways—particularly through controlled early inflammatory responses—despite unchanged viral titers (346,347). The observed disease exacerbation in this study supports the influence of infection timing and sequence on disease outcomes, a concept that has been confirmed by numerous studies in the past (185,325,348–350). Specifically, the immune system's response to an acute viral infection in the context of an existing chronic bacterial infection may lead to dysregulated immune signaling, increased inflammation, or altered macrophage function, thereby exacerbating pathology despite stable pathogen loads (351). The data from the current study are consistent with the hypothesis proposed by Cobelens and colleagues that immunologically active CMV infections-whether primary infection, reactivation, or reinfection-can drive the transition from latent TB infection to active TB disease (101). This is in line with the broader understanding that viral infections can serve as immune modulators, tipping the balance of immune homeostasis toward pathogen reactivation or increased disease severity (352,353). Together with the observations that latent MCMV exerts a different effect, this study indicate that it is not merely the presence of MCMV, but rather the phase of infection, that critically determines disease outcomes during coinfection.

Cytokine and chemokine profiles further illustrate the distinct immune dynamics depending on the timing of viral exposure. While latent MCMV infection resulted in cytokine shifts during *Mtb* coinfection, acute MCMV infection during chronic *Mtb* infection had minimal impact on chemokine responses like CXCL9 and CXCL10. CCL2 expression showed different kinetics, remaining persistently high in coinfected mice but declining in MCMV-only infected animals during later stages. Proinflammatory cytokines—including IL-1α, IL-1β, TNF, and IFN-γ—were significantly elevated at late time points (day 400 post-*Mtb* infection) in *Mtb*-only infected animals but remained markedly lower in coinfected mice. These results suggest that pre-existing latent MCMV infection modulates immune responses more than acute viral exposure during ongoing bacterial infection.

Age-related differences between experimental groups may also contribute to these findings. Mice with prior latent MCMV infection were approximately 130 days older at the time of *Mtb* exposure compared to those receiving MCMV 50 days after *Mtb* infection. Aging is associated with a phenomenon known as inflammaging—a chronic low-grade inflammatory state driven by immunosenescence and cumulative antigen exposure (354,355). Elevated baseline levels of proinflammatory mediators such as IL-6 and TNF may mask infection-induced cytokine shifts in older mice. Interestingly, latent MCMV itself may counterbalance inflammaging through regulatory Treg-mediated immunomodulation. Studies have shown that latent CMV expands Treg populations,

which suppress excessive inflammation and maintain viral latency by limiting effector T cell activation (356). In this model, latent MCMV-induced Treg activity may attenuate age-related inflammation, creating a buffered immune environment that alters cytokine landscapes during *Mtb* coinfection.

Overall, these findings indicate that the timing of MCMV infection relative to *Mtb* exposure is a determinant of immune responses, with distinct cytokine dynamics observed depending on whether MCMV was introduced before or after *Mtb* infection.

While age-related inflammaging and latent MCMV-induced immune modulation may alter cytokine landscapes, these immunoregulatory mechanisms could also influence viral persistence. Notably, by day 400 post-*Mtb* infection (equivalent to 350 days post-MCMV infection), MCMV was no longer detectable in both groups. This contrasts with the latency model, where viral genomes were still detectable in most mice six months after MCMV infection (5.1). This discrepancy may reflect time-dependent attrition of latent reservoirs and/or *Mtb* coinfection-driven immune pressure.

MCMV latency in mice is not universally lifelong, as latent genomes in lymphoid and stromal tissues exhibit progressive attrition over time. While viral reservoirs persist detectable in spleen, kidney, and salivary glands for months, studies demonstrate a >99% decline in latent genomes between 6–18 months post-infection. This attrition is accelerated in aged mice due to depletion of lymphatic endothelial cells (LECs), a key latency niche (357). In this coinfection model, the extended timeline (350 dpi ≈12 months) exceeds typical latency studies (≤6 months), allowing sufficient time for age-related mechanisms to eliminate residual virus. Consequently, viral genomes may fall below detection thresholds, explaining the absence of MCMV in our late-stage coinfected mice compared to shorter-term latency models.

MCMV latency is defined by genome persistence without production of infectious virus. However, even latent genomes can eventually be fully cleared. For example, latent MCMV genomes in splenic stromal cells decline by >99% between 6–18 months post-infection (270). Current findings align with this, suggesting that prolonged infection (12 months) permits immune-mediated resolution, whereas shorter-term models (6 months) retain detectable genomes. The timing and immunological context of MCMV infection relative to *Mtb* exposure thus appear to determine both viral persistence and immune outcomes. Undetectable MCMV-genome in this infection model, in contrast to shorter-term latency studies, likely reflects the combined effects of prolonged infection duration and coinfection-driven immune pressure. These findings suggest that pathogen interactions and host aging dynamically shape viral reservoir attrition, emphasizing the need to contextualize latency and clearance within infection timelines and comorbid conditions.

5.6 Immunoregulatory differences between acute and latent CMV infection

The findings suggest that the timing of MCMV infection influences the host immune response to *Mtb*, with distinct cytokine dynamics depending on whether MCMV precedes or follows *Mtb* infection.

Importantly, the phase of viral infection appears to be a key determinant of immune regulation during coinfection. Active MCMV infections are characterized by strong antiviral responses, including the induction of type-I IFNs, which play a central role in controlling viral replication (358). However, these responses are also known to exacerbate TB pathology, as type-I IFNs can suppress macrophage activation, inhibit the production of IL-1β and TNF, and promote IL-10 expression, thereby impairing bacterial containment (359). Although type-I IFNs were not measured in this study, their detrimental effects in TB suggest that they could mediate immune dysregulation during acute viral infections. Future research should focus on analyzing type-I IFN responses and downstream signaling pathways during early stages of coinfection.

In contrast, during the prolonged latency phase, immune regulation shifts significantly. Latent MCMV infection establishes a distinct immunological state characterized by long-term immune modulation. This state is associated with the expansion of Tregs and the production of immunosuppressive cytokines, such as viral IL-10, which help maintain latency by suppressing excessive inflammation (305,306,360). This immunoregulatory environment may benefit secondary infections like *Mtb* by preventing hyperinflammation while still supporting bacterial control (87). However, chronic low-grade inflammation driven by CMV during latency might also contribute to subtle immune dysregulation over time, potentially influencing disease progression (361).

These observations highlight the importance of differentiating between the immunological effects of active versus latent viral infections in coinfection models. While active MCMV infection likely worsens TB through type-I IFN-driven mechanisms, latent infection may foster a more balanced immune environment that could mitigate disease progression.

5.7 Conclusion

This study provides novel insights into CMV-*Mtb* coinfection using a C57BL/6 mouse model. Contrary to the initial hypothesis, pre-existing MCMV infection did not worsen TB but instead improved clinical outcomes, while acute MCMV infection during chronic TB exacerbated disease severity. This highlights the role of infection timing and sequence in shaping immune responses. Moreover, these findings challenge the assumption that chronic viral infections universally impair host immunity, instead suggesting that viral latency may shape immune dynamics in ways that can be beneficial in specific contexts.

Notably, this study found no evidence that *Mtb* coinfection reactivates latent MCMV. However, it is important to consider that the experimental model may not fully capture the complexity of viral latency and reactivation dynamics observed in human populations. Unlike controlled laboratory conditions, humans are consistently exposed to various environmental and immunological triggers that could facilitate HCMV reactivation or reinfection. Stress, concurrent infections, immune suppression, or aging are all known to influence CMV reactivation, potentially amplifying its impact on TB progression in real-world settings (267,362,363). This underlines the need for further investigations in clinical and epidemiological contexts to assess whether HCMV reactivation in individuals with latent TB poses a significant risk for disease progression and whether specific immune signatures can be used to identify those at increased risk.

Furthermore, while this study did not directly measure type-I IFNs, their role in acute MCMV infection remains an important area for future investigation. Type-I IFNs are known to suppress macrophage activation and inhibit IL-1β and TNF production while promoting IL-10 expression—mechanisms that could impair bacterial containment during TB. The absence of type-I IFN data represents a limitation of this study but highlights a critical avenue for future research into how acute viral infections exacerbate disease severity through IFN-driven pathways.

Overall, the recent findings highlight the intricate interplay between viral and bacterial infections and emphasize the importance of considering infection timing, host immune status, and technical limitations in detection methods when evaluating the impact of coinfections on disease outcomes.

References

1. Global tuberculosis report 2024. Geneva: World Health Organization; 2024. Licence: CC BY-NC-SA 3.0 IGO. Geneva; 2024 Oct.

2. Mandal S, Rao R, Joshi R. Estimating the Burden of Tuberculosis in India: A Modelling Study. Indian Journal of Community Medicine. 2023 Jul 1;48(3):436–42.

3. Robert Koch-Institut. Bericht zur Epidemiologie der Tuberkulose in Deutschland für 2022 [Internet]. Berlin; 2023 [cited 2025 Apr 20]. Available from: https://www.rki.de/DE/Content/InfAZ/T/Tuberkulose/Download/TB2022.pdf

4. MacPherson P, Lebina L, Motsomi K, Bosch Z, Milovanovic M, Ratsela A, et al. Prevalence and risk factors for latent tuberculosis infection among household contacts of index cases in two South African provinces: Analysis of baseline data from a cluster-randomised trial. PLoS One. 2020;15(3).

5. Lin PL, Flynn JL. Understanding Latent Tuberculosis: A Moving Target. The Journal of Immunology. 2010 Jul 1;185(1):15–22.

6. Robert D. Barker. Clinical tuberculosis. 6th Edition. Boca Raton: CRC Press; 2020.

7. Rodriguez-Takeuchi SY, Renjifo ME, Medina FJ. Extrapulmonary tuberculosis: Pathophysiology and imaging findings. Radiographics. 2019 Nov 1;39(7):2023–37.

8. Lee JY. Diagnosis and treatment of extrapulmonary tuberculosis. Vol. 78, Tuberculosis and Respiratory Diseases. Korean National Tuberculosis Association; 2015. p. 47–55.

9. Heye T, Stoijkovic M, Kauczor HU, Junghanss T, Hosch W. Extrapulmonale Tuberkulose: Die radiologische Bildgebung eines fast vergessenen Verwandlungskünstlers. RoFo Fortschritte auf dem Gebiet der Rontgenstrahlen und der Bildgebenden Verfahren. 2011;183(11):1019–29.

10. Prakoeswa FRS, Rumondor BB, Prakoeswa CRS. Acid-Fast Staining Revisited, a Dated but Versatile Means of Diagnosis. Open Microbiol J. 2022 Aug 17;16(1).

11. Jacobo-Delgado YM, Rodríguez-Carlos A, Serrano CJ, Rivas-Santiago B. Mycobacterium tuberculosis cell-wall and antimicrobial peptides: a mission impossible? Vol. 14, Frontiers in Immunology. Frontiers Media S.A.; 2023.

12. Cole ST BRPJGTCCHD et al. Deciphering the biology of Mycobacterium tuberculosis from the complete genome sequence. Nature. 1998 Jun;(393):537–44.

13. Maitra A, Munshi T, Healy J, Martin LT, Vollmer W, Keep NH, et al. Cell wall peptidoglycan in Mycobacterium tuberculosis: An Achilles' heel for the TB-causing pathogen. Vol. 43, FEMS Microbiology Reviews. Oxford University Press; 2019. p. 548–75.

14. Vilchèze C, Kremer L. Acid-Fast Positive and Acid-Fast Negative Mycobacterium tuberculosis: The Koch Paradox. Microbiology and Molecular Biology Reviews [Internet]. 2017 Dec;81(4). Available from: https://journals.asm.org/journal/spectrum

15. Sakula A. Robert koch: centenary of the discovery of the tubercle bacillus, 1882. Can Vet J. 1983 Apr;24(4):127-31. PMID: 17422248; PMCID: PMC1790283.

16. Cambau E, Drancourt M. Steps towards the discovery of Mycobacterium tuberculosis by Robert Koch, 1882. Vol. 20, Clinical Microbiology and Infection. Blackwell Publishing Ltd; 2014. p. 196–201.

17. Asante-Poku A, Huang H, Fan X. The impact of Mycobacterium tuberculosis complex in the environment on one health approach. Front Vet Sci. 2022;9.

18. Kanipe C, Palmer M V. Mycobacterium bovis and you: A comprehensive look at the bacteria, its similarities to Mycobacterium tuberculosis, and its relationship with human disease. Vol. 125, Tuberculosis. Churchill Livingstone; 2020.

19. Orgeur M, Sous C, Madacki J, Brosch R. Evolution and emergence of Mycobacterium tuberculosis. Vol. 48, FEMS Microbiology Reviews. Oxford University Press; 2024.

20. Sichewo PR, Etter EMC, Michel AL. Wildlife-cattle interactions emerge as drivers of bovine tuberculosis in traditionally farmed cattle. Prev Vet Med. 2020 Jan 1;174.

21. Silva ML, Cá B, Osório NS, Rodrigues PNS, Maceiras AR, Saraiva M. Tuberculosis caused by Mycobacterium africanum: Knowns and unknowns. Vol. 18, PLoS Pathogens. Public Library of Science; 2022.

22. Luca S, Mihaescu T. Maedica-a Journal of Clinical Medicine History of BCG Vaccine. Vol. 8, Maedica A Journal of Clinical Medicine. 2013.

23. Monteiro-Maia R, De Pinho RT. Oral bacillus Calmette-Guérin vaccine against tuberculosis: Why not? Mem Inst Oswaldo Cruz. 2014 Sep 1;109(6):838–45.

24. Martinez L, Cords O, Liu Q, Acuna-Villaorduna C, Bonnet M, Fox GJ, et al. Infant BCG vaccination and risk of pulmonary and extrapulmonary tuberculosis throughout the life course: a systematic review and individual participant data meta-analysis. Lancet Glob Health. 2022 Sep 1;10(9):e1307–16.

25. Schrager LK, Harris RC, Vekemans J. Research and development of new tuberculosis vaccines: A review . Vol. 7, F1000Research. F1000 Research Ltd; 2018.

26. Lai R, Ogunsola AF, Rakib T, Behar SM. Key advances in vaccine development for tuberculosis—success and challenges. Vol. 8, npj Vaccines. Nature Research; 2023.

27. Romano M, Squeglia F, Kramarska E, Barra G, Choi HG, Kim HJ, Ruggiero A, Berisio R. A Structural View at Vaccine Development against M. tuberculosis. Cells. 2023 Jan 14;12(2):317. doi: 10.3390/cells12020317. PMID: 36672252; PMCID: PMC9857197.

28. Zhuang L, Ye Z, Li L, Yang L, Gong W. Next-Generation TB Vaccines: Progress, Challenges, and Prospects. Vol. 11, Vaccines. Multidisciplinary Digital Publishing Institute (MDPI); 2023.

29. Alsayed SSR, Gunosewoyo H. Tuberculosis: Pathogenesis, Current Treatment Regimens and New Drug Targets. Vol. 24, International Journal of Molecular Sciences. Multidisciplinary Digital Publishing Institute (MDPI); 2023.

30. Lentz F, Reiling N, Martins A, Molnár J, Hilgeroth A. Discovery of novel enhancers of isoniazid toxicity in mycobacterium tuberculosis. Molecules. 2018;23(4).

31. World Health Organization. Meeting report of the WHO expert consultation on the definition of extensively drug-resistant tuberculosis, Geneva, Switzerland, 27–29 October 2020 [Internet]. Geneva: World Health Organization; 2021 [cited 2025 Apr 20]. Available from: https://apps.who.int/iris/handle/10665/340130

32. Keshavjee S, Farmer PE. Tuberculosis, Drug Resistance, and the History of Modern Medicine. New England Journal of Medicine. 2012 Sep 6;367(10):931–6.

33. Muthukrishnan L. Multidrug resistant tuberculosis – Diagnostic challenges and its conquering by nanotechnology approach – An overview. Vol. 337, Chemico-Biological Interactions. Elsevier Ireland Ltd; 2021.

34. Seung KJ, Keshavjee S, Rich ML. Multidrug-resistant tuberculosis and extensively drug-resistant tuberculosis. Cold Spring Harb Perspect Med. 2015 Sep 1;5(9).

35. Wulandari DA, Hartati YW, Ibrahim AU, Pitaloka DAE, Irkham. Multidrug-resistant tuberculosis. Vol. 559, Clinica Chimica Acta. Elsevier B.V.; 2024.

36. Houben RMGJ, Dodd PJ. The Global Burden of Latent Tuberculosis Infection: A Re-estimation Using Mathematical Modelling. PLoS Med. 2016 Oct 1;13(10).

37. Guidelines on the management of latent tuberculosis infection. World Health Organization; 2015. 33 p.

38. Vynnycky E, Fine PEM. The natural history of tuberculosis : the implications of age-dependent risks of disease and the role of reinfection. Epidemiol Infect. 1997;119(2):183–201.

39. Comstock GW LVWS. The prognosis of a positive tuberculin reaction in childhood and adolescence. Am J Epidemiol [Internet]. 1974 Feb;99(2). Available from: https://academic.oup.com/aje/article/99/2/131/162081

40. Kim HW, Kim JS. Treatment of latent tuberculosis infection and its clinical efficacy. Vol. 81, Tuberculosis and Respiratory Diseases. Korean National Tuberculosis Association; 2018. p. 6–12.

41. Kiazyk S, Ball TB. Latent tuberculosis infection: An overview. Canada Communicable Disease Report [Internet]. 2017 Apr 6;43(4):62–6. Available from: http://www.who.int/tb/

42. Fennelly KP, Martyny JW, Fulton KE, Orme IM, Cave DM, Heifets LB. Cough-generated Aerosols of Mycobacterium tuberculosis . Am J Respir Crit Care Med. 2004 Mar 1;169(5):604–9.

43. Shiloh MU. Mechanisms of mycobacterial transmission: How does Mycobacterium tuberculosis enter and escape from the human host. Vol. 11, Future Microbiology. Future Medicine Ltd.; 2016. p. 1503–6.

44. Kaufmann SHE. How can immunology contribute to the control of tuberculosis? Nat Rev Immunol [Internet]. 2001;1:20–30. Available from: www.nature.com/reviews/immunol

45. Cohen SB, Gern BH, Delahaye JL, Adams KN, Plumlee CR, Winkler JK, et al. Alveolar Macrophages Provide an Early Mycobacterium tuberculosis Niche and Initiate Dissemination. Cell Host Microbe. 2018 Sep 12;24(3):439-446.e4.

46. Russell DG. Who puts the tubercle in tuberculosis? Vol. 5, Nature Reviews Microbiology. 2007. p. 39–47.

47. Sakamoto K. The Pathology of Mycobacterium tuberculosis Infection. Vol. 49, Veterinary Pathology. 2012. p. 423–39.

48. Goenka A, Casulli J, Hussell T. Mycobacterium tuberculosis Joyrides Alveolar Macrophages into the Pulmonary Interstitium. Vol. 24, Cell Host and Microbe. Cell Press; 2018. p. 331–3.

49. Flynn JAL, Chan J. What's good for the host is good for the bug. Trends Microbiol. 2005;13(3):98–102.

50. Sankar P, Mishra BB. Early innate cell interactions with Mycobacterium tuberculosis in protection and pathology of tuberculosis. Vol. 14, Frontiers in Immunology. Frontiers Media SA; 2023.

51. Khader SA, Rangel-Moreno J, Fountain JJ, Martino CA, Reiley WW, Pearl JE, et al. In a Murine Tuberculosis Model, the Absence of Homeostatic Chemokines Delays Granuloma Formation and Protective Immunity. The Journal of Immunology. 2009 Dec 15;183(12):8004–14.

52. Rahman F. Characterizing the immune response to Mycobacterium tuberculosis: a comprehensive narrative review and implications in disease relapse. Vol. 15, Frontiers in Immunology. Frontiers Media SA; 2024.

53. Ndlovu H, Marakalala MJ. Granulomas and inflammation: Host-directed therapies for tuberculosis. Vol. 7, Frontiers in Immunology. Frontiers Media S.A.; 2016.

54. Reece ST, Kaufmann SHE. Floating between the poles of pathology and protection: Can we pin down the granuloma in tuberculosis? Vol. 15, Current Opinion in Microbiology. 2012. p. 63–70.

55. Guirado E, Schlesinger LS. Modeling the Mycobacterium tuberculosis granuloma - the critical battlefield in host immunity and disease. Front Immunol. 2013;4(APR).

56. Russell DG, Cardona PJ, Kim MJ, Allain S, Altare F. Foamy macrophages and the progression of the human tuberculosis granuloma. Vol. 10, Nature Immunology. 2009. p. 943–8.

57. Ulrichs T, Kaufmann SHE. New insights into the function of granulomas in human tuberculosis. Vol. 208, Journal of Pathology. 2006. p. 261–9.

58. Silva Miranda M, Breiman A, Allain S, Deknuydt F, Altare F. The tuberculous granuloma: An unsuccessful host defence mechanism providing a safety shelter for the bacteria? Vol. 2012, Clinical and Developmental Immunology. 2012.

59. Zhuang L, Yang L, Li L, Ye Z, Gong W. Mycobacterium tuberculosis: immune response, biomarkers, and therapeutic intervention. Vol. 5, MedComm. John Wiley and Sons Inc; 2024.

60. Chandra P, Grigsby SJ, Philips JA. Immune evasion and provocation by Mycobacterium tuberculosis. Vol. 20, Nature Reviews Microbiology. Nature Research; 2022. p. 750–66.

61. Bold TD, Ernst JD. Who Benefits from Granulomas, Mycobacteria or Host? Vol. 136, Cell. Elsevier B.V.; 2009. p. 17–9.

62. Lin Y, Zhang M, Barnes PF. Chemokine Production by a Human Alveolar Epithelial Cell Line in Response to Mycobacterium tuberculosis. Vol. 66, INFECTION AND IMMUNITY. 1998.

63. Wong KW. The Role of ESX-1 in Mycobacterium tuberculosis Pathogenesis . Microbiol Spectr. 2017 May 19;5(3).

64. Desjardins M, Huber LA, Parton RG, Griffiths G. Biogenesis of Phagolysosomes Proceeds through a Sequential Series of Interactions with the Endocytic Apparatus. J Cell Biol. 1994 Mar;124(5):677–88.

65. Coppens I, Romano JD. Sitting in the driver's seat: Manipulation of mammalian cell Rab GTPase functions by apicomplexan parasites. Vol. 112, Biology of the Cell. Wiley-Blackwell Publishing Ltd; 2020. p. 187–95.

66. Jin H, Tang Y, Yang L, Peng X, Li B, Fan Q, et al. Rab GTPases: Central Coordinators of Membrane Trafficking in Cancer. Vol. 9, Frontiers in Cell and Developmental Biology. Frontiers Media S.A.; 2021.

67. Eldridge BF, Lanzaro GC, Campbell GL, Reeves WC, Hardy JL, Lindsey HS, et al. Mosquito pools were assayed for virus accord-ing to the method described by method described by Lack of Acidification in Mycobacterium Phagosomes Produced by Exclusion of the Vesicular Proton-ATPase [Internet]. Vol. 5, J. Exp. Biol. Med. Sci. CRC Press; 1990. Available from: https://www.science.org

68. Queval CJ, Song OR, Carralot JP, Saliou JM, Bongiovanni A, Deloison G, et al. Mycobacterium tuberculosis Controls Phagosomal Acidification by Targeting CISH-Mediated Signaling. Cell Rep. 2017 Sep 26;20(13):3188–98.

69. Tiwari S, Casey R, Goulding CW, Hingley-Wilson S, Jacobs WR Jr. Infect and Inject: How Mycobacterium tuberculosis Exploits Its Major Virulence-Associated Type VII Secretion

System, ESX-1. Microbiol Spectr. 2019 May;7(3):10.1128/microbiolspec.bai-0024-2019. doi: 10.1128/microbiolspec.BAI-0024-2019. PMID: 31172908; PMCID: PMC6698389.

70. Huynh KK, Eskelinen EL, Scott CC, Malevanets A, Saftig P, Grinstein S. LAMP proteins are required for fusion of lysosomes with phagosomes. EMBO Journal. 2007 Jan 24;26(2):313–24.

71. Leake ES, Myrvik QN, Wright MJ. Phagosomal Membranes of Mycobacterium bovis BCG-Immune Alveolar Macrophages Are Resistant to Disruption by Mycobacterium tuberculosis H37Rv. INFECTION AND IMMUNITY. 1984.

72. Houben D, Demangel C, van Ingen J, Perez J, Baldeón L, Abdallah AM, et al. ESX-1-mediated translocation to the cytosol controls virulence of mycobacteria. Cell Microbiol. 2012 Aug;14(8):1287–98.

73. Weikert LF, Edwards K, Chroneos ZC, Hager C, Hoffman L, Shepherd VL, et al. SP-A enhances uptake of bacillus Calmette-Gu&in by macrophages through a specific SP-A receptor. Vol. 16, Lung Cell. Mol. Physiol. 1997.

74. Bob& DA, Frank' MM, Tenner' AJ. Clq acts synergistically with phorbol dibutyrate to activate CRl-mediated phagocytosis by human mononuclear phagocytes. Eur J Immunol [Internet]. 1988 [cited 2024 Aug 7];18:2001–7. Available from: https://onlinelibrary.wiley.com/doi/10.1002/eji.1830181220

75. McNab F, Mayer-Barber K, Sher A, Wack A, O'Garra A. Type I interferons in infectious disease. Vol. 15, Nature Reviews Immunology. Nature Publishing Group; 2015. p. 87–103.

76. Yu XH, Zheng XL, Tang CK. Nuclear Factor-κB Activation as a Pathological Mechanism of Lipid Metabolism and Atherosclerosis. Adv Clin Chem. 2015 Jan 1;70:1–30.

77. Grassin-Delyle S, Abrial C, Salvator H, Brollo M, Naline E, Devillier P. The Role of Toll-Like Receptors in the Production of Cytokines by Human Lung Macrophages. J Innate Immun. 2020 Jan 1;12(1):63–73.

78. Giacomini E, Iona E, Ferroni L, Miettinen M, Fattorini L, Orefici G, et al. Infection of Human Macrophages and Dendritic Cells with Mycobacterium tuberculosis Induces a Differential Cytokine Gene Expression That Modulates T Cell Response 1 [Internet]. Vol. 166, The Journal of Immunology. 2001. Available from: http://journals.aai.org/jimmunol/article-pdf/166/12/7033/1132156/7033.pdf

79. Mihret A. The role of dendritic cells in Mycobacterium tuberculosis infection. Virulence [Internet]. 2012;3(7):654–9. Available from: https://www.tandfonline.com/action/journalInformation?journalCode=kvir20

80. Khader SA, Partida-Sanchez S, Bell G, Jelley-Gibbs DM, Swain S, Pearl JE, et al. Interleukin 12p40 is required for dendritic cell migration and T cell priming after Mycobacterium tuberculosis infection. Journal of Experimental Medicine. 2006 Jul 10;203(7):1805–15.

81. Flynn JL, Chan J. IMMUNOLOGY OF TUBERCULOSIS. Annu Rev Immunol. 2001;

82. Flynn JL, Chan J, Triebold KJ, Dalton DK, Stewart TA, Bloom BR. An Essential Role for Interferon 7 in Resistance to Mycobacterium tuberculosis Infection.

83. Vaday GG, Franitza S, Schor H, Hecht I, Brill A, Cahalon L, et al. Combinatorial signals by inflammatory cytokines and chemokines mediate leukocyte interactions with extracellular matrix. J Leukoc Biol. 2001 Jun 1;69(6):885–92.

84. McDonald JC, LeBreton PR, Lee YT, Stenger S, Mazzaccaro RJ, Uyemura K, et al. Initiation of the adaptive immune response to Mycobacterium tuberculosis depends on antigen production in the local lymph node, not the lungs. Journal of Experimental Medicine [Internet]. 2008 Jan 21;56(9):2718. Available from: https://www.science.org

85. Koch R, Calmette A, Guérin C, Kaufmann SHE. Envisioning future strategies for vaccination against tuberculosis [Internet]. 2006. Available from: www.nature.com/reviews/immunol

86. Campbell KS, Hasegawa J. Natural killer cell biology: An update and future directions. Vol. 132, Journal of Allergy and Clinical Immunology. 2013. p. 536–44.

87. Cardona P, Cardona PJ. Regulatory T Cells in Mycobacterium tuberculosis Infection. Vol. 10, Frontiers in Immunology. Frontiers Media S.A.; 2019.

88. Tonaco MM, Moreira JD, Nunes FFC, Loures CMG, Souza LR, Martins JM, et al. Evaluation of profile and functionality of memory T cells in pulmonary tuberculosis. Immunol Lett. 2017 Dec 1;192:52–60.

89. Gupta A, Saqib M, Singh B, Pal L, Nishikanta A, Bhaskar S. Mycobacterium indicus pranii Induced Memory T-Cells in Lung Airways Are Sentinels for Improved Protection Against M.tb Infection. Front Immunol. 2019 Oct 18;10:2359. doi: 10.3389/fimmu.2019.02359. PMID: 31681272; PMCID: PMC6813244.

90. Narasimhan P, Wood J, Macintyre CR, Mathai D. Risk factors for tuberculosis. Pulmonary Medicine. Hindawi Publishing Corporation; 2013.

91. Russell DG, Barry CE, Flynn JL. Tuberculosis: What we don't know can, and does, hurt us. Vol. 328, Science. 2010. p. 852–6.

92. Cegielski JP, Mcmurray † D N. The relationship between malnutrition and tuberculosis: evidence from studies in humans and experimental animals. Vol. 8, INT J TUBERC LUNG DIS. 2004.

93. Kumar NP, Sridhar R, Banurekha V V., Jawahar MS, Fay MP, Nutman TB, et al. Type 2 diabetes mellitus coincident with pulmonary tuberculosis is associated with heightened systemic type 1, type 17, and other proinflammatory cytokines. Ann Am Thorac Soc. 2013 Oct;10(5):441–9.

94. Robert S. Wallis MBJWDB. Granulomatous Infections Due to Tumor Necrosis Factor Blockade: Correction. Clinical Infectious Diseases. 2004 Oct 15;39(8):1254–5.

95. Askling J, Fored CM, Brandt L, Baecklund E, Bertilsson L, Cöster L, et al. Risk and case characteristics of tuberculosis in rheumatoid arthritis associated with tumor necrosis factor antagonists in Sweden. Arthritis Rheum. 2005 Jul;52(7):1986–92.

96. Gómez-Reino JJ, Carmona L, Rodríguez Valverde V, Mola EM, Montero MD. Treatment of rheumatoid arthritis with tumor necrosis factor inhibitors may predispose to significant increase in tuberculosis risk: A multicenter active-surveillance report. Arthritis Rheum. 2003 Aug 1;48(8):2122–7.

97. Wolfe F, Michaud K, Anderson J, Urbansky K. Tuberculosis Infection in Patients with Rheumatoid Arthritis and the Effect of Infliximab Therapy. Vol. 50, Arthritis and Rheumatism. 2004. p. 372–9.

98. Corbett EL, Watt CJ, Neff Walker D;, Maher D, Williams BG, Raviglione MC, et al. The Growing Burden of Tuberculosis Global Trends and Interactions With the HIV Epidemic [Internet]. Available from: www.who.int/gtb/tbestimates

99. Kwan C, Ernst JD. HIV and tuberculosis: A deadly human syndemic. Vol. 24, Clinical Microbiology Reviews. 2011. p. 351–76.

100. Mendy J, Jarju S, Heslop R, Bojang AL, Kampmann B, Sutherland JS. Changes in Mycobacterium tuberculosis-specific immunity with influenza co-infection at time of TB diagnosis. Front Immunol. 2019;10(JAN).

101. Cobelens F, Nagelkerke N, Fletcher H. The convergent epidemiology of tuberculosis and human cytomegalovirus infection. F1000Res. 2018 Mar 6;7:280.

102. Ring S, Eggers L, Behrends J, Wutkowski A, Schwudke D, Kröger A, et al. Blocking IL-10 receptor signaling ameliorates Mycobacterium tuberculosis infection during influenza-induced exacerbation. JCI Insight. 2019;4(10).

103. Fowler K, Mucha J, Neumann M, Lewandowski W, Kaczanowska M, Grys M, et al. A systematic literature review of the global seroprevalence of cytomegalovirus: possible implications for treatment, screening, and vaccine development. BMC Public Health. 2022 Dec 1;22(1).

104. Sunil-Chandra NP, Jayasundara MVML, Gunathilaka MGRSS, Suminda SDH. Human cytomegalovirus (HCMV) trends in Sri Lanka: insights from a hospital-based seroprevalence analysis. BMC Infect Dis. 2025 Dec 1;25(1).

105. Cannon MJ, Schmid DS, Hyde TB. Review of cytomegalovirus seroprevalence and demographic characteristics associated with infection. Vol. 20, Reviews in Medical Virology. 2010. p. 202–13.

106. Zuhair M, Smit GSA, Wallis G, Jabbar F, Smith C, Devleesschauwer B, et al. Estimation of the worldwide seroprevalence of cytomegalovirus: A systematic review and meta-analysis. Vol. 29, Reviews in Medical Virology. John Wiley and Sons Ltd; 2019.

107. Hoehl S, Berger A, Ciesek S, Rabenau HF. Thirty years of CMV seroprevalence—a longitudinal analysis in a German university hospital. European Journal of Clinical Microbiology and Infectious Diseases. 2020 Jun 1;39(6):1095–102.

108. Manicklal S, Emery VC, Lazzarotto T, Boppana SB, Gupta RK. The "Silent" global burden of congenital cytomegalovirus. Clin Microbiol Rev. 2013 Jan;26(1):86–102.

109. Lachmann R, Loenenbach A, Waterboer T, Brenner N, Pawlita M, Michel A, et al. Cytomegalovirus (CMV) seroprevalence in the adult population of Germany. PLoS One. 2018 Jul 1;13(7).

110. Pass RF, Anderson B. Mother-to-child transmission of cytomegalovirus and prevention of congenital infection. J Pediatric Infect Dis Soc. 2014;3(SUPPL1).

111. Mocarski ES STPR. Fields Virology. In: Knipe DM HP, editor. Fields Virology [Internet]. 5th ed. Philadelphia: Lippincott Williams & Wilkins; 2007. p. 2701–72. Available from: https://www.researchgate.net/publication/239490323

112. Revello MG, Zavattoni M, Sarasini A, Percivalle E, Simoncini L, Gerna G. Human Cytomegalovirus in Blood of Immunocompetent Persons during Primary Infection: Prognostic Implications for Pregnancy [Internet]. Available from: https://academic.oup.com/jid/article/177/5/1170/803582

113. Griffiths P, Reeves M. Pathogenesis of human cytomegalovirus in the immunocompromised host. Vol. 19, Nature Reviews Microbiology. Nature Research; 2021. p. 759–73.

114. Bego MG, St. Jeor S. Human cytomegalovirus infection of cells of hematopoietic origin: HCMV-induced immunosuppression, immune evasion, and latency. Vol. 34, Experimental Hematology. 2006. p. 555–70.

115. Demmler-Harrison GJ. Congenital cytomegalovirus: Public health action towards awareness, prevention, and treatment. Journal of Clinical Virology. 2009 Dec;46(SUPPL. 4).

116. Mussi-Pinhata MM, Yamamoto AY, Brito RMM, De Isaac ML, De Carvalho E Oliveira PF, Boppana S, et al. Birth prevalence and natural history of congenital cytomegalovirus infection in a highly seroimmune population. Clinical Infectious Diseases. 2009 Aug 15;49(4):522–8.

117. Chiopris G, Veronese P, Cusenza F, Procaccianti M, Perrone S, Daccò V, et al. Congenital cytomegalovirus infection: Update on diagnosis and treatment. Vol. 8, Microorganisms. MDPI AG; 2020. p. 1–17.

118. Marsico C, Kimberlin DW. Congenital Cytomegalovirus infection: Advances and challenges in diagnosis, prevention and treatment. Vol. 43, Italian Journal of Pediatrics. BioMed Central Ltd.; 2017.

119. Perinat Med J, Casteels A, Naessens A, Gordts F, De Catte L, Bougatef A, et al. Casteels et al, Neonatal CMV screening Neonatal screening for congenital cytomegalovirus infections. 1999.

120. Kenneson A, Cannon MJ. Review and meta-analysis of the epidemiology of congenital cytomegalovirus (CMV) infection. Vol. 17, Reviews in Medical Virology. 2007. p. 253–76.

121. Grosse SD, Ross DS, Dollard SC. Congenital cytomegalovirus (CMV) infection as a cause of permanent bilateral hearing loss: A quantitative assessment. Vol. 41, Journal of Clinical Virology. 2008. p. 57–62.

122. Dollard SC, Grosse SD, Ross DS. New estimates of the prevalence of neurological and sensory sequelae and mortality associated with congenital cytomegalovirus infection. Rev Med Virol. 2007 Sep;17(5):355–63.

123. Zanghellini F, Boppana SB, Emery VC, Griffiths PD, Pass RF. Asymptomatic Primary Cytomegalovirus Infection: Virologic and Immunologic Features [Internet]. Available from: https://academic.oup.com/jid/article/180/3/702/810539

124. Crough T, Khanna R. Immimobiology of human cytomegalovirus: From bench to bedside. Vol. 22, Clinical Microbiology Reviews. 2009. p. 76–98.

125. Shin K, Seong GM, Yoo JR, Kim ET. Rapid and sensitive point-of-care diagnosis of human cytomegalovirus infection using RPA-CRISPR technology. Heliyon. 2024 Apr 15;10(7).

126. Brito LF, Brune W, Stahl FR. Cytomegalovirus (CMV) pneumonitis: Cell tropism, inflammation, and immunity. Vol. 20, International Journal of Molecular Sciences. MDPI AG; 2019.

127. Bigalke JM, Heldwein EE. Structural basis of membrane budding by the nuclear egress complex of herpesviruses. EMBO J. 2015 Dec 2;34(23):2921–36.

128. Sehrawat S, Kumar D, Rouse BT. Herpesviruses: Harmonious pathogens but relevant cofactors in other diseases? Vol. 8, Frontiers in Cellular and Infection Microbiology. Frontiers Media S.A.; 2018.

129. Mcgeoch DJ, Cook S, Dolan A, Jamieson FE, Telford EAR. Molecular Phylogeny and Evolutionary Timescale for the Family of Mammalian Herpesviruses. Vol. 247, J. Mol. Biol. 1995.

130. Dolan A, Cunningham C, Hector RD, Hassan-Walker AF, Lee L, Addison C, et al. Genetic content of wild-type human cytomegalovirus. Journal of General Virology. 2004;85(5):1301–12.

131. Charles OJ, Venturini C, Gantt S, Atkinson C, Griffiths P, Goldstein RA, et al. Genomic and geographical structure of human cytomegalovirus. Proc Natl Acad Sci U S A. 2023 Jul 25;120(30).

132. Cunha BA. Cytomegalovirus Pneumonia: Community-Acquired Pneumonia in Immunocompetent Hosts. Vol. 24, Infectious Disease Clinics of North America. 2010. p. 147–58.

133. Weller TH VWMPMM. Intranuclear inclusions in visceral disease. Journal of Pathology and Bacteriology. 1952;64(5):783–99.

134. Ho M. The history of cytomegalovirus and its diseases. Med Microbiol Immunol. 2008;197:65–73.

135. Ross SA, Novak Z, Pati S, Boppana SB. Diagnosis of Cytomegalovirus Infections.

136. Panda K, Parashar D, Viswanathan R. An Update on Current Antiviral Strategies to Combat Human Cytomegalovirus Infection. Vol. 15, Viruses. MDPI; 2023.

137. Fierro C, Brune D, Shaw M, Schwartz H, Knightly C, Lin J, et al. Safety and Immunogenicity of a Messenger RNA–Based Cytomegalovirus Vaccine in Healthy Adults: Results From a Phase 1 Randomized Clinical Trial. J Infect Dis. 2024 Sep 23;

138. Lischka P, Zimmermann H. Antiviral strategies to combat cytomegalovirus infections in transplant recipients. Vol. 8, Current Opinion in Pharmacology. 2008. p. 541–8.

139. Sullivan, V., Talarico, C., Stanat, S. et al. A protein kinase homologue controls phosphorylation of ganciclovir in human cytomegalovirus-infected cells. Nature 358, 162–164 (1992). https://doi.org/10.1038/358162a0. 1992.

140. Chen SJ, Wang SC, Chen YC. Antiviral agents as therapeutic strategies against cytomegalovirus infections. Vol. 12, Viruses. MDPI AG; 2019.

141. Humar A, Lebranchu Y, Vincenti F, Blumberg EA, Punch JD, Limaye AP, et al. The efficacy and safety of 200 days valganciclovir cytomegalovirus prophylaxis in high-risk kidney transplant recipients. American Journal of Transplantation. 2010;10(5):1228–37.

142. Lurain NS, Chou S. Antiviral drug resistance of human cytomegalovirus. Vol. 23, Clinical Microbiology Reviews. 2010. p. 689–712.

143. Santhanakrishnan K, Yonan N, Iyer K, Callan P, Al-aloul M, Venkateswaran R. Management of ganciclovir resistance cytomegalovirus infection with CMV hyperimmune globulin and

leflunomide in seven cardiothoracic transplant recipients and literature review. Transplant Infectious Disease. 2022 Feb 1;24(1).

144. Alfi O, From I, Yakirevitch A, Drendel M, Wolf M, Meir K, et al. Human Nasal Turbinate Tissues in Organ Culture as a Model for Human Cytomegalovirus Infection at the Mucosal Entry Site [Internet]. 2020. Available from: https://doi.org/10

145. Scrivano L, Sinzger C, Nitschko H, Koszinowski UH, Adler B. HCMV Spread and Cell Tropism are Determined by Distinct Virus Populations. 2011; Available from: www.plospathogens.org

146. Cimato G, Zhou X, Brune W, Frascaroli G. Human cytomegalovirus glycoprotein variants governing viral tropism and syncytium formation in epithelial cells and macrophages [Preprint]. bioRxiv [Internet]. 2024; Available from: https://doi.org/10.1101/2024.02.12.580040

147. Sinclair J. Human cytomegalovirus: Latency and reactivation in the myeloid lineage. Journal of Clinical Virology. 2008 Mar;41(3):180–5.

148. Sinclair J, Sissons P. Latency and reactivation of human cytomegalovirus. Vol. 87, Journal of General Virology. 2006. p. 1763–79.

149. Ye L, Qian Y, Yu W, Guo G, Wang H, Xue X. Functional Profile of Human Cytomegalovirus Genes and Their Associated Diseases: A Review. Vol. 11, Frontiers in Microbiology. Frontiers Media S.A.; 2020.

150. Nguyen CC, Kamil JP. Pathogen at the gates: Human cytomegalovirus entry and cell tropism. Vol. 10, Viruses. MDPI AG; 2018.

151. Kalejta RF, Albright ER. Expanding the Known Functional Repertoire of the Human Cytomegalovirus pp71 Protein. Vol. 10, Frontiers in Cellular and Infection Microbiology. Frontiers Media S.A.; 2020.

152. Kalejta RF. Functions of Human Cytomegalovirus Tegument Proteins Prior to Immediate Early Gene Expression.

153. Adamson CS, Nevels MM. Bright and early: Inhibiting human cytomegalovirus by targeting major immediate-early gene expression or protein function. Vol. 12, Viruses. MDPI AG; 2020.

154. Gruffat H, Marchione R, Manet E. Herpesvirus late gene expression: A viral-specific pre-initiation complex is key. Vol. 7, Frontiers in Microbiology. Frontiers Research Foundation; 2016.

155. Hook LM, Grey F, Grabski R, Tirabassi R, Doyle T, Hancock M, Landais I, Jeng S, McWeeney S, Britt W, Nelson JA. Cytomegalovirus miRNAs target secretory pathway genes to facilitate formation of the virion assembly compartment and reduce cytokine secretion. Cell Host Microbe. 2014 Mar 12;15(3):363-73. doi: 10.1016/j.chom.2014.02.004. PMID: 24629342; PMCID: PMC4029511.

156. Das S, Vasanji A, Pellett PE. Three-Dimensional Structure of the Human Cytomegalovirus Cytoplasmic Virion Assembly Complex Includes a Reoriented Secretory Apparatus. J Virol. 2007 Nov;81(21):11861–9.

157. Das S, Pellett PE. Spatial Relationships between Markers for Secretory and Endosomal Machinery in Human Cytomegalovirus-Infected Cells versus Those in Uninfected Cells. J Virol. 2011 Jun 15;85(12):5864–79.

158. Lee CH, Grey F. Systems Virology and Human Cytomegalovirus: Using High Throughput Approaches to Identify Novel Host-Virus Interactions During Lytic Infection. Vol. 10, Frontiers in Cellular and Infection Microbiology. Frontiers Media S.A.; 2020.

159. Jean Beltran PM, Cristea IM. The life cycle and pathogenesis of human cytomegalovirus infection: Lessons from proteomics. Vol. 11, Expert Review of Proteomics. Expert Reviews Ltd.; 2014. p. 697–711.

160. Akira S, Uematsu S, Takeuchi O. Pathogen recognition and innate immunity. Vol. 124, Cell. 2006. p. 783–801.

161. Medzhitov R. Recognition of microorganisms and activation of the immune response. Vol. 449, Nature. Nature Publishing Group; 2007. p. 819–26.

162. Boehme KW, Guerrero M, Compton T. Human Cytomegalovirus Envelope Glycoproteins B and H Are Necessary for TLR2 Activation in Permissive Cells. The Journal of Immunology. 2006 Nov 15;177(10):7094–102.

163. Gibson L, Donley S, Trzmielina S, Somasundaran M, Fisher D, Revello MG, et al. Cytomegalovirus (CMV) IE1- and pp65-specific CD8+ T cell responses broaden over time after primary CMV infection in infants. Journal of Infectious Diseases. 2007 Jun 15;195(12):1789–98.

164. Zhong B, Yang Y, Li S, Wang YY, Li Y, Diao F, et al. The Adaptor Protein MITA Links Virus-Sensing Receptors to IRF3 Transcription Factor Activation. Immunity. 2008 Oct 17;29(4):538–50.

165. Stahl FR, Heller K, Halle S, Keyser KA, Busche A, Marquardt A, et al. Nodular Inflammatory Foci Are Sites of T Cell Priming and Control of Murine Cytomegalovirus Infection in the Neonatal Lung. PLoS Pathog. 2013;9(12):1–18.

166. Lueder Y, Heller K, Ritter C, Keyser KA, Wagner K, Liu X, et al. Control of primary mouse cytomegalovirus infection in lung nodular inflammatory foci by cooperation of interferon-gamma expressing CD4 and CD8 T cells. PLoS Pathog. 2018 Aug 1;14(8).

167. Mihalić A, Železnjak J, Lisnić B, Jonjić S, Juranić Lisnić V, Brizić I. Immune surveillance of cytomegalovirus in tissues. Cell Mol Immunol [Internet]. 2024 Aug 12; Available from: http://www.ncbi.nlm.nih.gov/pubmed/39134803

168. Moretta A, Marcenaro E, Parolini S, Ferlazzo G, Moretta L. NK cells at the interface between innate and adaptive immunity. Vol. 15, Cell Death and Differentiation. 2008. p. 226–33.

169. Vivier E, Raulet DH, Moretta A, Caligiuri MA, Zitvogel L, Lanier LL, et al. Innate or adaptive immunity? The example of natural killer cells. Vol. 331, Science. 2011. p. 44–9.

170. Dell'Oste V, Biolatti M, Galitska G, Griffante G, Gugliesi F, Pasquero S, Zingoni A, Cerboni C, De Andrea M. Tuning the Orchestra: HCMV vs. Innate Immunity. Front Microbiol. 2020 Apr 15;11:661. doi: 10.3389/fmicb.2020.00661. PMID: 32351486; PMCID: PMC7174589.

171. Van De Berg PJ, Heutinck KM, Raabe R, Minnee RC, Young S La, Van Donselaar-Van Der Pant KA, et al. Human cytomegalovirus induces systemic immune activation characterized by a type 1 cytokine signature. Journal of Infectious Diseases. 2010 Sep 1;202(5):690–9.

172. Zangger N, Oderbolz J, Oxenius A. CD4 T Cell-Mediated Immune Control of Cytomegalovirus Infection in Murine Salivary Glands. Pathogens. 2021 Dec 1;10(12).

173. Hertoghs KML, Moerland PD, Van Stijn A, Remmerswaal EBM, Yong SL, Van De Berg PJEJ, et al. Molecular profiling of cytomegalovirus-induced human CD8+ T cell differentiation. Journal of Clinical Investigation. 2010 Nov 1;120(11):4077–90.

174. Gerna G, Sarasini A, Patrone M, Percivalle E, Fiorina L, Campanini G, et al. Human cytomegalovirus serum neutralizing antibodies block virus infection of endothelial/epithelial

cells, but not fibroblasts, early during primary infection. Journal of General Virology. 2008 Apr;89(4):853–65.

175. Zangger N, Oxenius A. T cell immunity to cytomegalovirus infection. Vol. 77, Current Opinion in Immunology. Elsevier Ltd; 2022.

176. Smith CJ, Venturi V, Quigley MF, Turula H, Gostick E, Ladell K, et al. Stochastic Expansions Maintain the Clonal Stability of CD8+ T Cell Populations Undergoing Memory Inflation Driven by Murine Cytomegalovirus. The Journal of Immunology. 2020 Jan 1;204(1):112–21.

177. Klenerman P, Oxenius A. T cell responses to cytomegalovirus. Vol. 16, Nature Reviews Immunology. Nature Publishing Group; 2016. p. 367–77.

178. Stockdale L, Nash S, Nalwoga A, Painter H, Asiki G, Fletcher H, et al. Human cytomegalovirus epidemiology and relationship to tuberculosis and cardiovascular disease risk factors in a rural Ugandan cohort. PLoS One. 2018 Feb 1;13(2).

179. Olaleye OD, Omilabu SA, Baba SS. Olaleye OD, Omilabu SA, Baba SS. Cytomegalovirus infection among tuberculosis patients in a chest hospital in Nigeria. Comp Immunol Microbiol Infect Dis. 1990;13(2):101-6. doi: 10.1016/0147-9571(90)90522-u. PMID: 2170073. Vol. 13, Comp. Immun. Microbiol. infect. Dis. 1990.

180. Stockdale L, Nash S, Nalwoga A, Gibson L, Painter H, Raynes J, et al. HIV, HCMV and mycobacterial antibody levels: a cross-sectional study in a rural Ugandan cohort. Tropical Medicine and International Health. 2019 Feb 1;24(2):247–57.

181. Müller J, Tanner R, Matsumiya M, Snowden MA, Landry B, Satti I, et al. Cytomegalovirus infection is a risk factor for tuberculosis disease in infants. JCI Insight. 2019 Dec 5;4(23).

182. Kim H, Shin SJ. Pathological and protective roles of dendritic cells in Mycobacterium tuberculosis infection: Interaction between host immune responses and pathogen evasion. Vol. 12, Frontiers in Cellular and Infection Microbiology. Frontiers Media S.A.; 2022.

183. Sinclair J, Reeves M. The intimate relationship between human cytomegalovirus and the dendritic cell lineage. Vol. 5, Frontiers in Microbiology. Frontiers Media S.A.; 2014.

184. Bayer C, Varani S, Wang L, Walther P, Zhou S, Straschewski S, et al. Human Cytomegalovirus Infection of M1 and M2 Macrophages Triggers Inflammation and Autologous T-Cell Proliferation. J Virol. 2013 Jan;87(1):67–79.

185. Olbrich L, Stockdale L, Roy RB, Song R, Cicin-Sain L, Whittaker E, et al. Understanding the interaction between cytomegalovirus and tuberculosis in children: The way forward. Vol. 17, PLoS Pathogens. Public Library of Science; 2021.

186. Marais BJ, Gie RP, Schaaf HS, Hesseling AC, Obihara CC, Starke JJ, et al. The natural history of childhood intra-thoracic tuberculosis: a critical review of literature from the pre-chemotherapy era [Internet]. Vol. 8, INT J TUBERC LUNG DIS. 2004. Available from: www.iuatld.org]

187. Tiwari D, Martineau AR. Inflammation-mediated tissue damage in pulmonary tuberculosis and host-directed therapeutic strategies. Vol. 65, Seminars in Immunology. Academic Press; 2023.

188. Wang YQ, Zhao XY. Human Cytomegalovirus Primary Infection and Reactivation: Insights From Virion-Carried Molecules. Vol. 11, Frontiers in Microbiology. Frontiers Media S.A.; 2020.

189. Loewendorf A, Benedict CA. Modulation of host innate and adaptive immune defenses by cytomegalovirus: Timing is everything: Symposium. In: Journal of Internal Medicine. 2010. p. 483–501.

190. Jackson SE, Redeker A, Arens R, van Baarle D, van den Berg SPH, Benedict CA, et al. CMV immune evasion and manipulation of the immune system with aging. Vol. 39, GeroScience. Springer International Publishing; 2017. p. 273–91.

191. Clement M, Marsden M, Stacey MA, Abdul-Karim J, Gimeno Brias S, Costa Bento D, et al. Cytomegalovirus-Specific IL-10-Producing CD4+T Cells Are Governed by Type-I IFN-Induced IL-27 and Promote Virus Persistence. PLoS Pathog. 2016 Dec 7;12(12).

192. Popkin DL, Watson MA, Karaskov E, Dunn GP, Bremner R, Virgin HW. Murine cytomegalovirus paralyzes macrophages by blocking IFN-induced promoter assembly [Internet]. 2003. Available from: www.pnas.orgcgidoi10.1073pnas.1835673100

193. Gredmark S, Söderberg-Nauclér C. Human Cytomegalovirus Inhibits Differentiation of Monocytes into Dendritic Cells with the Consequence of Depressed Immunological Functions. J Virol. 2003 Oct 15;77(20):10943–56.

194. Wolf AJ, Desvignes L, Linas B, Banaiee N, Tamura T, Takatsu K, et al. Initiation of the adaptive immune response to Mycobacterium tuberculosis depends on antigen production in the

local lymph node, not the lungs. Journal of Experimental Medicine. 2008 Jan 21;205(1):105–15.

195. Cooper AM. Cell-mediated immune responses in tuberculosis. Vol. 27, Annual Review of Immunology. 2009. p. 393–422.

196. Balthesen M, Messerle M, Reddehaset MJ. Lungs Are a Major Organ Site of Cytomegalovirus Latency and Recurrence. Vol. 67, JOURNAL OF VIROLOGY. 1993.

197. Wolf AJ, Desvignes L, Linas B, Banaiee N, Tamura T, Takatsu K, et al. Initiation of the adaptive immune response to Mycobacterium tuberculosis depends on antigen production in the local lymph node, not the lungs. Journal of Experimental Medicine. 2008 Jan 21;205(1):105–15.

198. Poole E, Juss JK, Krishna B, Herre J, Chilvers ER, Sinclair J. Alveolar macrophages isolated directly from human cytomegalovirus (HCMV)-seropositive individuals are sites of HCMV reactivation in vivo. Journal of Infectious Diseases. 2015 Jun 15;211(12):1936–42.

199. Cook CH, Trgovcich J, Zimmerman PD, Zhang Y, Sedmak DD. Lipopolysaccharide, Tumor Necrosis Factor Alpha, or Interleukin-1β Triggers Reactivation of Latent Cytomegalovirus in Immunocompetent Mice. J Virol. 2006 Sep 15;80(18):9151–8.

200. Caceres N, Llopis I, Marzo E, Prats C, Vilaplana C, de Viedma DG, et al. Low dose aerosol fitness at the innate phase of murine infection better predicts virulence amongst clinical strains of Mycobacterium tuberculosis. PLoS One. 2012 Jan 3;7(1).

201. Zhan L, Tang J, Sun M, Qin C. Animal models for tuberculosis in translational and precision medicine. Vol. 8, Frontiers in Microbiology. Frontiers Media S.A.; 2017.

202. Torrelles JB, Soldevilla P, Vilaplana C, Cardona PJ. Mouse Models for Mycobacterium tuberculosis Pathogenesis: Show and Do Not Tell. 2022; Available from: https://doi.org/10.3390/pathogens12010049

203. Dunn PL, North RJ. Persistent infection with virulent but not avirulent Mycobacterium tuberculosis in the lungs of mice causes progressive pathology. Vol. 45, J. Med. Microbiol. 1996.

204. Apt A, Kramnik I. Man and mouse TB: Contradictions and solutions. Vol. 89, Tuberculosis. 2009. p. 195–8.

205. Rhoades ER. Progression of chronic pulmonary tuberculosis in mice aerogenically infected with virulent Mycobacterium tuberculosis. Tubercle and Lung Disease. 1997 Jan 1;78(1):57–66.

206. David N. McMurray, Disease model: pulmonary tuberculosis, Trends in Molecular Medicine, Volume 7, Issue 3, 2001, Pages 135-137, ISSN 1471-4914, https://doi.org/10.1016/S1471-4914(00)01901-8. (https://www.sciencedirect.com/science/article/pii/S1471491400019018).

207. Driver ER, Ryan GJ, Hoff DR, Irwin SM, Basaraba RJ, Kramnik I, et al. Evaluation of a mouse model of necrotic granuloma formation using C3HeB/FeJ mice for testing of drugs against Mycobacterium tuberculosis. Antimicrob Agents Chemother. 2012 Jun;56(6):3181–95.

208. Chackerian AA, Alt JM, Perera T V., Dascher CC, Behar SM. Dissemination of Mycobacterium tuberculosis is influenced by host factors and precedes the initiation of T-cell immunity. Infect Immun. 2002;70(8):4501–9.

209. Wallgren A. The Time-Table of Tuberculosis.

210. Filipe-Santos O, Bustamante J, Chapgier A, Vogt G, de Beaucoudrey L, Feinberg J, et al. Inborn errors of IL-12/23- and IFN-γ-mediated immunity: molecular, cellular, and clinical features. Vol. 18, Seminars in Immunology. Academic Press; 2006. p. 347–61.

211. Cooper AM, Magram J, Ferrante J, Orme IM. Interleukin 12 (IL-12) Is Crucial to the Development of Protective Immunity in Mice Intravenously Infected with Mycobacterium tuberculosis. Vol. 186, J. Exp. Med. 1997.

212. Cooper AM, Dalton DK, Stewart TA, Griffin JP, Russell DG, Orme IM. Disseminated Tuberculosis in Interferon 7 Gene-disrupted Mice.

213. Cooper AM. Mouse Model of Tuberculosis [Internet]. Available from: www.perspectivesinmedicine.org

214. Soldevilla P, Vilaplana C, Cardona PJ. Mouse Models for Mycobacterium tuberculosis Pathogenesis: Show and Do Not Tell. Vol. 12, Pathogens. MDPI; 2023.

215. Kramnik I, Beamer G. Mouse models of human TB pathology: roles in the analysis of necrosis and the development of host-directed therapies.

216. A Mouse Model for Cytomegalovirus Infection. 1999.

217. Gabel M, Baumann NS, Oxenius A, Graw F. Investigating the dynamics of MCMV-specific CD8+ T cell responses in individual hosts. Front Immunol. 2019;10(JUN).

218. Dupont L, Reeves MB. Cytomegalovirus latency and reactivation: recent insights into an age old problem. Reviews in Medical Virology. John Wiley and Sons Ltd; 2016. p. 75–89.

219. Reddehase MJ, Rgen Podlech J, Grzimek NKA. Mouse models of cytomegalovirus latency: overview [Internet]. Available from: www.elsevier.com/locate/jcv

220. Brizić I, Lisnić B, Krstanović F, Brune W, Hengel H, Jonjić S. Mouse Models for Cytomegalovirus Infections in Newborns and Adults. Curr Protoc. 2022 Sep 1;2(9).

221. Shanley JD, Morningstar J, Colin AM. Inhibition of Murine Cytomegalovirus Lung Infection and Interstitial Pneumonitis by Acyclovir and 9-(1,3-Dihydroxy-2-Propoxymethyl)Guanine. Vol. 28, ANTIMICROBIAL AGENTS AND CHEMOTHERAPY. 1985.

222. Reddehase MJ, Lemmermann NAW. Mouse Model of Cytomegalovirus Disease and Immunotherapy in the Immunocompromised Host: Predictions for Medical Translation that Survived the “Test of Time.” 2018; Available from: www.mdpi.com/journal/viruses

223. Riddell SR, Watanabe KS, Goodrich JM, Li CR, Agha ME, Greenberg PD. Restoration of Viral Immunity in Immunodeficient Humans by the Adoptive Transfer of T Cell Clones [Internet]. Available from: www.sciencemag.org

224. Bukowski JF WJDGWRM. Adoptive transfer studies demonstrating the antiviral effect of natural killer cells in vivo. J Exp Med. 1985 Apr 1;161(2):409–26.

225. Bukowski JF, Woda BA, Welsh’ RM. Pathogenesis of Murine Cytomegalovirus Infection in Natural Killer Cell-Depleted Mice [Internet]. Vol. 52, JOURNAL OF VIROLOGY. 1984. Available from: https://journals.asm.org/journal/jvi

226. Vivier E, Tomasello E, Baratin M, Walzer T, Ugolini S. Functions of natural killer cells. Vol. 9, Nature Immunology. 2008. p. 503–10.

227. Lee SH, Girard S, Macina D, Busà M, Zafer A, Belouchi A, et al. Susceptibility to mouse cytomegalovirus is associated with deletion of an activating natural killer cell receptor of the C-type lectin superfamily [Internet]. 2001. Available from: http://genetics.nature.com/supplementary_info/

228. Björkström NK, Strunz B, Ljunggren HG. Natural killer cells in antiviral immunity. Vol. 22, Nature Reviews Immunology. Nature Research; 2022. p. 112–23.

229. Arase H, Mocarski ES, Campbell AE, Hill AB, Lanier LL. 8. C. A. Nelson, in Developmental Neurocognition: Speech and Face Processing in the First Year of Life [Internet]. Vol. 10, J. Cogn. Neurosci. MIT Press; 2001. Available from: www.sciencemag.org/cgi/content/full/296/5571/1321/DC1

230. Handke W, Luig C, Popović B, Krmpotić A, Jonjić S, Brune W. Viral Inhibition of BAK Promotes Murine Cytomegalovirus Dissemination to Salivary Glands. J Virol. 2013 Mar 15;87(6):3592–6.

231. Harvey DM, Levine AJ. Harvey DM, Levine AJ. p53 alteration is a common event in the spontaneous immortalization of primary BALB/c murine embryo fibroblasts. Genes Dev. 1991 Dec;5(12B):2375-85. doi: 10.1101/gad.5.12b.2375. PMID: 1752433.

232. Jordan S, Krause J, Prager A, Mitrovic M, Jonjic S, Koszinowski UH, et al. Virus Progeny of Murine Cytomegalovirus Bacterial Artificial Chromosome pSM3fr Show Reduced Growth in Salivary Glands due to a Fixed Mutation of MCK-2. J Virol. 2011 Oct;85(19):10346–53.

233. Karsten Tischer B, Smith GA, Osterrieder N. En passant mutagenesis: A Two Markerless red recombination system. Methods in Molecular Biology. 2010;634:421–30.

234. Zurbach KA, Moghbeli T, Snyder CM. Resolving the titer of murine cytomegalovirus by plaque assay using the M2-10B4 cell line and a low viscosity overlay. Virol J. 2014 Apr 18;11(1).

235. Bankhead P, Loughrey MB, Fernández JA, Dombrowski Y, McArt DG, Dunne PD, et al. QuPath: Open source software for digital pathology image analysis. Sci Rep. 2017 Dec 1;7(1).

236. Stockdale L, Nash S, Farmer R, Raynes J, Mallikaarjun S, Newton R, et al. Cytomegalovirus antibody responses associated with increased risk of tuberculosis disease in ugandan adults. Journal of Infectious Diseases. 2020;221(7):1127–34.

237. Darboe F, Reijneveld JF, Maison DP, Martinez L, Suliman S. Unmasking the hidden impact of viruses on tuberculosis risk. Vol. 45, Trends in Immunology. Elsevier Ltd; 2024. p. 649–61.

238. Krmpotic A, Bubic I, Polic B, Lucin P, Jonjic S. Pathogenesis of murine cytomegalovirus infection. Vol. 5, Microbes and Infection. Elsevier Masson SAS; 2003. p. 1263–77.

239. Voigt V, Forbes CA, Tonkin JN, Degli-Esposti MA, C Smith HR, Yokoyama WM, et al. Murine cytomegalovirus m157 mutation and variation leads to immune evasion of natural killer cells [Internet]. 2003. Available from: www.pnas.orgcgidoi10.1073pnas.2233572100

240. Smith HRC, Heusel JW, Mehta IK, Kim S, Dorner BG, Naidenko O V, et al. Recognition of a virus-encoded ligand by a natural killer cell activation receptor [Internet]. 2002. Available from: www.pnas.orgcgidoi10.1073pnas.092258599

241. Bubić I, Wagner M, Krmpotić A, Saulig T, Kim S, Yokoyama WM, et al. Gain of Virulence Caused by Loss of a Gene in Murine Cytomegalovirus. J Virol. 2004 Jul 15;78(14):7536–44.

242. Oduro JD, Redeker A, Lemmermann NAW, Ebermann L, Marandu TF, Dekhtiarenko I, et al. Murine cytomegalovirus (CMV) infection via the intranasal route offers a robust model of immunity upon mucosal CMV infection. Journal of General Virology. 2016 Jan 1;97(1):185–95.

243. Busche A, Marquardt A, Bleich A, Ghazal P, Angulo A, Messerle M. The Mouse Cytomegalovirus Immediate-Early 1 Gene Is Not Required for Establishment of Latency or for Reactivation in the Lungs. J Virol. 2009 May;83(9):4030–8.

244. Liu XF, Wang X, Yan S, Zhang Z, Abecassis M, Hummel M. Epigenetic control of cytomegalovirus latency and reactivation. Viruses. 2013 May 22;5(5):1325–45.

245. Cook CH, Zhang Y, Sedmak DD, Martin LC, Jewell S, Ferguson RM. PULMONARY CYTOMEGALOVIRUS REACTIVATION CAUSES PATHOLOGY IN IMMUNOCOMPETENT MICE.

246. Brizić I, Šušak B, Arapović M, Huszthy PC, Hiršl L, Kveštak D, et al. Brain-resident memory CD8+ T cells induced by congenital CMV infection prevent brain pathology and virus reactivation. Eur J Immunol. 2018 Jun 1;48(6):950–64.

247. Flynn JAL, Chan J. Immune cell interactions in tuberculosis. Vol. 185, Cell. Elsevier B.V.; 2022. p. 4682–702.

248. Zhuang L, Yang L, Li L, Ye Z, Gong W. Mycobacterium tuberculosis: immune response, biomarkers, and therapeutic intervention. Vol. 5, MedComm. John Wiley and Sons Inc; 2024.

249. Kumar VG, Urs TA, Ranganath RR. MPT 64 Antigen detection for rapid confirmation of M.tuberculosis isolates. BMC Res Notes. 2011;4.

250. Stamm CE, Pasko BL, Chaisavaneeyakorn S, Franco LH, Nair VR, Weigele BA, et al. Screening Mycobacterium tuberculosis Secreted Proteins Identifies Mpt64 as a Eukaryotic Membrane-Binding Bacterial Effector. 2019; Available from: https://doi.org/10.1128/mSphere

251. Tan CSE, Frederico B, Stevenson PG. Herpesvirus delivery to the murine respiratory tract. J Virol Methods. 2014 Sep 15;206:105–14.

252. Brizić I, Lisnić B, Brune W, Hengel H, Jonjić S. Cytomegalovirus Infection: Mouse Model. Curr Protoc Immunol. 2018 Aug 1;122(1):e51.

253. Speck SH, Ganem D. Viral latency and its regulation: lessons from the gammaherpesviruses. 2010.

254. Lieberman PM. Epigenetics and Genetics of Viral Latency. Vol. 19, Cell Host and Microbe. Cell Press; 2016. p. 619–28.

255. Forte E, Zhang Z, Thorp EB, Hummel M. Cytomegalovirus Latency and Reactivation: An Intricate Interplay With the Host Immune Response. Vol. 10, Frontiers in Cellular and Infection Microbiology. Frontiers Media S.A.; 2020.

256. Isham IM, Najimudeen SM, Cork SC, Gupta A, Abdul-Careem MF. Comparison of quantitative PCR and digital PCR assays for quantitative detection of infectious bronchitis virus (IBV) genome. J Virol Methods. 2024 Feb 1;324.

257. Brands C, Morcock D, Estes J, Deleage C. Next-generation viral RNA/DNA in situ hybridization applications in human immunodeficiency virus/simian immunodeficiency virus research. Journal of Visualized Experiments. 2020 Jun 1;2020(160):1–13.

258. Kondo Y, Shen L, Yan PS, Hui T, Huang M, Issa JPJ. Chromatin immunoprecipitation microarrays for identification of genes silenced by histone H3 lysine 9 methylation [Internet]. 2004. Available from: www.microarrays.org.

259. Mitrović M, Arapović J, Jordan S, Fodil-Cornu N, Ebert S, Vidal SM, et al. The NK Cell Response to Mouse Cytomegalovirus Infection Affects the Level and Kinetics of the Early CD8 + T-Cell Response . J Virol. 2012 Feb 15;86(4):2165–75.

260. Alexandre YO, Cocita CD, Ghilas S, Dalod M. Deciphering the role of DC subsets in MCMV infection to better understand immune protection against viral infections. Vol. 5, Frontiers in Microbiology. Frontiers Research Foundation; 2014.

261. Reddehase MJ, Lemmermann NAW. Mouse model of cytomegalovirus disease and immunotherapy in the immunocompromised host: Predictions for medical translation that survived the “test of time.” Vol. 10, Viruses. MDPI AG; 2018.

262. Munks MW, Cho KS, Pinto AK, Sierro S, Klenerman P, Hill AB. Four Distinct Patterns of Memory CD8 T Cell Responses to Chronic Murine Cytomegalovirus Infection 1 [Internet].

Vol. 177, The Journal of Immunology. 2006. Available from: http://journals.aai.org/jimmunol/article-pdf/177/1/450/1221716/zim01306000450.pdf

263. Seefried M, Hundhausen N, Kroeger I, Büttner-Herold M, Hoffmann P, Edinger M, et al. Murine cytomegalovirus reactivation concomitant with acute graft-versus-host disease is controlled by antibodies. JCI Insight. 2023 Mar 8;8(5).

264. Holzki JK, Dağ F, Dekhtiarenko I, Rand U, Casalegno-Garduño R, Trittel S, et al. Type I Interferon Released by Myeloid Dendritic Cells Reversibly Impairs Cytomegalovirus Replication by Inhibiting Immediate Early Gene Expression. J Virol. 2015 Oct;89(19):9886–95.

265. Zhang S, Springer LE, Rao HZ, Espinosa Trethewy RG, Bishop LM, Hancock MH, et al. Hematopoietic cell-mediated dissemination of murine cytomegalovirus is regulated by NK cells and immune evasion. PLoS Pathog. 2021 Jan 28;17(1).

266. Brisse E, Imbrechts M, Put K, Avau A, Mitera T, Berghmans N, et al. Mouse Cytomegalovirus Infection in BALB/c Mice Resembles Virus-Associated Secondary Hemophagocytic Lymphohistiocytosis and Shows a Pathogenesis Distinct from Primary Hemophagocytic Lymphohistiocytosis. The Journal of Immunology. 2016 Apr 1;196(7):3124–34.

267. Shimada T, Higashida-Konishi M, Izumi K, Hama S, Oshige T, Oshima H, et al. Risk factors associated with cytomegalovirus reactivation in patients receiving immunosuppressive therapy for rheumatic diseases: a retrospective study. Sci Rep. 2022 Dec 1;12(1).

268. Vu A, Glassman I, Campbell G, Yeganyan S, Nguyen J, Shin A, et al. Host Cell Death and Modulation of Immune Response against Mycobacterium tuberculosis Infection. Vol. 25, International Journal of Molecular Sciences. Multidisciplinary Digital Publishing Institute (MDPI); 2024.

269. Dibbern J, Eggers L, Schneider BE. Sex differences in the C57BL/6 model of Mycobacterium tuberculosis infection. Sci Rep. 2017 Dec 1;7(1).

270. Sitnik KM, Krstanović F, Gödecke N, Rand U, Kubsch T, Maaß H, et al. Fibroblasts are a site of murine cytomegalovirus lytic replication and Stat1-dependent latent persistence in vivo. Nat Commun. 2023 Dec 1;14(1).

271. Zhang S, Caldeira-Dantas S, Smith CJ, Snyder CM. Persistent viral replication and the development of T-cell responses after intranasal infection by MCMV. Med Microbiol Immunol. 2019 Aug 1;208(3–4):457–68.

272. Nhamoyebonde S, Leslie A. Biological differences between the sexes and susceptibility to tuberculosis. Journal of Infectious Diseases. 2014;209(SUPPL. 3).

273. vom Steeg LG, Klein SL. SeXX Matters in Infectious Disease Pathogenesis. Vol. 12, PLoS Pathogens. Public Library of Science; 2016.

274. Pujantell M, Altfeld M. Consequences of sex differences in Type I IFN responses for the regulation of antiviral immunity. Vol. 13, Frontiers in Immunology. Frontiers Media S.A.; 2022.

275. Traub S, Demaria O, Chasson L, Serra F, Desnues B, Alexopoulou L. Sex Bias in Susceptibility to MCMV Infection: Implication of TLR9. PLoS One. 2012 Sep 20;7(9).

276. Perry WA, Gardiner BJ, Price LL, Rodriguez-Garcia M, Chow JK, Snydman DR. Female sex and advanced age are associated with invasive cytomegalovirus disease in solid organ transplant recipients. Transplant Infectious Disease. 2022 Dec 1;24(6).

277. Geurs TL, Hill EB, Lippold DM, French AR. Sex differences in murine susceptibility to systemic viral infections. J Autoimmun. 2012 May;38(2–3).

278. Hertz D, Dibbern J, Eggers L, von Borstel L, Schneider BE. Increased male susceptibility to Mycobacterium tuberculosis infection is associated with smaller B cell follicles in the lungs. Sci Rep. 2020 Dec 1;10(1).

279. Klein SL, Flanagan KL. Sex differences in immune responses. Vol. 16, Nature Reviews Immunology. Nature Publishing Group; 2016. p. 626–38.

280. Klein SL. Immune cells have sex and so should journal articles. Vol. 153, Endocrinology. 2012. p. 2544–50.

281. Picarda G, Benedict CA. Cytomegalovirus: Shape-Shifting the Immune System. The Journal of Immunology. 2018 Jun 15;200(12):3881–9.

282. Furman D, Jojic V, Sharma S, Shen-Orr SS, Angel CJL, Onengut-Gumuscu S, et al. Cytomegalovirus infection enhances the immune response to influenza. Sci Transl Med. 2015 Apr 1;7(281).

283. Pera A, Vasudev A, Tan C, Kared H, Solana R, Larbi A. CMV induces expansion of highly polyfunctional CD4+ T cell subset coexpressing CD57 and CD154. J Leukoc Biol. 2017 Feb 1;101(2):555–66.

284. Pera A, Campos C, Corona A, Sanchez-Correa B, Tarazona R, Larbi A, et al. CMV latent infection improves CD8+ T response to SEB due to expansion of polyfunctional CD57+ cells in young individuals. PLoS One. 2014 Feb 12;9(2).

285. Sandalova E, Laccabue D, Boni C, Tan AT, Fink K, Ooi EE, et al. Contribution of herpesvirus specific CD8 T cells to anti-viral T cell response in humans. PLoS Pathog. 2010 Aug;6(8):47–8.

286. Barton ES, White DW, Cathelyn JS, Brett-McClellan KA, Engle M, Diamond MS, et al. Herpesvirus latency confers symbiotic protection from bacterial infection. Nature. 2007 May 17;447(7142):326–9.

287. Domingo-Gonzalez R, Prince O, Cooper A, Khader SA. Cytokines and Chemokines in Mycobacterium tuberculosis Infection . Microbiol Spectr. 2016 Oct 14;4(5).

288. Salazar-Mather TP, Hokeness · K L. Cytokine and Chemokine Networks: Pathways to Antiviral Defense. Vol. 303, CTMI. Springer-Verlag; 2006.

289. Mayer-Barber KD, Andrade BB, Barber DL, Hieny S, Feng CG, Caspar P, et al. Innate and Adaptive Interferons Suppress IL-1α and IL-1β Production by Distinct Pulmonary Myeloid Subsets during Mycobacterium tuberculosis Infection. Immunity. 2011 Dec 23;35(6):1023–34.

290. Flynn JL, Goldstein MM, Chan J, Triebold,' KJ, Pfeffersps K, Lowensteln CJ, et al. Tumor Necrosis Factor-u Is Required in the Protective Immune Response Against Mycobacterium tuberculosis in Mice. Vol. 2, Immunity. 1995.

291. Bean AGD, Roach DR, Briscoe H, France MP, Korner H, Sedgwick JD, et al. Structural Deficiencies in Granuloma Formation in TNF Gene-Targeted Mice Underlie the Heightened Susceptibility to Aerosol Mycobacterium tuberculosis Infection, Which Is Not Compensated for by Lymphotoxin 1 [Internet]. Vol. 162, The Journal of Immunology. 1999. Available from: http://journals.aai.org/jimmunol/article-pdf/162/6/3504/1097197/im069903504o.pdf

292. Chang D, Dela Cruz C, Sharma L. Beneficial and Detrimental Effects of Cytokines during Influenza and COVID-19. Vol. 16, Viruses. Multidisciplinary Digital Publishing Institute (MDPI); 2024.

293. Silvério D, Gonçalves R, Appelberg R, Saraiva M. Advances on the Role and Applications of Interleukin-1 in Tuberculosis. Vol. 12, mBio. American Society for Microbiology; 2021.

294. Yuk JM, Kim JK, Kim IS, Jo EK. TNF in Human Tuberculosis: A Double-Edged Sword. Vol. 24, Immune Network. Korean Association of Immunologists; 2024.

295. Dorhoi A, Kaufmann SHE. Tumor necrosis factor alpha in mycobacterial infection. Vol. 26, Seminars in Immunology. Academic Press; 2014. p. 203–9.

296. Green AM, DiFazio R, Flynn JL. IFN-γ from CD4 T Cells Is Essential for Host Survival and Enhances CD8 T Cell Function during Mycobacterium tuberculosis Infection . The Journal of Immunology. 2013 Jan 1;190(1):270–7.

297. Boni FG, Hamdi I, Koundi LM, Shrestha K, Xie J. Cytokine storm in tuberculosis and IL-6 involvement. Vol. 97, Infection, Genetics and Evolution. Elsevier B.V.; 2022.

298. Guzmán-Beltrán S, Carreto-Binaghi LE, Carranza C, Torres M, Gonzalez Y, Muñoz-Torrico M, et al. Oxidative stress and inflammatory mediators in exhaled breath condensate of patients with pulmonary tuberculosis. A pilot study with a biomarker perspective. Antioxidants. 2021 Oct 1;10(10).

299. Kumar NP, Moideen K, Banurekha V V., Nair D, Babu S. Plasma proinflammatory cytokines are markers of disease severity and bacterial burden in pulmonary tuberculosis. Open Forum Infect Dis. 2019 Jun 5;6(7).

300. Munn DH, Mellor AL. Indoleamine 2,3 dioxygenase and metabolic control of immune responses. Vol. 34, Trends in Immunology. 2013. p. 137–43.

301. Li Q, Harden JL, Anderson CD, Egilmez NK. Tolerogenic Phenotype of IFN-γ–Induced IDO+ Dendritic Cells Is Maintained via an Autocrine IDO–Kynurenine/AhR–IDO Loop. The Journal of Immunology. 2016 Aug 1;197(3):962–70.

302. Cobbold SP, Adams E, Farquhar CA, Nolan KF, Howie D, Lui KO, et al. Infectious tolerance via the consumption of essential amino acids and mTOR signaling [Internet]. 2009. Available from: www.pnas.org/cgi/content/full/

303. Jürgens B, Hainz U, Fuchs D, Felzmann T, Heitger A. Interferon-γ-triggered indoleamine 2,3-dioxygenase competence in human monocyte-derived dendritic cells induces regulatory activity in allogeneic T cells. Blood. 2009;114(15):3235–43.

304. Munn DH, Sharma MD, Baban B, Harding HP, Zhang Y, Ron D, et al. GCN2 kinase in T cells mediates proliferative arrest and anergy induction in response to indoleamine 2,3-dioxygenase. Immunity. 2005 May;22(5):633–42.

305. Almanan M, Raynor J, Sholl A, Wang M, Chougnet C, Cardin RD, et al. Tissue-specific control of latent CMV reactivation by regulatory T cells. PLoS Pathog. 2017 Aug 1;13(8).

306. Slobedman B, Mocarski ES. Mechanisms modulating immune clearance during human cytomegalovirus latency. Vol. 109, Proceedings of the National Academy of Sciences of the United States of America. 2012. p. 14291–2.

307. Mishra BB, Rathinam VAK, Martens GW, Martinot AJ, Kornfeld H, Fitzgerald KA, et al. Nitric oxide controls the immunopathology of tuberculosis by inhibiting NLRP3 inflammasome-dependent processing of IL-1β. Nat Immunol. 2013 Jan;14(1):52–60.

308. Mao K, Chen S, Chen M, Ma Y, Wang Y, Huang B, et al. Nitric oxide suppresses NLRP3 inflammasome activation and protects against LPS-induced septic shock. Cell Res. 2013 Feb;23(2):201–12.

309. Hernandez-Cuellar E, Tsuchiya K, Hara H, Fang R, Sakai S, Kawamura I, et al. Cutting Edge: Nitric Oxide Inhibits the NLRP3 Inflammasome. The Journal of Immunology. 2012 Dec 1;189(11):5113–7.

310. Slight SR, Khader SA. Chemokines shape the immune responses to tuberculosis. Vol. 24, Cytokine and Growth Factor Reviews. 2013. p. 105–13.

311. Tokunaga R, Zhang W, Naseem M, Puccini A, Berger MD, Soni S, et al. CXCL9, CXCL10, CXCL11/CXCR3 axis for immune activation – A target for novel cancer therapy. Vol. 63, Cancer Treatment Reviews. W.B. Saunders Ltd; 2018. p. 40–7.

312. Arbués A, Schmidiger S, Reinhard M, Borrell S, Gagneux S, Portevin D. CXCL9, granzyme B and TNF-α orchestrate protective in vitro granulomatous responses across Mycobacterium tuberculosis complex lineages [Internet]. 2024. Available from: https://elifesciences.org/reviewed-preprints/99062v1

313. Wehrens EJ, Wong KA, Gupta A, Khan A, Benedict CA, Zuniga EI. IL-27 regulates the number, function and cytotoxic program of antiviral CD4 T cells and promotes cytomegalovirus persistence. PLoS One. 2018 Jul 1;13(7).

314. Morita Y, Masters EA, Schwarz EM, Muthukrishnan G. Interleukin-27 and Its Diverse Effects on Bacterial Infections. Vol. 12, Frontiers in Immunology. Frontiers Media S.A.; 2021.

315. Indramohan M, Sieve AN, Break TJ, Berg RE. Inflammatory monocyte recruitment is regulated by interleukin-23 during systemic bacterial infection. Infect Immun. 2012;80(12):4099–105.

316. Khader SA, Guglani L, Rangel-Moreno J, Gopal R, Fallert Junecko BA, Fountain JJ, et al. IL-23 Is Required for Long-Term Control of Mycobacterium tuberculosis and B Cell Follicle Formation in the Infected Lung . The Journal of Immunology. 2011 Nov 15;187(10):5402–7.

317. Chemaitelly H, Ayoub HH, Coyle P, Tang P, Hasan MR, Yassine HM, et al. Differential protection against SARS-CoV-2 reinfection pre- and post-Omicron. Nature [Internet]. 2025 Feb 5; Available from: http://www.ncbi.nlm.nih.gov/pubmed/39910292

318. Yang C, Liu Z, Yang Y, Cocka LJ, Li Y, Zeng W, et al. Chronic viral infection impairs immune memory to a different pathogen. PLoS Pathog. 2024 Mar 1;20(3).

319. Smith CJ, Caldeira-Dantas S, Turula H, Snyder CM. Murine CMV Infection Induces the Continuous Production of Mucosal Resident T Cells. Cell Rep. 2015 Nov 10;13(6):1137–48.

320. Nandi B, Behar SM. Regulation of neutrophils by interferon-γ limits lung inflammation during tuberculosis infection. Journal of Experimental Medicine. 2011 Oct 24;208(11):2251–62.

321. Shanmuganathan G, Orujyan D, Narinyan W, Poladian N, Dhama S, Parthasarathy A, et al. Role of Interferons in Mycobacterium tuberculosis Infection. Clin Pract. 2022 Oct 1;12(5):788–96.

322. Lyadova I V. Neutrophils in Tuberculosis: Heterogeneity Shapes the Way? Vol. 2017, Mediators of Inflammation. Hindawi Limited; 2017.

323. Netea MG, Domínguez-Andrés J, Barreiro LB, Chavakis T, Divangahi M, Fuchs E, et al. Defining trained immunity and its role in health and disease. Vol. 20, Nature Reviews Immunology. Nature Research; 2020. p. 375–88.

324. Urdahl KB, Shafiani S, Ernst JD. Initiation and regulation of T-cell responses in tuberculosis. Vol. 4, Mucosal Immunology. Nature Publishing Group; 2011. p. 288–93.

325. Obar JJ, Shepardson KM. Coinfections in the lung: How viral infection creates a favorable environment for bacterial and fungal infections. PLoS Pathog. 2023 May 1;19(5).

326. Elder E, Krishna B, Williamson J, Aslam Y, Farahi N, Wood A, Romashova V, Roche K, Murphy E, Chilvers E, Lehner PJ, Sinclair J, Poole E. Monocytes Latently Infected with Human

Cytomegalovirus Evade Neutrophil Killing. iScience. 2019 Feb 22;12:13-26. doi: 10.1016/j.isci.2019.01.007. Epub 2019 Jan 8. PMID: 30677738; PMCID: PMC6352302.

327. Baasch S, Ruzsics Z, Henneke P. Cytomegaloviruses and Macrophages—Friends and Foes From Early on? Vol. 11, Frontiers in Immunology. Frontiers Media S.A.; 2020.

328. Guirado E, Schlesinger LS, Kaplan G. Macrophages in tuberculosis: Friend or foe. Vol. 35, Seminars in Immunopathology. 2013. p. 563–83.

329. Baasch S, Giansanti P, Kolter J, Riedl A, Forde AJ, Runge S, et al. Cytomegalovirus subverts macrophage identity. Cell. 2021 Jul 8;184(14):3774-3793.e25.

330. Deng Y, Ostermann E, Brune W. A cytomegalovirus inflammasome inhibitor reduces proinflammatory cytokine release and pyroptosis. Nat Commun. 2024 Dec 1;15(1).

331. Kropp KA, Robertson KA, Sing G, Rodriguez-Martin S, Blanc M, Lacaze P, et al. Reversible Inhibition of Murine Cytomegalovirus Replication by Gamma Interferon (IFN-γ) in Primary Macrophages Involves a Primed Type I IFN-Signaling Subnetwork for Full Establishment of an Immediate-Early Antiviral State. J Virol. 2011 Oct;85(19):10286–99.

332. Popkin DL, Virgin HW. Murine Cytomegalovirus Infection Inhibits Tumor Necrosis Factor Alpha Responses in Primary Macrophages. J Virol. 2003 Sep 15;77(18):10125–30.

333. Murray PJ, Wynn TA. Protective and pathogenic functions of macrophage subsets. Vol. 11, Nature Reviews Immunology. 2011. p. 723–37.

334. Cilfone NA, Perry CR, Kirschner DE, Linderman JJ. Multi-Scale Modeling Predicts a Balance of Tumor Necrosis Factor-α and Interleukin-10 Controls the Granuloma Environment during Mycobacterium tuberculosis Infection. PLoS One. 2013 Jul 15;8(7).

335. Rajni, Rao N, Meena LS. Biosynthesis and Virulent Behavior of Lipids Produced by Mycobacterium tuberculosis : LAM and Cord Factor: An Overview . Biotechnol Res Int. 2011 Dec 19;2011:1–7.

336. Ding Y, Bei C, Xue Q, Niu L, Tong J, Chen Y, et al. Transcriptomic Analysis of Mycobacterial Infected Macrophages Reveals a High MOI Specific Type I IFN Signaling. Infect Immun. 2023 Jul 1;91(7).

337. Yu S, Ge H, Li S, Qiu HJ. Modulation of Macrophage Polarization by Viruses: Turning Off/On Host Antiviral Responses. Vol. 13, Frontiers in Microbiology. Frontiers Media S.A.; 2022.

338. Malmgaard L, Melchjorsen J, Bowie AG, Mogensen SC, Paludan SR. Viral Activation of Macrophages through TLR-Dependent and-Independent Pathways 1 [Internet]. Vol. 173, The Journal of Immunology. 2004. Available from: http://journals.aai.org/jimmunol/article-pdf/173/11/6890/1182564/6890.pdf

339. Sarti E. Modulating Macrophage Activation and c-Myc Inhibition for Enhanced Immune Response against Mycobacterium tuberculosis. 2025.

340. Newton HJ, Ang DKY, Van Driel IR, Hartland EL. Molecular pathogenesis of infections caused by Legionella pneumophila. Vol. 23, Clinical Microbiology Reviews. 2010. p. 274–98.

341. Yang J, Zhang L, Qiao W, Luo Y. Mycobacterium tuberculosis: Pathogenesis and therapeutic targets. Vol. 4, MedComm. John Wiley and Sons Inc; 2023.

342. Escoll P, Song OR, Viana F, Steiner B, Lagache T, Olivo-Marin JC, et al. Legionella pneumophila Modulates Mitochondrial Dynamics to Trigger Metabolic Repurposing of Infected Macrophages. Cell Host Microbe. 2017 Sep 13;22(3):302-316.e7.

343. Upadhyay S, Mittal E, Philips JA. Tuberculosis and the art of macrophage manipulation. Vol. 76, Pathogens and Disease. Oxford University Press; 2018.

344. Roca FJ, Whitworth LJ, Redmond S, Jones AA, Ramakrishnan L. TNF Induces Pathogenic Programmed Macrophage Necrosis in Tuberculosis through a Mitochondrial-Lysosomal-Endoplasmic Reticulum Circuit. Cell. 2019 Sep 5;178(6):1344-1361.e11.

345. Karki R, Sharma BR, Tuladhar S, Williams EP, Zalduondo L, Samir P, et al. Synergism of TNF-α and IFN-γ Triggers Inflammatory Cell Death, Tissue Damage, and Mortality in SARS-CoV-2 Infection and Cytokine Shock Syndromes. Cell. 2021 Jan 7;184(1):149-168.e17.

346. Gonzalez AJ, Ijezie EC, Balemba OB, Miura TA. Attenuation of Influenza A Virus Disease Severity by Viral Coinfection in a Mouse Model [Internet]. 2018. Available from: https://doi.org/10

347. Devi P, Khan A, Chattopadhyay P, Mehta P, Sahni S, Sharma S, et al. Co-infections as Modulators of Disease Outcome: Minor Players or Major Players? Vol. 12, Frontiers in Microbiology. Frontiers Media S.A.; 2021.

348. Kumar N, Sharma S, Barua S, Tripathi BN, Rouse BT. Virological and Immunological Outcomes of Coinfections [Internet]. 2018. Available from: https://journals.asm.org/journal/cmr

349. Karvonen A, Jokela J, Laine AL. Importance of Sequence and Timing in Parasite Coinfections. Vol. 35, Trends in Parasitology. Elsevier Ltd; 2019. p. 109–18.

350. McArdle AJ, Turkova A, Cunnington AJ. When do co-infections matter? Vol. 31, Current Opinion in Infectious Diseases. Lippincott Williams and Wilkins; 2018. p. 209–15.

351. Garduno A, Martinez GS, Ostadgavahi AT, Kelvin D, Cusack R, Martin-Loeches I. Parallel Dysregulated Immune Response in Severe Forms of COVID-19 and Bacterial Sepsis via Single-Cell Transcriptome Sequencing. Biomedicines. 2023 Mar 1;11(3).

352. Gogoi D, Baruah PJ, Narain K. Immunopathology of emerging and re-emerging viral infections: an updated overview. Vol. 68, Acta Virologica. Frontiers Media SA; 2024.

353. Traylen CM, Patel HR, Fondaw W, Mahatme S, Williams JF, Walker LR, et al. Virus reactivation: A panoramic view in human infections. Vol. 6, Future Virology. 2011. p. 451–63.

354. Diaz-Nicieza C, Sahyoun L, Michalaki C, Johansson C, Culley FJ. Ageing results in an exacerbated inflammatory response to LPS by resident lung cells. Immunity and Ageing . 2024 Dec 1;21(1).

355. Frasca D, Blomberg BB. Inflammaging decreases adaptive and innate immune responses in mice and humans. Vol. 17, Biogerontology. Springer Netherlands; 2016. p. 7–19.

356. Almanan M, Raynor J, Sholl A, Wang M, Chougnet C, Cardin RD, et al. Tissue-specific control of latent CMV reactivation by regulatory T cells. PLoS Pathog. 2017 Aug 1;13(8).

357. Coplen CP, Sonar SA, Nikolich JŽ. Late-life Attenuation of Cytomegalovirus-mediated CD8 T Cell Memory Inflation: Shrinking of the Cytomegalovirus Latency Niche. The Journal of Immunology. 2024 Oct 1;

358. Paulus C, Krauss S, Nevels M. A human cytomegalovirus antagonist of type I IFN-dependent signal transducer and activator of transcription signaling [Internet]. 2006. Available from: www.pnas.orgcgidoi10.1073pnas.0600007103

359. McNab FW, Ewbank J, Howes A, Moreira-Teixeira L, Martirosyan A, Ghilardi N, et al. Type I IFN Induces IL-10 Production in an IL-27–Independent Manner and Blocks Responsiveness to IFN-γ for Production of IL-12 and Bacterial Killing in Mycobacterium tuberculosis –Infected Macrophages . The Journal of Immunology. 2014 Oct 1;193(7):3600–12.

360. Forte E, Zhang Z, Thorp EB, Hummel M. Cytomegalovirus Latency and Reactivation: An Intricate Interplay With the Host Immune Response. Vol. 10, Frontiers in Cellular and Infection Microbiology. Frontiers Media S.A.; 2020.

361. van den Berg SPH, Lanfermeijer J, Jacobi RHJ, Hendriks M, Vos M, van Schuijlenburg R, et al. Latent CMV Infection Is Associated With Lower Influenza Virus-Specific Memory T-Cell Frequencies, but Not With an Impaired T-Cell Response to Acute Influenza Virus Infection. Front Immunol. 2021 May 5;12.

362. Mariotti J, Legrand F, Furst S, Giordano L, Magri F, Richiardi L, et al. Risk Factors for Early Cytomegalovirus Reactivation and Impact of Early Cytomegalovirus Reactivation on Clinical Outcomes after T Cell-Replete Haploidentical Transplantation with Post-Transplantation Cyclophosphamide. Transplant Cell Ther. 2022 Mar 1;28(3):169.e1-169.e9.

363. Styczynski J. Who Is the Patient at Risk of CMV Recurrence: A Review of the Current Scientific Evidence with a Focus on Hematopoietic Cell Transplantation. Vol. 7, Infectious Diseases and Therapy. Springer Healthcare; 2018.

List of figures

List of tables

Acknowledgements

I never imagined I would make it this far – far enough to be writing these lines.
I dedicate this dissertation to my father, whose passing during my doctoral studies broke my heart.
I also dedicate it to my mother, who continues to find courage despite illness.
And I dedicate it to all those who keep going, even when it feels impossible.

First and foremost, I would like to express my heartfelt gratitude to **Dr. Bianca Schneider**, who gave me the opportunity to pursue this project in her lab. This time has been both rewarding and challenging, and I am deeply thankful for her guidance, from which I have grown both personally and professionally. I can truly say that I am leaving this PhD a better scientist in every sense – a journey to which she contributed significantly.

I am also very grateful to **PD Dr. Norbert Reiling, Prof. Dr. Stefan Taube, and Prof. Dr. Rudolf Manz**, my examination committee, for taking the time to read my work, engage in discussions about the data, and offer valuable perspectives that helped shape the direction of this project.

My sincere thanks also go to **Prof. Dr. Wolfram Brune** and **Dr. Eleonore Ostermann**, from our collaboration at the LIV. Wolfram gave me the opportunity to pursue the virological part of my project in his lab and was always approachable – whether I needed advice or simply more virus. Eleonore was incredibly generous with her time and knowledge. She walked me through data analyzes, taught me everything I needed to know about virus production, and was my go-to person for every question.

I would also like to sincerely thank the team from the histology facility – **PD. Dr. Sebastian Marwitz, Prof. Dr. Torsten Goldmann, Christian Rosero, and Jasmin Tiebach**– for their kind support and expertise. Their help was invaluable in enabling the methodological and scientific diversity that this dissertation ultimately reflects. Thank you for always being approachable, helpful, and generous with your time and knowledge.

I also want to thank my wonderful lab mates: **David, Linda, Lars, and Lara**, as well as all the trainees we had along the way. I found not only amazing colleagues in you, but also true friends. Working with you in the lab was as joyful as spending time together outside of it – often over far too much raclette cheese. Thank you for your support in every way over the past years.

Finally, I thank the wonderful people in my life who stand by my side outside the lab – who laugh and cry with me, and whose unwavering support has helped me become the person I am today.

Curriculum vitae

JAQUELINE MARSCHNER

Education

Since 09/2020	**University of Lübeck** PhD candidate (Lab of Dr. Bianca Schneider) Major: Infection Biology/Immunology Thesis title: The impact of cytomegalovirus coinfection on the outcome of tuberculosis in C57BL/6 mice
10/2017 – 01/2020	**University of Hamburg** M.Sc. Molecular Life Sciences Major: Immune therapies Thesis title: Development and evaluation of an optimized lentiviral CRISPR donor construct for improved knock-in efficiency in NIH3T3
10/2013 – 10/2016	**University of Jena** B.Sc. Biochemistry/Molecular Biology Major: Molecular Genetics Thesis title: Characterization of transgenic *sfrp1* in *Nothobranchius furzeri*
08/2010 – 06/2012	**School of Life Science (UKE)** State-certified biological technical assistant Major: Practical Laboratory Techniques and Biological Analysis Thesis title: Characterization of Pyruvate-Carboxylase

Conferences (a selection)

26/09/2023 – 29/09/2023	**SFI-DGfI JOINT MEETING Strasbourg (France)** Topics: Cancer immunotherapy, innate and adaptive immune responses and host-pathogen interactions in viral infections • Contribution Poster: "Viral triggers of tuberculosis disease: a case for cytomegalovirus?"
10/10/2022 – 15/10/2022	**DGfI Autumn School Merseburg (Germany)** Topics: Immunology including lymphocyte development, antigen recognition, immune repertoire formation, and innate/adaptive immune mechanisms • Contribution Poster: "Viral triggers of tuberculosis disease: a case for cytomegalovirus?"
26/09/2022 – 28/09/2022	**2nd Summer School „Infection Biology" Greifswald (Germany)** Topics: Bacterial and viral interactions with hosts, co-infection mechanisms, and pathophysiology • Contribution Poster: "Viral triggers of tuberculosis disease: a case for cytomegalovirus?"

Awards & Scholarships

30/11/2023 – 01/12/2023	**New Developments in Immunology, Inflammation and Infection-Conference, Research Center Borstel** • 1st Prize in the Category Oral Presentations
26/09/2023 – 29/09/2023	**Travel Grant for SFI-DGfI JOINT MEETING, Strasbourg, France** 1st • Funded by the DGfI
26/06/2023 – 28/06/2023	**LCI Summer School, Fintel, Germany** • 2nd Prize in the Speed Talks Category

Publications

The impact of cytomegalovirus coinfection on tuberculosis in the mouse model

Jaqueline Marschner, Sebastian Marwitz, Lars Eggers, Linda von Borstel, David Hertz, Torsten Goldmann, Eleonore Ostermann, Wolfram Brune, Bianca E. Schneider (submitted)

Sex differences in vaccine induced immunity and protection against Mycobacterium tuberculosis

Gishnu Harikumar Parvathy, Dhananjay Bhandiwad, Lars Eggers, Linda von Borstel, Jochen Behrends, Martina Hein, David Hertz, **Jaqueline Marschner**, Zane Orinska, Stefan H E Kaufmann, Mario Alberto Flores-Valdez, Hanna Lotter, Bianca E Schneider doi: https://doi.org/10.1101/2024.04.20.590403

Erklärung

Hiermit versichere ich, dass ich die vorliegende Arbeit selbständig angefertigt habe und keine weiteren als die angegebenen Quellen und Hilfsmittel verwendet wurden.

Weder vorher noch gleichzeitig habe ich andernorts einen Zulassungsantrag gestellt oder diese Dissertation vorgelegt. Ich habe mich bisher noch keinem Promotionsverfahren unterzogen.

Hamburg, 20.04.2025

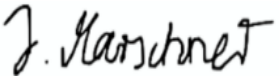

Jaqueline Marschner